

Pannexin1 in human pluripotent stem cells and its influence on early cell fate decisions

By © Rebecca J. Noort (Frohlich)

A thesis submitted to the School of Graduate Studies in partial fulfillment of the requirements for the degree of **Master of Science in Medicine (Cancer & Development)**

October 2021

Division of BioMedical Sciences, Faculty of Medicine
Memorial University of Newfoundland
St. John's, Newfoundland, Canada, A1B 3V6

Scientific Abstract

Human development requires cells to work together within their environment to successfully differentiate and organize into complex tissues. Pannexin1 (PANX1) is a channel-forming protein that facilitates cell-cell communication by conveying small messenger molecules across cellular membranes. PANX1 is expressed in the early embryo and persists in most adult tissues. Dysfunctional PANX1 activity has been implicated in several human pathologies including oocyte cell death and neurological disease. Given its expression in the early embryo and its link to disease, we investigated PANX1's involvement in cell fate specification to the embryonic germ layers and during complex, 3-dimensional human cerebral organoid development. Using immunofluorescence, flow cytometry and quantitative RT-PCR, we find that human induced pluripotent stem cells (iPSCs) express PANX1. iPSCs subjected to CRISPR-Cas9 *PANX1* genetic ablation show no changes in cellular morphology, pluripotency gene expression, proliferation, or apoptosis. However, spontaneously differentiated *PANX1* knockout iPSCs have enhanced ability to generate mesoderm and endoderm germ layers compared to control. Furthermore, PANX1 is dynamically expressed and localized across different neural cell types at distinct stages of human cerebral organoid development. Taken together, our results suggest that PANX1-mediated cell communication actively participates in cell fate specification and human cerebral organoid development.

General Summary

Stem cells have the unique ability to turn themselves into many different types of cells. Deciding what sort of adult cell it will become is one of the most important decisions a stem cell will make. Like all cell types, stem cells rely on the messages communicated throughout their environment to direct their behaviours and decisions. Pannexin1 (PANX1) is a protein that facilitates cell-cell communication by conveying specific signals from one cell to its neighbours. These signals can direct recipient cells to grow, migrate, and even die. Because PANX1 is expressed in the embryo and remains widely expressed throughout adult tissues, we investigated how cell-cell communication mediated by PANX1 channels influences the life and decisions of stem cells. We find that human stem cells express the PANX1 protein, but they do not require it to stay alive. However, stem cells lacking PANX1 have an altered ability to communicate with their surroundings, which affects their decisions about what adult cell type they will become. Therefore, we conclude that cell-cell communication through PANX1 channels helps direct stem cells' behaviours and decisions.

Co-Authorship

Data presented in Figure 3.1, Figure 3.2, Figure 3.3, Figure 3.4, and Figure 3.5 (with slight modification) were published in *Frontiers in Cell and Developmental Biology*:

Noort RJ*, Christopher GA*, Esseltine JL. Pannexin 1 Influences Lineage Specification of Human iPSCs. *Front Cell Dev Biol.* 2021;9:659397.

*contributed equally

Dr. Jessica L. Esseltine designed and engineered the *PANX1*^{-/-} human iPSCs used throughout this study.

I performed the differentiation and sample preparation for **Figure 3.4C**, however the immunofluorescence images for this panel were captured by Grace A. Christopher. For **Figure 3.5**, Grace performed the differentiation, RNA extraction and cDNA synthesis while I performed the qPCR and flow cytometry assays. I performed all other experiments myself.

Funding

This work was supported through the Natural Sciences and Engineering Research Council Discovery Grant RGPIN-2019-04345, Memorial University Faculty of Medicine startup funds and the Medical Research Endowment Fund to Jessica L. Esseltine. Funding for Rebecca J. Noort was provided through a Faculty of Medicine Dean's Fellowship, the F.A. Aldrich Graduate Fellowship and the Natural Sciences and Engineering Research Council Canadian Graduate Scholarship.

Ethics Statement

The induced pluripotent stem cell studies presented here were approved by the Human Ethics Research Board (HREB # 2018.201). Refer to Section 6.1 for full details.

Conflict of Interest

The work presented in this study was conducted in the absence of any commercial relationships or agreements that would be deemed as a potential conflict of interest.

Acknowledgements

I am grateful to Dr. Dale Laird for generously providing us with the female control and *PANX1* iPSCs in addition to the human PANX1 antibody used in this study. I thank Stephanie Tucker and Chris Corkum of the MUN Faculty of Medicine imaging and flow cytometry core facility for providing training and support on the Olympus Fluoview FV1000 confocal microscope and CytoFLEX flow cytometer. I am grateful to Dr. Jaqueline Vanderluit who provided me with training and access to her phase contrast microscope (Zeiss AxioObserver) and cryostat and to Dr. Matthew Parsons for his assistance setting up the FIJI macro for performing automatic area measurements in embryoid bodies and cerebral organoids. I thank Dr. Karen Mearow for the use of her tissue culture suite and the equipment therein. Additionally, I acknowledge Dr. Qi Yuan for use of the Olympus Fluoview FV10i-W3 confocal microscope and Dr. Jules Dore for access and use of the Viiia7 Real Time PCR System. Finally, I wish to acknowledge Leon Chew and Adam Añonuevo who provided training and technical support relating to the cerebral organoids.

I am grateful to my former industry supervisor, Dr. Melanie Kardel, for teaching me how to work efficiently under pressure and stay sane. To my talented former colleagues, thank you for teaching me all kinds of wonderful techniques and for the conversations we shared.

I thank Dr. Jessica Esseltine for her guidance throughout my master's program and for teaching me how to write with clarity. Without her help, my thesis would likely consist of figures and nothing else. I also thank my advisory committee members, Drs. Matthew Parsons and Craig Moore, for their thoughtful evaluation of my project and resulting thesis.

To my family, thank you for teaching me perseverance and for instilling within me a passion to learn new things every day. Most of all, thank you for your love and support. Josh, although I was not thrilled initially, I want to thank you for bringing me to Newfoundland and for encouraging me to return to school after a long hiatus. Your assurances and encouragement helped me transition out of my comfort zone to seek new opportunities that I would have passed up if we stayed in Vancouver. Thank you for your constant support in all my endeavours.

Table of Contents

Scientific Abstract	i
General Summary	ii
Co-Authorship	iii
Funding	iv
Ethics Statement	iv
Conflict of Interest	iv
Acknowledgements	v
Table of Contents	vii
List of Tables	1
List of Figures	2
List of Abbreviations and Symbols	3
1 Introduction	8
1.1 Early Embryonic Development	8
1.2 Germ Layer Emergence	12
1.3 Stem Cells Overview	13
1.4 Induced Pluripotent Stem Cells	15
1.5 Modelling Human Germ Layer Formation with PSC-Derived Embryoid Bodies	18
1.6 Human Brain Development Overview	19
1.7 Cerebral Organoids as a Model of Human Cortical Development	22
1.8 Cellular Communication	27
1.9 Pannexin Overview	27
1.10 Pannexin1 Biology	29
1.11 Pannexin1 Pathologies	32
1.12 Pannexin1 in Brain Development	34
1.13 Pannexin1 in Stem Cells	36
1.14 Research Objectives and Hypotheses	37
2 Materials & Methods	39
2.1 Induced Pluripotent Stem Cell lines	39

2.2	CRISPR-Cas9 human iPSC Knockout Generation	39
2.3	Human iPSC Culture.....	40
2.4	Embryoid Body Generation for Spontaneous Differentiation.....	42
2.5	Directed Differentiation to the Three Germ Layers.....	43
2.6	Cerebral Organoid Culture.....	44
2.6.1	Embryoid Body formation	45
2.6.2	Neuroectoderm Induction	45
2.6.3	Neuroepithelial expansion	45
2.6.4	Cerebral Organoid Maturation	46
2.6.5	Pharmacological inhibition of PANX1 in Cerebral Organoids	46
2.7	Human iPSC Monolayer Differentiation to Neural Progenitor Cells and Neurons	46
2.7.1	iPSC Differentiation into Neural Progenitor Cells	46
2.7.2	NPC Differentiation into Neurons	47
2.8	Gene expression analysis with quantitative reverse transcription polymerase chain reaction (qPCR)	48
2.9	Immunofluorescence (IF)	52
2.9.1	Setup of Monolayer Cultures for IF	52
2.9.2	Monolayer Culture Fixation	53
2.9.3	Immunofluorescence Staining of Monolayer Cultures	53
2.9.4	Embryoid Body and Cerebral Organoid Fixation	57
2.9.5	Whole-Mount Immunostaining of Embryoid Bodies and Cerebral Organoids	57
2.9.6	Cryogenic Tissue Processing and Immunofluorescent Labeling	57
2.10	Imaging	59
2.10.1	Phase Contrast	59
2.10.2	Confocal Microscopy	59
2.10.3	Image Analysis and Colocalization with FIJI	60
2.11	Flow Cytometry	61
2.12	SDS-PAGE & Western Blot.....	63
2.13	Statistics	65
3	Results.....	66
3.1	Human iPSCs Express PANX1	66

3.2	<i>PANX1</i> Knockout iPSCs are Morphologically Indistinguishable from Control	66
3.3	<i>PANX1</i> Knockout Embryoid Bodies Have Skewed Germ Layer Differentiation Potential	73
3.4	Exogenous Pressures Override <i>PANX1</i> ^{-/-} Germ Lineage Bias	80
3.5	<i>PANX1</i> Expression in Neural Progenitor Cells and Neurons	83
3.6	Human Cerebral Organoids Express <i>PANX1</i>	89
3.7	Pharmacological Channel Inhibition with Probenecid Decreases Organoid Size.....	100
4	Discussion	103
4.1	Human iPSCs Express <i>PANX1</i>	103
4.2	<i>PANX1</i> is Dispensable for Human iPSC Morphology, Survival, and Pluripotency Gene Expression.....	104
4.3	<i>PANX1</i> Influences Germ Layer Specification.....	105
4.4	<i>PANX1</i> is Expressed in NPCs, Neurons, and Astrocyte-Like Cells.....	107
4.4.1	<i>PANX1</i> Localizes to the Apical Region of Cerebral Organoid Neuroepithelia	109
4.4.2	Pharmacological <i>PANX1</i> Inhibition Reduces Cerebral Organoid Size	110
4.5	Study Limitations.....	112
4.6	Conclusions	115
4.7	Outlook and Future Directions	116
5	References	119
6	Appendices	127
6.1	Human Ethics Research Statement.....	129
6.2	R Heatmap Code	130
6.3	FIJI Area Measurement Macro.....	132

List of Tables

Table 2.1 Components of Neuron Differentiation Medium	48
Table 2.2 Oligo Sets for qPCR	51
Table 2.3 Primary Antibodies for Flow Cytometry, Immunofluorescence (IF), and Western Blots	55
Table 2.4 Secondary Antibodies and Dyes for Flow Cytometry, IF, and Western Blot	56
Table 2.5 Composition of Mowial®488-DABCO Mounting Medium.....	56
Table 3.1 Mean Putative PANX1 Glycosylation Species Frequency	86

List of Figures

Figure 1.1 Early embryonic development and germ layer emergence involves discrete signaling pathways and gene expression.....	11
Figure 1.2 Comparison of cerebral organoids and the developing human cerebral cortex.....	26
Figure 1.3 Pannexin1 subunit topology and heptameric channel	31
Figure 3.1 PANX1 expression and genetic ablation in iPSCs.....	68
Figure 3.2 <i>PANX1</i> knockout iPSCs are morphologically indistinguishable from control iPSCs	72
Figure 3.3 <i>PANX1</i> ^{-/-} embryoid bodies exhibit skewed lineage specification during spontaneous differentiation.....	76
Figure 3.4 Immunofluorescent analysis of <i>PANX1</i> ^{-/-} embryoid bodies.....	79
Figure 3.5 Exogenous pressures override <i>PANX1</i> ^{-/-} lineage bias.....	82
Figure 3.6 PANX1 is expressed in iPSC-derived neural progenitor cells and neurons.....	85
Figure 3.7 PANX1 immunofluorescence in monolayer neural progenitor cells and neurons.....	88
Figure 3.8 PANX1 is expressed at the earliest points of cerebral organoid development	92
Figure 3.9 PANX1 is expressed in the apical domain of polarized neuroepithelial cells	95
Figure 3.10 PANX1 localization in neural progenitor cells, neurons, and GFAP-positive glia within cerebral organoids	99
Figure 3.11 Probenecid-treated cerebral organoids display stunted growth	102
Figure 6.1 <i>GAPDH</i> transcript expression is stable across all cell lines and tissues assessed in this study.....	128
Figure 6.2 Example of csv file imported into R	131
Figure 6.3 Example of csv file converted to a dataframe (df).....	131

List of Abbreviations and Symbols

% – percent

(v/v) – volume per volume

(w/v) – weight per volume

-/- – homozygous genetic knockout

+/- – with or without

± - plus or minus

°C – degrees Celsius

µg – microgram

µL – microliter

µm – micrometer

µM – micromolar

1X – one time

2X – two times

3X – three times

ATP – adenosine triphosphate

BC – British Columbia

BCA – bicinchoninic acid

BDNF – brain-derived neurotrophic factor

BMP – bone morphogenic protein

BMP4 – bone morphogenic protein 4

bp – base pairs

BSA – bovine serum albumin

Ca²⁺ – calcium

CAN – Canada

CAS – chemical abstracts service

cDNA – complimentary deoxyribonucleic acid

CO₂ – carbon dioxide

CRISPR-Cas9 – clustered regularly interspersed palindromic repeats – Cas9
C_T – threshold cycle
DEU – Deutschland (Germany)
df – dataframe
diH₂O – deionized water
DMEM – Dulbecco's Modified Eagle Medium
DMSO – dimethyl sulfoxide
DNA – deoxyribonucleic acid
E6 – Essential 6
E8 – Essential 8
EB – embryoid body
ECL – enhanced chemiluminescence
ER – endoplasmic reticulum
FACS – fluorescence activated cell sorting
FBS – fetal bovine serum
FGF – fibroblast growth factor
FGF2 – fibroblast growth factor 2
FMO – fluorescence-minus-one
FOXA2 – forkhead box A2
GDNF – glial cell-derived neurotropic factor
GFAP – glial fibrillary acidic protein
GFP – green fluorescent protein
gRNA – guide ribonucleic acid
GSK3 β – glycogen synthase kinase 3 beta
hESC – human embryonic stem cell
HRP – horseradish peroxidase
ICC – immunocytochemistry
IL – Illinois

iPSC – induced pluripotent stem cell
JPN – Japan
KLF4 – Kruppel like factor 4
KO(s) – knockout(s)
L – Liter
LDEV – lactate dehydrogenase elevating virus
MA – Massachusetts
MAP2 – microtubule associated protein 2
MAPK – mitogen-associated protein kinase
MD – Maryland
MEFs – murine embryonic fibroblasts
MEM – Eagle minimum essential medium
MFI – median fluorescence intensity
mg – milligram
Mg²⁺ – magnesium
min – minute
MIXL1 – mix paired-like homeobox
mL – milliliter
mm – millimeter
mM – millimolar
MN – Minnesota
NANOG – NANOG homeobox
NCAM1 – neural cell adhesion molecule
NCBI – National Center for Biotechnology Information
NEAA – non-essential amino acids
NIH – National Institute of Health
NIM – Neural induction medium
NJ – New Jersey

NPC – neural progenitor cell
NSC – neural stem cell
NY – New York
OCT3/4 – see abbreviation for POU5F1
OKS – OCT4, KLF4, SOX2
OKSM – OCT4, KLF4, SOX2, c-MYC
ON – Ontario
OR – Oregon
oRG – outer radial glia
P0 – Passage #0
PA – Pennsylvania
PANX1 – pannexin1
PANX2 – pannexin2
PANX3 – pannexin3
PAX6 – paired box 6
PBS – phosphate buffered saline
PBS-T – phosphate buffered saline with 0.1% (v/v) Tween® 20
PCR – polymerase chain reaction
pH – power of hydrogen
POU5F1 – POU class 5 homeobox
PSC – pluripotent stem cell
QC – Quebec
qPCR – quantitative polymerase chain reaction
RAS – gene family first identified in rat sarcoma
RG – radial glia
RNA – ribonucleic acid
ROCKi – rho-associated kinase inhibitor
SDS-PAGE – sodium dodecyl sulfate polyacrylamide gel electrophoresis

SEM – standard error of the mean
sgRNA – single guide ribonucleic acid
SOX17 – SRY-box transcription factor 17
SOX2 – SRY-box transcription factor 2
TBS – tris buffered saline
TBST – tris buffered saline with 0.1% (v/v) TWEEN®20
TGFβ – transforming growth factor beta
TUJ1 – beta-tubulin III
UK – United Kingdom
USA – United States of America
V – volts
VA – Virginia
ZO-1 – zona occludens-1
vRG – ventricular radial glia
VZ – ventricular zone
WI – Wisconsin
WNT – Wingless/int family of genes
WT – wildtype
x g – times gravity
 ΔC_T – delta threshold cycle
 $\Delta\Delta C_T$ – delta-delta threshold cycle

1 Introduction

1.1 Early Embryonic Development

Human embryonic development follows a series of intricately choreographed events involving large cellular migrations, cell rearrangements, changes in cell morphology, and cell fate specification. Following fertilization, the resulting single-celled zygote undergoes three rounds of cell division called cleavage to attain an 8-celled sphere (also called blastomeres, reviewed in (1)). Each of these 8 individual blastomeres are equivalent in their ability to produce the entire embryo. During each cleavage event, the number of cells doubles but the size of the developing embryo remains unchanged. Shortly after the 8-cell stage, the developing embryo undergoes a process called compaction whereby the cells form tight junctions with each other, generating a cluster called a morula. Cells at the morula's exterior become polarized whereas those at the inside remain apolar leading to the production of a blastocyst (reviewed in (2)). The human blastocyst is a cavitated sphere-like structure containing ~256 cells with discrete functions. Trophectoderm cells arising from the outer layer of the morula constitute the blastocyst's exterior and surround a fluid-filled space called the blastocoel as well as an inner cell mass at one pole of the developing embryo (Figure 1.1A) (1, 3). As embryogenesis progresses, the trophectoderm cells will contribute to placenta formation. Inside the blastocyst, the inner cell mass is comprised of two different cell types: hypoblast and epiblast cells. While the hypoblast cells will give rise to the embryo's extraembryonic yolk sac, the epiblast

cells will produce all bodily cell types of the resulting organism (1, 3, 4). The proliferative and multi-tissue potential of the epiblast cells are discussed in greater detail below.

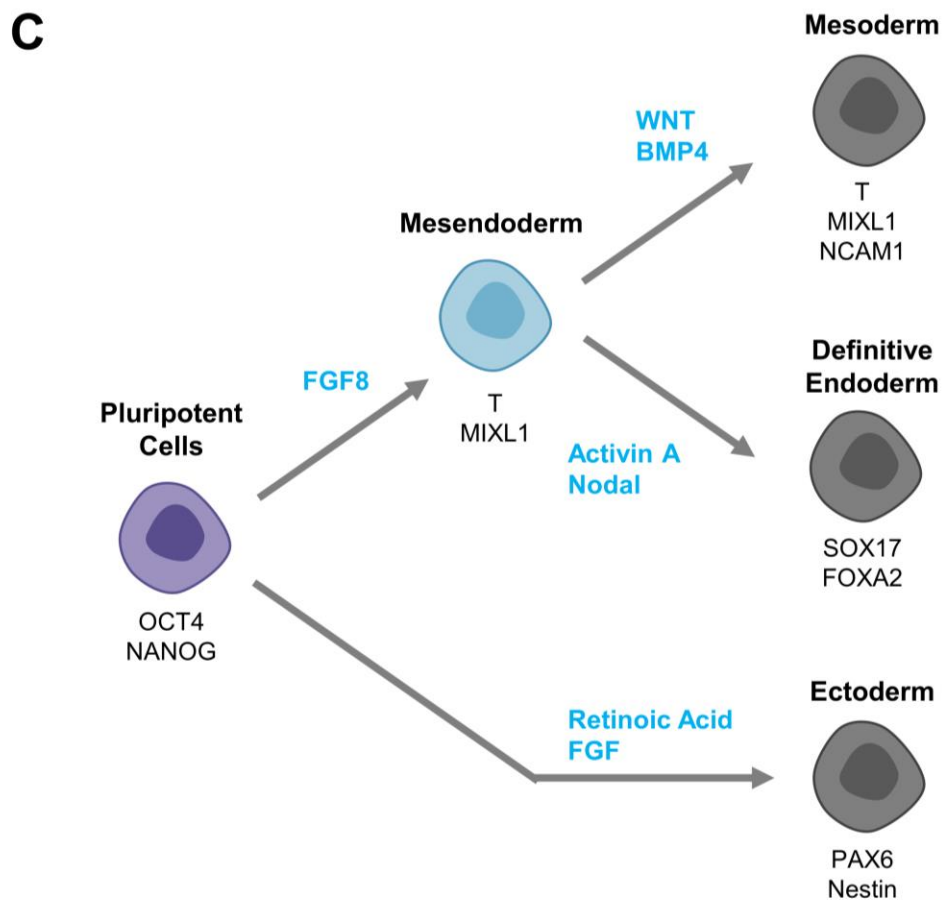
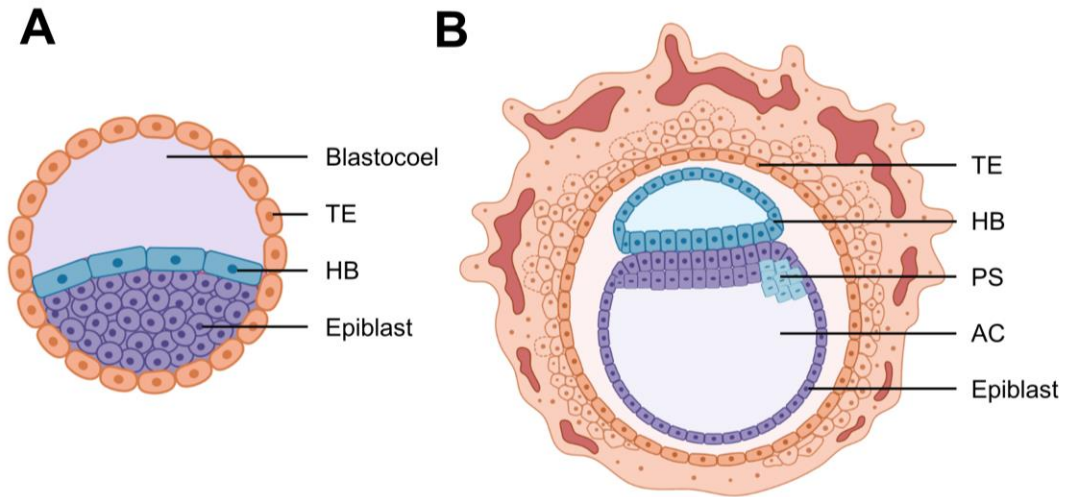


Figure 1.1 Early embryonic development and germ layer emergence involves discrete signaling pathways and gene expression

(A) The human preimplantation blastocyst (at embryonic day 6) is a cavitated sphere surrounded by a layer of polarized trophectoderm (TE) cells which will later contribute to placenta formation. The epiblast cells are sequestered at one pole of the blastocyst and will give rise to the developing embryo's bodily organs. The layer of hypoblast cells (HB) which overlay the epiblast cells will become the extraembryonic yolk sac. **(B)** Following implantation on embryonic day 7 the developing human embryo undergoes morphological transformations to generate a disc-like multilayered structure called the gastrula. The epiblast cells within rearrange themselves so that they surround the amniotic cavity (AC). By embryonic day 14, the primitive streak (PS) emerges at the posterior epiblast region and gastrulation commences. **(C)** During gastrulation, pluripotent epiblast cells in the embryo commit to the three germ layers (mesoderm, definitive endoderm, and ectoderm) in response to various signals. Multipotent mesendoderm cells arise in response to FGF8 signaling. Mesoderm is subsequently produced in regions of high BMP4 signaling and is characterized by expression of Brachyury (T), MIXL1, and NCAM1. Activin A/Nodal signaling leads to the formation of definitive endoderm, characterized by expression of SOX17 and FOXA2. Finally, retinoic acid and FGF signaling encourages ectoderm cell specification characterized by PAX6 and Nestin expression. Clip art in **(A, B)** from BioRender.com with slight modification.

1.2 Germ Layer Emergence

In embryogenesis, the epiblast cells inside the blastocyst give rise to the three germ layers through a process called gastrulation (5). These three primary germ layers (ectoderm, mesoderm, and definitive endoderm) eventually give rise to all bodily cells and tissues (reviewed in (4)). For example, the ectoderm layer contributes to skin and the nervous system, while mesoderm produces connective tissues like blood and muscle, and definitive endoderm gives rise to organs like the liver and intestines (4, 6). Many decades of developmental biology research have revealed exquisite signal transduction pathways that facilitate gastrulation and the subsequent emergence of the three germ layers from epiblast cells (refer to Figure 1.1C).

During gastrulation, a groove-like structure called the primitive streak is formed on the posterior region of the embryo (4, 5) (Figure 1.1B). In response to FGF8 signaling, a subset of the epiblast cells migrates through the primitive streak to become bipotent mesendoderm cells which can specify to either mesoderm or definitive endoderm depending on regional signaling gradients across the embryo (4, 6-8). Mesoderm is produced in regions of high BMP4 signaling and is characterized by Brachyury (T), MIXL1, and NCAM1 expression (9). On the other hand, mesendoderm cells exposed to high levels of Activin A/Nodal signaling specify to definitive endoderm characterized by expression of SOX17 and FOXA2 (8).

In contrast to mesoderm and definitive endoderm, the ectoderm germ layer is formed at the anterior side of the embryo from the remaining epiblast cells which did not ingress through the primitive streak (4, 5). Early ectoderm precursors are characterized by PAX6 and Nestin expression and undergo specification to other intermediates such as neural ectoderm progenitors which contribute to central nervous system development (10). Heightened retinoic acid and FGF signaling in conjunction with the blockade of BMP and TGF β signaling pathways encourages cell specification to a neural ectoderm fate (10, 11). Collectively, gastrulation signaling pathways direct cell fates of the early embryo, establishing the embryonic body plan and subsequent tissue emergence.

1.3 Stem Cells Overview

Human stem cells have emerged as an excellent resource to study human cell fate specification events and model human organogenesis. All stem cells exhibit two primary functions: The first is the ability to self-renew and create identical copies of themselves; the second is to differentiate toward (become) terminal cell types that are locked in form and function (12-14). The ability of a stem cell to differentiate into a wide range of terminal cell types is called potency. Furthermore, there are multiple kinds of stem cells which vary in their potency. From most to least potent, stem cells are categorized as either totipotent, pluripotent, or multipotent.

Totipotent (from the Latin, *totus*, or “whole/entire”) stem cells exhibit the highest degree of potency and can differentiate into every type of cell required to

form a fertile, living organism (3). For example, the fusion of a sperm and ova forms a totipotent, single-celled zygote which will undergo cellular divisions and subsequent differentiation to produce all extraembryonic structures like the placenta and all postnatal bodily organs (3).

Slightly less potent pluripotent (from the Latin, *pluris*, or “more”) stem cells give rise to an organism’s bodily tissues during embryogenesis but have limited ability to form extraembryonic structures (3, 15). Thus, pluripotent stem cells cannot form a fertile, living organism. During embryogenesis, pluripotent epiblast cells are found within the inner cell mass of early and late pre-implantation blastocysts (2, 3, 15). Pluripotent stem cells can also be reprogrammed from terminally differentiated cell types as discussed in Section 1.4.

The first to be discovered but the least potent of the stem cells are multipotent stem cells (from the Latin, *multi*, or “many”) which have limited self-renewal capacity and give rise to a select number of related downstream cell types (3, 15). Many types of multipotent stem cells reside across the adult body, comprising tissue-specific stem cell populations involved in tissue homeostasis and repair. For example, in the adult bone marrow niche, hematopoietic (blood) stem cells continually produce and replenish the many kinds of blood cells required over an organism’s lifespan (15). In addition to their roles in adult tissues, multipotent progenitors also participate in embryonic and fetal developmental programs. In the developing brain, multipotent neural stem cells (NSCs) proliferate symmetrically to increase the size of the NSC pool and later,

asymmetrically divide to produce terminally differentiated cells like neurons and glia (16, 17).

In vivo, the proliferative and differentiative capabilities of the various stem cells (totipotent, pluripotent, and multipotent) drive the expansion of a one-cell zygote into an elaborate multicellular organism with diverse tissues and cell types. While the totipotent and pluripotent stem cells do not persist beyond the earliest time points of embryogenesis, multipotent stem cells continue to replenish and refresh the cells of various tissues over the course of an organism's lifespan. Stem cells cultured *in vitro* retain many of the properties of their *in vivo* counterparts including their ability to self-renew and differentiate. Consequently, stem cells are a useful tool for studying human tissue development and pathology.

1.4 Induced Pluripotent Stem Cells

Pluripotent stem cells (PSCs) can proliferate indefinitely in culture and possess the ability to form the three embryonic germ layers (mesoderm, definitive endoderm, and ectoderm) from which bodily tissues are derived (18, 19). It is possible to obtain human PSCs directly from the epiblast of pre-implantation embryos or derive them from adult somatic cells via genetic reprogramming. Human PSCs isolated from the inner cell mass of a pre-implantation blastocyst are called human embryonic stem cells (hESCs) due to their embryonic origins (20) whereas adult somatic cells subjected to genetic reprogramming are called human induced pluripotent stem cells (iPSCs) (18).

Through genetic reprogramming, terminally differentiated adult somatic cells (such as dermal fibroblasts) undergo dramatic epigenetic remodeling and metabolic alterations to become pluripotent stem cells (reviewed in (21, 22)). Typically, this is accomplished by overexpressing four exogenous transcription factors (OCT3/4, KLF4, SOX2, c-MYC; OKSM), known as the “Yamanaka Factors” in adult somatic cells (18). OCT3/4, KLF4, and SOX2 (OKS) act as pioneer transcription factors by binding to open chromatin and unfurling condensed chromatin to reveal the promoters of repressed genes including those required for pluripotent stemness (21). Meanwhile, c-MYC over-expression enhances the transcription of genes associated with cellular proliferation (a hallmark of stem cells) as well as the transcription of other genes that have active promoters including those of the newly activated pluripotency gene regulatory network (21). Along with the changes at the genetic level, the reprogramming process shifts cellular metabolism from oxidative phosphorylation to glycolysis (22) and reactivates telomerase thereby extending telomere length (23). Additionally, the reprogrammed cells acquire expression of the cell-cell adhesion protein E-cadherin and a subsequent epithelial-like phenotype akin to that of blastocyst cells (24). Thus, the reprogrammed cells look and behave quite differently from the somatic cells they were created from.

While the origins of hESCs and human iPSCs differ, both exhibit comparable morphology, proliferation, potency, and *in vitro* culture requirements (18). Human PSCs are frequently cultured as colonies on culture dishes coated with a thin

layer of extracellular matrix proteins such as laminins, collagens, vitronectins, or mixtures thereof (18, 20, 25, 26). Within the colonies, individual PSCs exhibit tight packing with their neighbours, a large nucleus-to-cytoplasm ratio, and prominent, dark nucleoli (20). In addition to their distinct morphology, human PSCs are also characterized by expression of transcription factors like NANOG, OCT3/4, and SOX2 as well as surface antigens including SSEA3/4, TRA-1-60, and TRA-1-81 (18, 20, 26). Retention of pluripotent stemness and the ability of the PSCs to self-renew requires exogenously applied signaling molecules which act on pathways that continuously activate the OCT3/4, NANOG, SOX2 pluripotency regulatory network. (4, 25-28). While there are numerous signaling molecules that can act on the relevant pathways, the cytokines TGF β and FGF2 are commonly used for PSC maintenance *in vitro* (27). TGF β acts on the TGF signaling pathway to activate the pluripotency transcription factor NANOG (29). FGF2 signaling is slightly more complex and utilizes the RAS/MAPK signaling cascade to indirectly activate NANOG (reviewed in (29)). By leveraging these signaling pathways, pluripotent stem cells can proliferate indefinitely in culture whilst retaining their stemness. Furthermore, PSCs' ability to differentiate into other cell types (18) makes them a useful tool to investigate human cell fate specification and model various steps in human development (20).

1.5 Modelling Human Germ Layer Formation with PSC-Derived Embryoid Bodies

As in the developing embryo, human pluripotent stem cells grown in laboratory culture conditions also form the three germ layers and derivative tissues (9). PSCs in culture can model the germ layer emergence observed during gastrulation (30) by directed or spontaneous differentiation strategies. In directed differentiation, PSCs are supplied with exogenous growth factors or chemicals that modulate the specific signaling pathways active in gastrulation, as outlined in Section 1.2. For example, chemical inhibition of downstream participants of the TGF β signaling pathway forces PSC commitment to ectoderm (31-33) whereas GSK3 β inhibition with the small molecule CHIR99021 activates the canonical WNT/ β -catenin pathway and drives PSC differentiation toward mesoderm and definitive endoderm (7, 34). While directed differentiation is often rapid and highly efficient, it can mask cells' innate lineage preferences that arise in part due to interactions with their neighbours and environment. Spontaneous differentiation techniques facilitate assessment of intrinsic lineage preferences due to cell-cell and cell-environment interactions in the absence of externally applied cues.

A useful property of PSCs in culture is their ability to form spherical structures called embryoid bodies (EBs) (19, 30). EBs recapitulate the gross morphology and germ layer potential of post-implantation embryos (19) but do not form an organism. EBs are especially useful for human developmental

studies as EBs permit investigation of 3-dimensional cell-cell and cell-matrix organization during germ layer emergence without the need for human embryos (13, 19, 30). EBs are created by singularizing PSCs and allowing the cells to form a unified sphere. To prevent cells from attaching to the cultureware, anti-adherent surface coatings like agarose or detergents are utilized so cells must adhere to each other rather than the culture surface (35, 36). In the absence of externally applied signaling molecules (spontaneous differentiation) the PSCs within the EBs will communicate with one another and spontaneously commit to mesoderm, definitive endoderm, and ectoderm (13, 19, 34, 37). Consequently, spontaneous differentiation using EB culture provides a platform to evaluate cells' intrinsic germ lineage preferences as the cells rely on communication with each other rather than guidance from exogenous signals (19). While EBs are particularly useful for evaluating the generation of the three germ layers, EBs are largely disorganized and do not display the cellular patterning or organization exhibited by the developing gastrula. Nevertheless, EBs can act as a starting point for 3D directed differentiation strategies which imitate aspects of organ development.

1.6 Human Brain Development Overview

Human brain development is a protracted process which begins following gastrulation and continues after birth (38). During the embryonic and fetal periods, the various brain tissues are formed and organized while the refinement

of neuronal connections occurs postnatally. Here, we focus on how select brain cells are produced during the prenatal period.

Following gastrulation, the ectoderm specifies toward four possible downstream lineages: neuroectoderm, neural crest, non-neural ectoderm, and the cranial placode (10). BMP4 signaling gradients govern the ectoderm lineage trajectory, where low levels of BMP4 signaling in conjunction with WNT inhibition confer a neuroectoderm fate (10). The neuroectodermal cells acquire tight junctions, adherens junctions, and apical-basal polarity, forming a pseudostratified layer of columnar neuroepithelium which gives rise to the neural plate and subsequent neural tube (39-41). The caudal (tail) end of the neural tube will eventually become the hindbrain and spinal cord whereas the rostral (head) end will become forebrain structures like the cerebral cortex (38). As brain development progresses the ends of the neural tube close and the resulting lumen undergoes conformational changes, developing into brain ventricles filled with cerebrospinal fluid.

Several types of multipotent neural stem and progenitor cells reside along the edge of the ventricles where they form a cell-dense region called the ventricular zone (VZ) (38, 41). Initially, neuroepithelial cells predominate in the VZ but slightly before neurogenesis (production of neurons) the neuroepithelial cells differentiate to produce downstream progenitor cells called ventricular radial glia (vRG) (39). Like neuroepithelial cells, vRG exhibit apical-basal polarity, self-renew, possess adherens junctions, and express markers such as SOX2 and

PAX6 (39, 41, 42). However, vRG are distinguishable from neuroepithelial cells in that vRG possess glycogen granules, lack tight junctions, and acquire expression of several glial markers (39). Eventually displacing the neuroepithelial cells in the VZ, vRG proliferate to increase the size of the progenitor pool and differentiate to produce a variety of neural cell types (39). From human E25-E42, vRG at the apical side of the VZ proliferate symmetrically to expand their numbers and increase the size of the developing brain (42). Around human E42 the vRG start dividing asymmetrically to produce an identical daughter cell and an intermediate progenitor cell that will eventually become a neuron (38, 42). The intermediate progenitor cell migrates out of the ventricular zone into a subventricular zone where it proliferates to increase neuronal numbers (42).

By primate mid-gestation, the subventricular zone is divided by an inner fiber layer which delineates an inner (apically situated and closer to the ventricles) and outer subventricular zone (42). In primates, the intermediate progenitor cells reside in the outer subventricular zone along with an additional type of progenitor cell called outer radial glia (oRG). Like their vRG counterparts, oRG express SOX2 and PAX6, self-renew, and divide asymmetrically to produce neurons (42). Interestingly, oRGs are generally absent in rodents and are thought to facilitate heightened brain expansion of the human cerebral cortex (42). Neurons produced by progenitor cells in the ventricular and outer subventricular zones migrate away to populate layers of the developing cortical plate (17, 38). During the embryonic and fetal periods, waves of neuron migration produce

different cortical layers, some of which are transient and do not persist into adulthood (reviewed in (38)). However, by the end of the fetal period, the cerebral cortex attains six defined neuronal layers that are produced in an inside-out fashion where the newest neurons produced reside at the outermost (basal) facet.

While neurons constitute a large proportion of brain cells in the cerebral cortex there are also populations of non-neuronal cells. Following neurogenesis, radial glia begin to divide asymmetrically to produce glial progenitor cells capable of division which migrate and differentiate to downstream glial cell types such as astrocytes and oligodendrocytes (38). Collectively, neuroectoderm-derived cell types such as neurons and glia work together to facilitate signal transmission and maintain tissue homeostasis in the brain (43).

Most of our understanding of human brain development comes from studies on model organisms and limited human brain samples (44). While animal models have afforded many insights, a human-centric model could reveal nuances of human brain development that are different or lacking in model organisms.

1.7 Cerebral Organoids as a Model of Human Cortical Development

Human organoids are artificially grown 3D structures which resemble the cellular composition, development, and functionality of human organs (45, 46). Created from PSCs, cerebral organoids are self-organizing structures which form many of the neural cell types found in the human cerebral cortex (refer to Figure

1.2) (17). Cerebral organoids start out as EBs which are directed toward ectoderm and subsequent neuroepithelium (17, 44). The neuroepithelial cells self-organize into rosette-like structures with tightly packed nuclei and apical-basal polarity (17, 44). The apical side (innermost) of the neuroepithelium hollows out whilst the neuroepithelial layer thickens, forming a ventricular-like zone surrounding a fluid-filled space resembling a ventricle (17, 33). Like their ventricular zone counterparts *in vivo*, the organoid ventricular-like zone contains vRG which proliferate and give rise to other cell types such as neurons (17, 47). As the organoid matures, discrete neuronal layers form and glial cell types like astrocytes emerge (44, 47). While cerebral organoids can model various brain regions including dorsal forebrain, hindbrain, choroid plexus, hippocampus, meninges, and retina (17, 44, 47), they have a tendency to form forebrain regions which exhibit the layered structure and various cell types observed in developing human cerebral cortex (17). However, cerebral organoids typically lack vascularization, resident immune cells called microglia, and the cortical layer thickness observed in the human brain (reviewed in (44)). Encouragingly, refinement to the organoid culture system now enables vascularization (48, 49) and microglial incorporation (50). Even without these advances, the cerebral organoid system has successfully recapitulated human development pathologies such as microcephaly (17) and Miller-Dieker syndrome (51) which are not adequately modeled in rodents. As such, the cerebral organoid culture system is

useful for evaluating cellular interactions and brain pathologies unique to the human context.

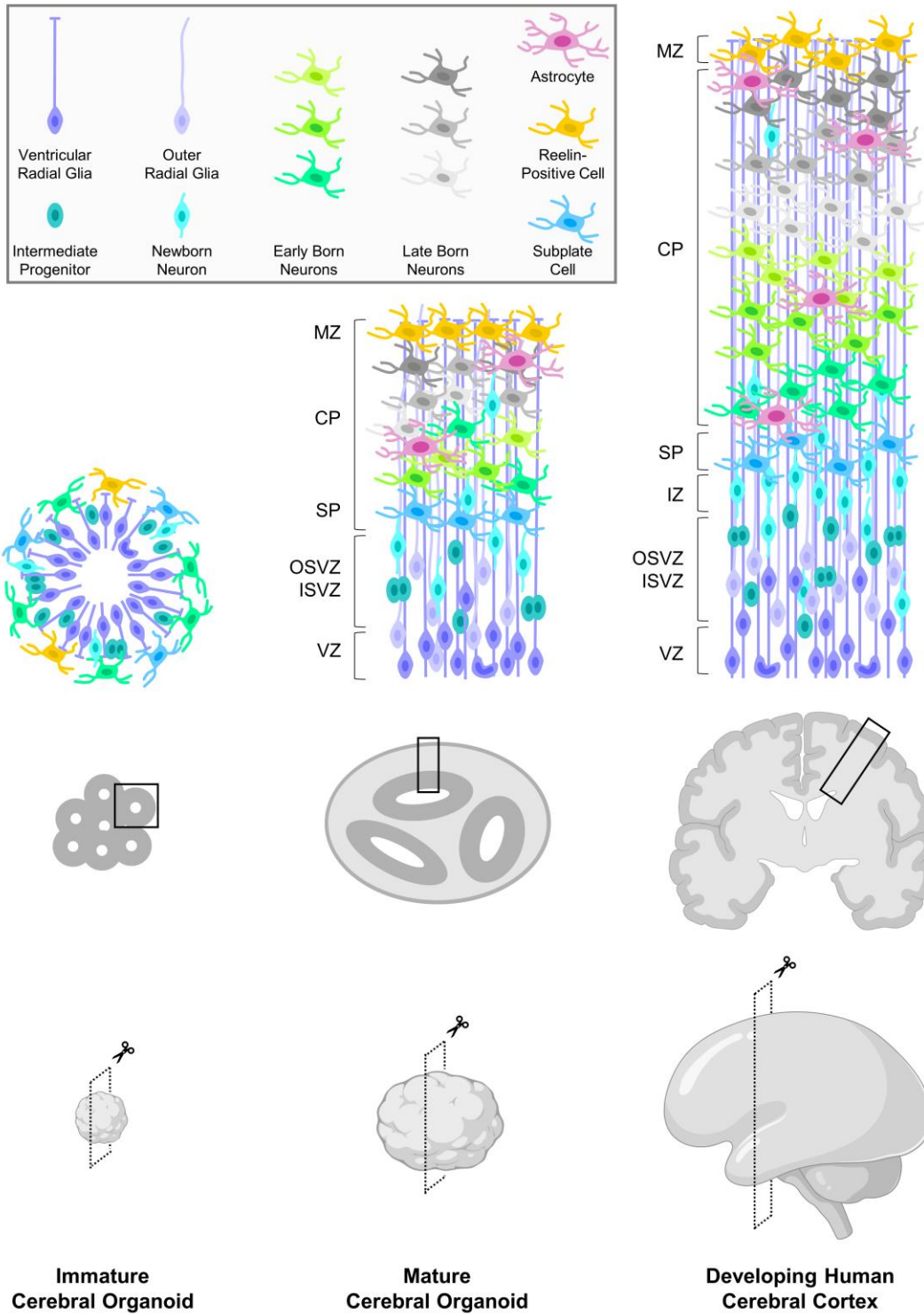


Figure 1.2 Comparison of cerebral organoids and the developing human cerebral cortex

Cerebral organoids partially model the cellular composition and organization observed in the developing human cerebral cortex. Cerebral organoids are much smaller than the developing human cerebral cortex (images not to scale). Immature cerebral organoids (by day 10) contain multiple rosette-like arrangements of neuroepithelium which contain ventricular radial glia surrounding a small, fluid-filled ventricular-like space. As cerebral organoids mature (day 40+), the ventricular-like zones (VZ) become thicker and additional cell types are present. As in the developing human cerebral cortex, mature cerebral organoids possess outer radial glia which populate the outer subventricular zone (OSVZ) but lack a well-defined intermediate zone (IZ). In mature cerebral organoids, neurons of the cortical plate (CP)-like region are generally organized into an early born and late born layer. However, in the developing human cortex, early and late born neurons are arranged as six well-defined layers. Cell types that are typically underrepresented or absent in mature cerebral organoids include endothelial cells, microglia, and oligodendrocytes. ISVZ, inner subventricular zone; SP, subplate; MZ, marginal zone. Cerebral organoid and human brain clip art from BioRender.com.

1.8 Cellular Communication

Cells must work together within their environment to orchestrate the series of events required for successful differentiation and arrangement into complex tissues. Interruption of cell communication can drastically alter cell fate potentials and skew differentiation. For example, β -catenin knockout mice have impaired WNT signaling and die in early embryogenesis as they fail to produce mesoderm and all its derivative tissues (heart, kidney, blood, bone, etc.) (52). Cellular communication occurs via several different mechanisms. For example, gap junctional intercellular communication mediated by the connexin protein family enables the direct transmission of signals between the cytoplasm of adjacent cells (53). Additionally, cells can deploy signaling molecules into the extracellular space to indirectly communicate with distant cells (endocrine signaling), neighbouring cells (paracrine signaling), or with themselves (autocrine signaling) (54, 55). Pannexins (PANX) are a class of mechanosensitive pore forming proteins that facilitate paracrine and autocrine signaling by conveying messenger molecules across cellular membranes (53). These channels are increasingly recognized for their beneficial contributions to tissue homeostasis and detrimental roles in pathological conditions.

1.9 Pannexin Overview

In humans, there are three pannexin protein (PANX) isoforms: PANX1, PANX2, and PANX3 (56). Of these, PANX1 is the most prevalent with broad expression across many tissues including but not limited to the brain,

gastrointestinal tract, kidneys, and ovaries (57) (Human ProteinAtlas). PANX2, on the other hand, is generally restricted to the skin, central nervous system, and testes while PANX3 is primarily found in bone and connective tissue (56-59). Synthesis and assembly of PANX proteins into functional channels occurs through the conventional endoplasmic reticulum (ER)-Golgi apparatus pathway (60, 61). PANX proteins are subject to posttranslational modifications including glycosylation (62), which can affect channel localization to specific membrane compartments. For example, PANX1 proteins can adopt three distinct glycosylated forms: Gly0, newly translated and non-glycosylated; Gly1, an N-linked high mannose form which permits ER to Golgi transport; and Gly2, a complex carbohydrate addition produced in the Golgi apparatus which facilitates PANX1 channel trafficking to the plasma membrane (63). While the three human PANX isoforms vary in their subcellular localization depending on cell type and developmental stage, some general rules apply. PANX1 and PANX3 can localize to the plasma membrane and within intracellular compartments (57, 59, 60, 64, 65). PANX2, on the other hand, is typically retained intracellularly (57, 66, 67).

Owing to its wide expression patterns, PANX1 is by far the best characterized pannexin isoform. Additionally, *PANX1* is currently the only pannexin family member with reported germline mutations resulting in disease (68, 69). Given its nearly ubiquitous expression throughout the body and implications in disease, PANX1 is particularly salient.

1.10 Pannexin1 Biology

Individual human PANX1 proteins consist of a chain of 426 amino acids that cross the plasma membrane four times, forming 2 extracellular loops and situating the N and C-terminal tails in the cytoplasmic domain (70) (refer to Figure 1.3). PANX1 channels are comprised of seven individual subunits which assemble to form a heptamer (71-73). Since PANX1 channels on the plasma membrane are heavily glycosylated at amino acid position N254 on the second extracellular loop (64), they are unable to dock with PANX1 channels from a neighbouring cell due to steric hinderance (53). Consequently, PANX1 channels on the plasma membrane facilitate transfer of small signaling molecules between the cell cytosol and the extracellular space rather than directly between the cytosols of two adjacent cells.

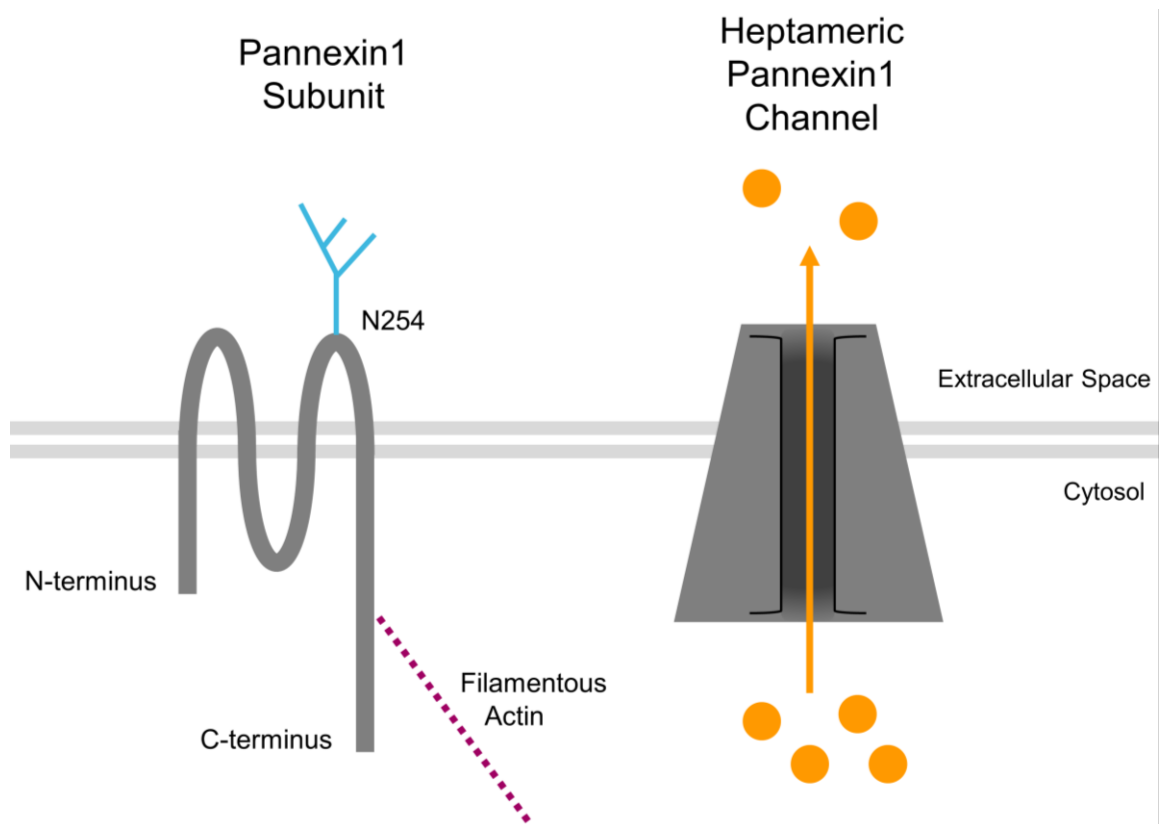


Figure 1.3 Pannexin1 subunit topology and heptameric channel

PANX1 subunits are 4-pass transmembrane proteins that are often glycosylated at amino acid position N254 on the second extracellular loop. Heavy glycosylation (shown in blue) along with PANX1 interaction with the actin cytoskeleton (shown by dashed purple line) is linked to PANX1 trafficking to the plasma membrane. Seven PANX1 subunits assemble to form a channel that permits movement of ions, metabolites and other signaling molecules less than 1kDa in size (orange) across cell membranes in response to various stimuli.

PANX1 is most thoroughly characterized for its role as an ATP release channel in diverse cellular functions (53). Stimuli including mechanical stretch, high extracellular ATP and K⁺, and high cytoplasmic Ca²⁺ can transiently promote PANX1 channel opening while irreversible PANX1 channel opening is triggered upon cleavage of its carboxyl-terminal tail (54, 57, 74). Immunoprecipitation experiments revealed that F-actin, β-actin, and actin-related protein 3 interact with the PANX1 C-tail (57, 61, 67). Actin microfilaments may help anchor PANX1 channels to the plasma membrane and open the channels during cytoskeletal rearrangement or cell stretching (57). These mechanosensitive properties suggest a role for PANX1 in cell migration and motility where cells undergo dramatic alterations to their cytoskeleton (75).

1.11 Pannexin1 Pathologies

PANX1 channel functions are implicated in pathologies including ischemic stroke, epilepsy, HIV infection, and oocyte death (58, 69, 70). During inflammation, P2X₇ purinergic receptors stimulate PANX1 channels to open and release ATP (57). Similarly, apoptosis triggers irreversible PANX1 channel opening through activated caspase 3 and 7 which cleave the PANX1 C-terminal tail resulting in mass efflux of ATP out of the cell (57, 74). The ATP serves as a “find me, eat me” signal which recruits phagocytic cells to the area resulting in clearance of the apoptotic cell (76). PANX1 channels also play a detrimental role in viral pathogenesis. For example, HIV can use PANX1 channels to gain access into lymphocytes (77). Once inside the cell, HIV leverages PANX1 channels’ ATP

release function to destabilize the plasma membrane so that it fuses with those of uninfected cells thereby facilitating viral spread (70, 78).

Under ischemic conditions, PANX1 channels of murine hippocampal neurons release ATP which contributes to subsequent membrane depolarization and neuronal death (79, 80). Similarly, NMDAR (N-methyl-D-aspartate receptor) activation facilitates PANX1 channel opening and subsequent ionic dysregulation which can potentiate seizure-like activity (81). More recent work performed in human cortical brain slices revealed that PANX1 channels initiate epileptic activity via their ATP release function and subsequent activation of P2X₇R (58).

While the native PANX1 protein is implicated in several pathologies, there are also several reported inheritable human *PANX1* mutations which result in disease. To date, four different autosomal dominant human *PANX1* mutations are implicated in a phenotype called oocyte death where oocytes degenerate before fertilization or shortly thereafter (69). The aberrant PANX1 proteins p.21_23delTEP, p.K345E, p.C346S, and p.Q392* exhibit defective glycosylation and enhanced channel activation resulting in improper ATP release from human oocytes (69). Unlike the human patients, heterozygous female knock-in mice harbouring these four mutations were fertile and healthy (69). The authors determined that human oocytes express much more PANX1 protein than murine oocytes but when female mice are engineered with oocyte-specific overexpression of the *PANX1*^{Q392*} mutation they become infertile and their oocytes degenerate prior to fertilization (69). A different, homozygous mutation

(p.R217H) in *PANX1* is attributed to multisystem dysfunction in a female patient whose clinical presentations include kyphosis, primary ovarian failure, hearing loss, and intellectual disabilities (68). The p.R217H mutation displayed normal glycosylation and trafficking to the cell surface but had reduced channel function (68). In contrast to the many pathological conditions attributed to *PANX1*, this channel also has physiological roles in vasoconstriction, taste sensation, airway defence (54), and positively regulating neural progenitor cell proliferation (16).

1.12 Pannexin1 in Brain Development

Animal studies have revealed *PANX1* expression in various brain regions and in diverse neural cell types including neural stem and progenitor cells, neurons, and astrocytes (16, 82, 83). Gene expression analyses revealed that murine *PANX1* is abundantly expressed in the cerebral cortex, cerebellum, and olfactory bulbs during embryonic development, peaking at murine embryonic day 18 and declining thereafter (82). The decline of murine *PANX1* expression is accompanied by increased *PANX2* expression which predominates throughout the postnatal period and into adulthood (82, 83). Gene expression analyses curated by BrainSpan indicate that a similar pattern occurs in the human system – where *PANX1* expression in various brain structures is high at the beginning of the fetal period but diminishes thereafter, whereas *PANX2* predominates and persists into adulthood (Brainspan.org). Although *PANX1* expression in adult brains is diminished compared to fetal brains, the Human Protein atlas reports moderate-to-high *PANX1* protein abundance in the adult human cerebral cortex.

Many insights of PANX1's role in brain development come from studies conducted on postnatal mice. While many neurons are generated in the embryonic and fetal periods, neural stem and progenitor cells within the ventricular zones continue to proliferate and produce neurons after birth (16). In the postnatal murine brain, ATP released into the extracellular space by PANX1 channels activates P2X₇ and P2Y purinergic receptors. In turn, the activation of these receptors stimulates the proliferation of neural stem and progenitor cells (16) while impeding neurogenesis (75). Pharmacological PANX1 inhibition with probenecid (a non-specific blocker of various channel types including pannexins) decreases murine neural progenitor proliferation, while overexpression of PANX1 protein increases proliferation (16). Collectively, these results suggest that PANX1-mediated ATP release in neural stem and progenitor cells retards neurogenesis and encourages expansion of the progenitor pool. (16). It is worth noting, however, that brain development differs between mice and humans. Human brains experience dramatic cortical expansion and gyration (folding) whereas murine brains have relatively a small cerebral cortex and a smooth (lissencephalic) surface (51). Enhanced human brain size and gyrification is attributed to additional progenitor cells called outer radial glia which are generally absent in the murine brain (44, 47). Consequently, human brain disorders such as microcephaly (small brain) and Miller-Dieker syndrome (smooth brain) are ineffectively modeled using a murine system (44). While roles for PANX1 in postnatal murine neural progenitors are well-established, it is unclear whether these findings also apply to humans.

1.13 Pannexin1 in Stem Cells

Current PANX1 studies have failed to capture the earliest stages of embryonic and fetal development, instead relying on E14 mice and older. Recently, PANX1 expression was reported in human pluripotent stem cells (84) although the role of PANX1 in these cells and their downstream progeny is currently unknown. The lack of information on PANX1 channel function in pluripotent stem cells, embryonic tissue emergence, and cerebral cortex development in a human context warrants further investigation. Fortunately, human iPSCs make inquiries such as these possible.

Human iPSCs are highly versatile and capable of modelling PANX1 functions in pluripotency, germ layer emergence, and human brain development. iPSCs are scalable as they self-renew indefinitely in maintenance culture conditions. Furthermore, they exhibit tremendous plasticity as they can differentiate to any cell type of the body under spontaneous or directed differentiation methods. Their ability to form EBs and cerebral organoids confers a means of investigating PANX1-mediated communication within a 3D context. iPSCs are amenable to CRISPR-Cas9 genetic engineering and can be reprogrammed from patients harbouring pathological genetic mutations, enabling loss-of-function and clinical variant studies. Taken together, iPSCs are a powerful tool to investigate human development and the role of PANX1 therein.

1.14 Research Objectives and Hypotheses

Here, we utilize human control and *PANX1* knockout iPSCs to investigate the role of PANX1 in human pluripotent stem cells, during cell fate specification into the three embryonic germ layers, and in a cerebral organoid model of human brain development. Additionally, we examine PANX1 expression and localization at the cellular and subcellular levels across these culture systems. **We hypothesize that PANX1-mediated communication facilitates human iPSC fate decisions and cerebral organoid development.**

Our objectives to specifically test this hypothesis are as follows:

Objective 1) Evaluate how *PANX1* genetic ablation affects human iPSC morphology, proliferation, apoptosis, and pluripotency gene expression.

Objective 2) Determine the effect of *PANX1* gene knockout on spontaneous germ layer commitment in human iPSC-derived EBs.

Objective 3) Evaluate PANX1 expression and localization throughout human cerebral organoid development.

Objective 4) Determine the effect of PANX1 pharmacological inhibition on human cerebral organoid development.

Our results indicate that PANX1 is not required for human iPSC maintenance but that it influences iPSC differentiation to the germ layers. Gene and protein expression analyses demonstrate that spontaneously differentiated *PANX1*^{-/-} iPSCs have a greater tendency to produce mesoderm and endoderm than control iPSCs. In human cerebral organoids, immunofluorescent imaging reveals PANX1 expression in neural precursor cells, neurons, astrocyte-like cells, and at the apical side of ventricular-like zones. Finally, we noted that pharmacological inhibition of PANX1 can reduce human cerebral organoid size. Taken together, we propose a new role for PANX1 channels in regulating stem cell fate specification.

2 Materials & Methods

2.1 Induced Pluripotent Stem Cell lines

Female wildtype human induced pluripotent stem cells were created from dermal fibroblasts isolated from an apparently healthy 30-year-old female as described in Esseltine et al., 2017 (85) and obtained through a material transfer agreement with The University of Western Ontario. A wildtype male human iPSC line (GM25256) was purchased from the Coriell Institute for Medical Research (Cat# GM25256, Coriell, Camden, NJ, USA).

2.2 CRISPR-Cas9 human iPSC Knockout Generation

PANX1 knockout human iPSCs in the female background were created as described previously (86). Briefly, female wildtype human iPSCs were transfected using the Mirus TransIT®-LT1 Transfection Reagent (Cat# MIR-2304, Mirus Bio LLC, Madison, WI, USA) with the pSpCas9(BB)-2A-GFP plasmid (Cat# 48138, Addgene, Cambridge, MA, USA) according to the manufacturer's instructions. The plasmid encodes for the Cas9 protein along with a cloning backbone for a single guide RNA (sgRNA) and a green fluorescence protein (GFP) selection marker (87). The sgRNA against *PANX1* was designed to target the third exon using the Sanger Institute CRISPR finder (<http://www.sanger.ac.uk/htgt/wge/>) and was selected based on its low exonic off-target predictions (human *PANX1*: Sanger sgRNA ID 1087081842 (5'-GCTGCGAAACGCCAGAACAG-3')). After transfection, GFP-expressing single cells were sorted using fluorescence

activated cell sorting (FACS) and re-plated at low density to permit easy isolation of individual clones. The resulting individual clones were examined for ablation of the target gene at the genomic level via PCR and Sanger sequencing while ablation of the PANX1 protein was assessed via immunofluorescence microscopy, flow cytometry, and Western blotting (refer to sections 2.9.3, 2.11, and 2.12 for detailed information). Resultant human iPSC knockouts were maintained in culture according to Section 2.3.

2.3 Human iPSC Culture

Human iPSCs were routinely cultured as colonies in feeder-free (lacking murine embryonic fibroblasts) conditions in humidified 37°C Heracell™ VIOS 160i CO₂ cell culture incubator (Cat# 51030284, ThermoFisher) buffered with 5% CO₂ and atmospheric oxygen. Human iPSCs were grown on Nunclon Delta surface 6-well dishes (Cat# 140685, ThermoFisher) coated with Geltrex (Cat# A141330, ThermoFisher). The male iPSC line was fed daily with mTeSR Plus medium (Cat# 100-0276, STEMCELL Technologies, Vancouver, BC, CAN) whereas female iPSC lines were fed daily with Essential 8 medium (Cat# A1517001, ThermoFisher). mTeSR Plus is a proprietary adaptation of mTeSR1 (described in (26-28)) whereas Essential 8 medium (E8) is based on the published formulation described by Chen et al., (25). Both media are designed to maintain the pluripotency of human iPSCs in feeder-free culture systems. Dishes were coated with Geltrex by diluting ice cold Geltrex at 1:100 dilution into ice cold Dulbecco's Modified Eagle's Medium (DMEM; Cat# 319-005-CL, WISENT Inc, Montreal, QC,

CAN) and incubating at 37°C in a humidified incubator for 1 hour. After incubation, the residual coating material was aspirated and replaced with mTeSR Plus or Essential 8. Colonies were passaged every 4-5 days when they exhibited tight cell packing, smooth borders, and phase-bright smattering at colony centers. Individual iPSCs within the colonies exhibited prominent nucleoli and high nucleus-to-cytoplasm ratio as is characteristic for human pluripotent stem cells (18, 20). Regions of spontaneous differentiation in the iPSC cultures were visually identified using a phase contrast microscope (Cat# 319-005-CL, Olympus, Tokyo, JPN) and manually removed from the culture by scratch aspiration prior to passaging. Spontaneous differentiation did not exceed 5% of the total cell-occupied area. After regions of spontaneous differentiation were removed, residual culture media was aspirated and each well was washed once with Ca²⁺ and Mg²⁺-free PBS (Cat# 21-040-CV, Corning Inc, Corning, NY, USA). Wells were incubated with 1 mL gentle cell dissociation buffer (Cat# 13151014, ThermoFisher) at room temperature until colonies were visibly broken apart, approximately 3-5 minutes (88). Gentle cell dissociation buffer was then replaced with 1 mL of Essential 8 or mTeSR Plus to stop the reaction. Colonies were then scraped from the dish surface and broken into small aggregates of cells (roughly 50 – 200 µm in diameter) using a cell lifter (Cat# 03-421-105, ThermoFisher). The resultant aggregates were seeded into fresh Geltrex-coated wells containing mTeSR Plus or Essential 8 at split ratios of 1:5-1:50, depending on how soon cells were needed for experimentation. Human iPSCs were maintained in culture for 20 weeks after thawing at which point the culture was terminated and a fresh

vial of low-passage iPSCs was thawed from liquid nitrogen. We confirmed our human iPSC cell banks have normal copy number at various mutation hotspots using the hPSC Genetic Analysis Kit (Cat # 07550, STEMCELL Technologies).

Single cell human iPSC passaging was achieved using StemPro Accutase (Cat# A1110501, ThermoFisher). Spent culture media was removed from the iPSCs and the wells were washed once with $\text{Ca}^{2+}/\text{Mg}^{2+}$ -free PBS followed by treatment with a thin layer of Accutase for 8 minutes at 37°C. Contents of the wells were triturated in the Accutase to create a single cell suspension which was subsequently transferred into a collection tube containing a 2X volume of DMEM to stop the reaction. The collection tube was centrifuged at 300 x gravity for 5 minutes and the supernatant was decanted. Cells were plated in medium supplemented with Rho-associated kinase inhibitor (ROCKi), Y-27632 (Cat# Y-5301, LC Laboratories, Woburn, MA, USA) to promote survival of singularized human iPSCs (89).

2.4 Embryoid Body Generation for Spontaneous Differentiation

EBs of 9000 cells each were created in 96-well round-bottom plates (Cat# 163320, ThermoFisher) coated with 1% agarose (Cat# 800-015-EG, WISENT Inc.) prepared in deionized water to confer a non-adherent surface which promotes iPSC self-aggregation (35, 90). In later experiments, 96-well round-bottom plates (Cat# 353077, Corning, Corning Inc, Corning, NY, USA) were rinsed with 5% w/v Pluronic F-127 (Cat# P2443, MilliporeSigma, Burlington, MA,

USA) prepared in deionized water, to confer anti-adherent surface properties to the plastic (91).

On day 0, a single cell human iPSC suspension was created via Accutase dissociation as described above. The single cell pellet was re-suspended in Essential 6, which lacks the essential pluripotency factors TGF β and FGF2 (Cat# A1516401, ThermoFisher), with 10 μ M Y-27632 to promote cell survival (37). Viable cell counts were performed on a Bio-Rad TC20™ automated cell counter (Cat# 145010, Bio-Rad, Hercules, CA, USA) using trypan blue (Cat# 15250061, ThermoFisher) and the cell density was adjusted to 9000 viable cells per 100 μ L of Essential 6 + 10 μ M Y-27632 (STEMCELL Technologies Document #DX21849 | Version 1_2_0). On days 2 and 4, 50 μ L of Essential 6 without Y-27632 was added to each well to promote spontaneous differentiation. On day 5 EBs were collected for analysis using wide-bore pipet tips as not to damage the EBs. For prolonged culture, day 5 EBs were transferred to Pluronic™ F-127-rinsed 6-well dishes (Cat # 140675, ThermoFisher) containing 3 mL Essential 6. The dishes were shaken up/down & side/side once per day to evenly distribute EBs across the dish and prevent EB merging. Half medium changes (remove 1.5 mL spent medium and add 1.5 mL fresh medium) were performed every other day up to day 10 or 14 when EBs were collected with wide bore tips for analyses.

2.5 Directed Differentiation to the Three Germ Layers

To direct human iPSCs to the three germ layers, we used the STEMdiff™ Trilineage Differentiation Kit (Cat#05320, STEMCELL) according to the

manufacturer's instructions (Document # 10000003454 Version 01) with slight modifications. Before use in the Trilineage Differentiation Kit, iPSCs were switched from Essential 8 medium to mTeSR Plus (Cat# 100-0276, STEMCELL). iPSCs were maintained in mTeSR Plus medium for approximately 1 week wherein iPSCs were fed daily and passaged as small aggregates as needed. When iPSC colonies in mTeSR Plus exhibited signs of confluence (circular, white smattering at colony centers, tight cell packing) the cells were singularized using Accutase as described previously and plated onto Geltrex-coated cultureware containing mTeSR Plus with 10 μ M Y-27632. Human iPSCs for mesoderm differentiation were plated at a density of 50,000 viable cells/cm² whereas iPSCs for ectoderm and definitive endoderm differentiation were plated at 200,000 viable cells/cm². Twenty-four hours after plating (on protocol day 1), the spent medium was removed and replaced with either ectoderm, endoderm, or mesoderm medium. Germ lineage medium was refreshed daily until the mesoderm and endoderm endpoints on day 5 or the ectoderm endpoint on day 7. Resulting germ layers were collected for analysis at their specified culture endpoints.

2.6 Cerebral Organoid Culture

Cerebral organoids were generated using the STEMdiff™ Cerebral Organoid Kit (Cat# 08570 & 08571, STEMCELL Technologies) according to the manufacturer's instructions but with slight modification to the neuroepithelial expansion steps (see Section 2.6.3). Cerebral organoid development was

initiated in several discrete steps: EB formation (Section 2.6.1), neuroectoderm induction (Section 2.6.2), neuroepithelial expansion (Section 2.6.3) and cerebral organoid maturation (Section 2.6.4).

2.6.1 Embryoid Body formation

On day 0, single cells were re-suspended in EB Formation Medium supplemented with 10 μ M Y-27632 and the resulting EBs were formed in 1% agarose-coated or 5% Pluronic™ F-127-rinsed 96-well round-bottom plates as described in Section 2.4. On days 2 and 4, each EB was fed with 100 μ L of EB Formation Medium without Y-27632.

2.6.2 Neuroectoderm Induction

On day 5, the resulting EBs were transferred with wide-bore pipet tips to new Pluronic™ F-127-rinsed cultureware (Cat# 353078, Corning) containing Neural Induction Medium.

2.6.3 Neuroepithelial expansion

On day 7 the organoids were removed from their cultureware and subjected to high throughput Geltrex embedding in Expansion Medium (personal correspondence that will appear in Chew et al., 2021 (92)). Briefly, ice cold liquid Geltrex was added at 1:50 dilution to ice-cold Expansion Medium. Up to 32 organoids were quickly transferred into the cold Expansion Medium with Geltrex and re-plated into one well of a fresh Pluronic™ F-127-coated 6-well dish (Cat#

140685, ThermoFisher). The plate was shaken (side-to-side and up/down) once daily to prevent organoids from merging.

2.6.4 Cerebral Organoid Maturation

On day 10, each cerebral organoid was transferred with a wide bore pipet into its own well of a Pluronic™ F-127-rinsed culture dish (Cat# 353047, Corning) containing Maturation Medium. The culture dish was placed on an orbital shaker set to 80 revolutions per minute with an approximate relative centrifugal force of 0.20194 x gravity. After day 10, half media feeds with Maturation Medium were performed every 4-5 days until the end of the assay – up to 120 days.

2.6.5 Pharmacological inhibition of PANX1 in Cerebral Organoids

We used probenecid (PBN; Cat# 2006, AAT Bioquest, Sunnyvale, CA, USA) at a concentration of 1 mM in organoid culture media from day 5 until the assay endpoint at day 40 to block PANX1 channel function (16, 93).

2.7 Human iPSC Monolayer Differentiation to Neural Progenitor Cells and Neurons

2.7.1 iPSC Differentiation into Neural Progenitor Cells

Human iPSCs were differentiated into neural progenitor cells (NPCs) using Gibco™ PSC Neural Induction Medium (Cat A1647801, ThermoFisher) according to the manufacturer's instructions and the protocol outlined by Yan and colleagues (94) with several modifications. Briefly, human iPSCs singularized with Accutase were seeded at 200,000 cells/cm² onto Geltrex-coated dishes

containing PSC Neural Induction Media: Neurobasal Media (Cat# 21103049, ThermoFisher), 1X Neural Induction supplement (Cat# A16477-01, ThermoFisher) and 10 μ M Y-27632. Complete medium changes were performed daily until the first passage (day 7) using PSC Neural Induction Medium without Y-27632. At passage 1, 200,000 cells/cm² were seeded onto fresh Geltrex-coated wells containing Neural Stem Cell (NSC) Expansion Medium: 49% Neurobasal, 49% Advanced DMEM/F12 media (Cat# 12634010, ThermoFisher), 1X Neural Induction Supplement and 10 μ M Y-27632. Cells were fed daily with NSC Expansion Medium without Y-27632 and seeded into new Geltrex-coated wells every 7 days until 21 cumulative days in culture. After 21 cumulative days in culture the resultant NPCs were cryopreserved, assessed for NPC marker expression, or differentiated to neurons as per Section 2.7.2.

2.7.2 NPC Differentiation into Neurons

NPCs were differentiated to neurons using a monolayer method according to the procedure described by Yan and colleagues (94). NPCs were passaged as single cells and seeded at a density of 50,000 cells/cm² onto culture dishes coated with 10 μ g/mL laminin (Cat# 354232, Corning) containing Neuron Differentiation Medium (see Table 2.1) supplemented with 10 μ M Y-27632. Half medium changes with Neuron Differentiation Medium were performed every other day for 14 days. Resultant neurons were evaluated by qPCR, Western blot, and immunofluorescence imaging.

Table 2.1 Components of Neuron Differentiation Medium

Reagent	Vendor	Catalog	Final Concentration
Neurobasal™ Medium	ThermoFisher	21103049	~96% v/v
B-27™ (50X)	ThermoFisher,	17504044	1X (2% v/v)
GlutaMAX™ (200 mM Stock)	ThermoFisher,	35050061	2 mM (1% v/v)
MEM NEAA (Non-Essential Amino Acids) 100X	WISENT Inc	321-011-EL	1X (1% v/v)
BDNF (brain-derived neurotropic factor)	STEMCELL Technologies	78005	20 ng/mL
GDNF (glial cell-derived neurotropic factor)	STEMCELL Technologies	78058	20 ng/mL
L(+)-ascorbic acid	VWR, Radnor, PA, USA	97061-072	200 µM

2.8 Gene expression analysis with quantitative reverse transcription polymerase chain reaction (qPCR)

Undifferentiated human iPSCs, differentiated cells, and organoids were collected for RNA extraction and qPCR gene expression analysis. RNA was extracted using the PureLink™ RNA isolation kit (Cat # 12183018A, ThermoFisher) according to the manufacturers' instructions. Briefly, cells were washed 1X with Ca²⁺/Mg²⁺-free PBS and ruptured using freshly prepared lysis buffer supplemented with 1% (v/v) 2-mercaptoethanol (Cat# AAJ6674230, FisherScientific, Waltham, MA, USA). Cell lysates were homogenized using spin column shredders (Cat# 79654, Qiagen, Hilden, DEU) and homogenized RNA was purified via RNA binding columns while genomic DNA was removed via on-column DNase digestion (Cat# 12185010, ThermoFisher) according to manufacturers' protocols. Purified RNA was quantified using a NanoDrop™ 2000

spectrophotometer (Cat# ND-2000, ThermoFisher), and stored at -80°C until use. High quality RNA was identified by a $\lambda_{260/280}$ of ≥ 2.0 and $\lambda_{260/230}$ of ≥ 2.0 .

RNA was converted into complementary DNA (cDNA) using the High-Capacity cDNA Reverse Transcription Kit (Cat# 4368814, ThermoFisher) according to the manufacturer's instructions in a Bio-Rad T100™ Thermal Cycler (Cat# 1861096, Bio-Rad). Typically, 500 ng of RNA were used per cDNA reaction. Reverse transcription cycle conditions were as follows: 25°C for 1 minute, 37°C for 2 hours, 85°C for 5 minutes, 4°C hold. The resulting cDNA was stored at -30°C until use.

Quantitative RT-PCR (qPCR) was performed using intercalating dye chemistry (95). Oligonucleotide sets were designed for specific target amplification and minimal primer dimer formation using NCBI Primer-BLAST (NIH, Bethesda, MD, USA; <https://www.ncbi.nlm.nih.gov/tools/primer-blast/>) and IDT's Oligo Analyzer Tool (IDT, Newark, NJ, USA). For some targets, we purchased pre-designed oligonucleotide sets from IDT as indicated in Table 2.2. We used Bio-Rad SsoAdvanced™ Universal SYBR® Green Supermix (Cat# 1725274, Bio-Rad) and 10 μ M of each oligonucleotide for qPCR reactions. Reactions were performed in triplicate or duplicate in 0.1 mL, sub-semi skirted low profile 96-well plates (Cat# LP-96, FroggaBio, Toronto, ON, CAN) as 10 μ L reactions. The plate was sealed using Bio-Rad microseal 'B' seal film (Cat# MSB1001, Bio-Rad) and centrifuged for 2 minutes at 800 x gravity to eliminate air bubbles in wells. qPCR was performed on Vii7 Real Time PCR System (Cat#

4453545, ThermoFisher) with a 96-well block attachment. Standard run time cycling parameters were as follows: one cycle of 50°C for 2 minutes, one cycle of 95°C for 30 seconds, 40 cycles of 95°C for 10 seconds, 60°C for 1 minute, followed by a melt curve from 60°C to 95°C.

Table 2.2 Oligo Sets for qPCR

Target	Forward Primer (5'-3')	Reverse Primer (5'-3')	Amplicon Size (bp)
CXCR4	AGG GGA TCA GTA TAT ACA CTT CAG	AGA AGG GAA GCG TGA TGA CA	276
FOXA2	Hs.PT.58.22972176		
GAPDH	TGC TTT TAA CTC TGG TAAA G	CAC TTG ATT TTG GAG GGA TC	198
GFAP	CTG CTC AAT GTC AAG CTG G	AAT GGT GAT CCG GTT CTC C	84
GJA1	GGT CTG AGT GCC TGA ACT TGC CT	AGC CAC ACC TTC CCT CCA GCA	184
HNF1B	AGC CAG TCG GTT TTA CAG CA	CTT GGG AGG TGT TGA GGC TT	229
KDR	GTA CAT AGT TGT CGT TGT AGG	TCA ATC CCC ACA TTT AGT TC	132
MAP2	GGA GAC AGA GAT GAG AAT TCC T	GAA TTG GCT CTG ACC TGG T	82
MIXL1	GCT TTC AGT TAC CCT CCC AGA TAA C	GCA CAG GAA GTA CAA TAA CAA GTG C	270
NANOG	TGC TGA GAT GCC TCA CAC GGA	TGA CCG GGA CCT TGT CTT CCT T	155
NCAM1	GCC TGA AGC CCG AAA CAA C	CAC TGG GTT CCC CTT GGA	117
NES	CTG CGG GCT ACT GAA AAG TT	TCC AGG AGG GTC CTG TAC G	161
PANX1	GGC AAA GGG AAA GCG AAA G	CCA GGA GAA AGA ACT TGG AGA G	337
PANX2	CTA CAT CCT CGG CAC CAA GA	GGG TAC GGG ATT TCC TTC TC	168
PANX3	Hs.PT.58.4636086		
PAX6	CAG CTC GGT GGT GTC TTT G	CCG TTG GAC ACG TTT TGA TTG	167
PDGFRA	CTG CTG ATG AAA GCA CAC GG	AAC TCC ATT CCT CGG GCA AC	289
POU5F1	TGG GCT CGA GAA GGA TGT G	GCA TAG TCG CTG CTT GAT CG	78
SOX17	GAG CCA AGG GCG AGT CCC GTA	CCT TCC ACG ACT TGC CCA GCA T	141
T	Hs.PT.58.1243965		
WT1	GTA GCC CCG ACT CTT GTA CG	AGT CCT GGT GTG GGT CTT CA	297

Data were analyzed using QuantStudio™ real-time PCR software (Version 1.3, ThermoFisher). Gene expression for each sample were normalized to the reference gene (*GAPDH*) which was stably expressed across all tissues and cell lines used in this study (refer to Figure 6.1) to generate a deltaC_T (ΔC_T) (96). Samples where C_T values were \geq the C_T value of the no-template control were considered qPCR non-detects and were excluded from further analysis.

Heatmaps were generated from the average $2^{-\Delta C_T}$ value from each condition using R Studio (version 3.6.1) software with the ggplots.2 package and row clustering. Refer to Section 6.2 for the heatmap code.

Fold change expression of genes relative to a control sample (such as control (wildtype) human iPSC cell population) were evaluated using the $\Delta\Delta C_T$ method as described in Schmittgen and Livak, 2008 (96). Fold change results from the average of 2-3 technical replicates were plotted in GraphPad PRISM (Version 6.07, GraphPad, San Diego, CA, USA).

2.9 Immunofluorescence (IF)

2.9.1 Setup of Monolayer Cultures for IF

For immunofluorescence imaging, monolayer cell cultures (like human iPSCs, neurons, and neural progenitors) were cultured on glass coverslips coated with hESC-qualified matrix, LDEV (lactate dehydrogenase elevating virus)-free Matrigel® (Cat# 354277, Corning) that was thawed overnight on ice and diluted 1:125 (as per the specific lot number) in ice-cold DMEM. A single

autoclaved circular glass coverslip (Cat# 12CIR1602811G, FisherScientific) was aseptically placed into a well of a 24-well plate (Cat #353047, Corning) and 0.25 mL of prepared Matrigel® coating solution was added. The cultureware was incubated at room temperature for 30 minutes followed by aspiration of coating liquid and replacement with cell culture medium. Cells were seeded into the prepared wells and cultured to their respective end points as per Sections 2.3, 2.5, and 2.7.

2.9.2 Monolayer Culture Fixation

Cells grown as monolayers on coverslips were prepared for immunofluorescence microscopy by removing the spent culture media and washing once with $\text{Ca}^{2+}/\text{Mg}^{2+}$ -free PBS. Cultures were fixed with a 10% solution of normal buffered formalin (Cat# CA71007-344, VWR) at room temperature for 10 minutes. Formalin was removed and the wells were washed 1X with $\text{Ca}^{2+}/\text{Mg}^{2+}$ -free PBS prior to immunostaining according to Section 2.9.3.

2.9.3 Immunofluorescence Staining of Monolayer Cultures

Fixed cells on coverslips were permeabilized in $\text{Ca}^{2+}/\text{Mg}^{2+}$ -free PBS supplemented with 0.1% (v/v) TWEEN® 20 (Cat# BP337-500, FisherScientific) hereto referred as PBS-T for 20 minutes followed by 10 minutes in $\text{Ca}^{2+}/\text{Mg}^{2+}$ -free PBS supplemented with 0.1% (v/v) Triton X-100 (Cat# T5832, MilliporeSigma). Primary antibodies were prepared in PBS-T with 3% (w/v) bovine serum albumin (BSA; Cat# 800-095-EL, WISENT Inc) + 0.1% (w/v) NaN_3 and primary staining was performed overnight at 4°C. Primary antibodies (refer to Table 2.3 below)

were washed thrice with PBS-T for 10 minutes each. Secondary antibodies and dyes (refer to Table 2.4 below) were prepared in PBS-T and incubated on samples for 2 hours at room temperature in the dark. Secondary antibodies were washed thrice for 30 minutes each with PBS-T. Coverslips were mounted onto glass microscopy slides (Cat# 3800285, Leica, Wetzlar, DEU) using Mowial®488 reagent with 1,4-diazabicyclo[2.2.2]octane (DABCO) antifade compound prepared according to methods described by Cold Spring Harbor (97) and the formulation detailed in

Table 2.5. Slides were dried at 4°C for >12 hours before imaging with confocal microscopy (see Section 2.10.2).

Table 2.3 Primary Antibodies for Flow Cytometry, Immunofluorescence (IF), and Western Blots

Marker	Supplier	Catalog #	Host Species	Flow Cytometry Dilution	IF Dilution	Western Blot Dilution
β -III Tubulin (TUJ1)	R&D Systems, Minneapolis, MN, USA	MAB1195	mouse	-	1:200	-
β -catenin	Santa Cruz Biotechnology, Dallas, TX, USA	Sc-7963	mouse	-	1:500	-
Caspase3 (active)	BD Biosciences, San Jose, CA, USA	559565	rabbit	1:5000	-	-
GAPDH	MilliporeSigma	MAB374	mouse	-	-	1:5000
GFAP	Cell Signaling Technology (Danvers, MA, USA)	3670	mouse	-	1:300	-
Ki67	Abcam	ab16667	rabbit	1:1000	1:250	-
N-cadherin	BD Biosciences	610920	mouse	-	1:500	-
Nestin	ThermoFisher	14-9843-82	mouse	-	1:500	-
OCT4-BV421	BioLegend	653712	mouse	1:50	1:40	-
PANX1	Dr. Dale Laird (64)	N/A	rabbit	1:400	1:500	1:2000
PAX6-PerCPCy5.5	BD Biosciences	562388	mouse	1:200	1:100	-
SOX17	R&D Systems	AF1924	goat	-	1:1000	-
SOX17-APC	R&D Systems	IC1924A	goat	1:200	-	-
SOX2	R&D Systems	AF2018	goat	-	1:200	-
T	Abcam	ab209665	rabbit	1:400	1:1000	-
T-AF488	R&D Systems	IC2085G	goat	1:50	-	-
ZO-1	ThermoFisher	33-910	Mouse	-	1:500	-

Table 2.4 Secondary Antibodies and Dyes for Flow Cytometry, IF, and Western Blot

Marker	Supplier	Catalog #	Fluor	Host	Flow Cytometry Dilution	IF Dilution	Western Blot Dilution
Donkey-anti-goat	ThermoFisher	A32849	Alexa Fluor® 647	Donkey IgG	-	1:1000	-
donkey-anti-mouse	ThermoFisher	A31570	Alexa Fluor® 555	Donkey IgG	1:3000	1:1000	-
Donkey-anti-Rabbit	ThermoFisher	A21206	Alexa Fluor® 488	Donkey IgG	1:3000	1:1000	-
donkey-anti-rabbit	ThermoFisher	A31572	Alexa Fluor® 555	Donkey IgG	1:3000	1:1000	-
Donkey-anti-rabbit	ThermoFisher	A31573	Alexa Fluor® 647	Donkey IgG	1:3000	1:1000	-
Goat-anti-Mouse	ThermoFisher	31430	horseradish peroxidase	Goat IgG	-	-	1:5000
Goat-anti-Mouse	ThermoFisher	A32728	Alexa Fluor® 647	Goat IgG	-	1:1000	-
Goat-anti-Rabbit	ThermoFisher	31460	horseradish peroxidase	Goat IgG	-	-	1:5000
Goat-anti-Rabbit	ThermoFisher	A21206	Alexa Fluor® 488	Goat IgG	-	1:1000	-
Hoechst 33342	FisherScientific	H3570	Hoechst	Dye	-	1:1000	-
Phalloidin	ThermoFisher	A34055	Alexa Fluor® 555	Dye	-	1:500	-
TO-PRO-3 Iodide (642/661)	ThermoFisher	T3605	TO-PRO-3 Iodide (642/661)	Dye	-	1:1000	-
Zombie-NIR™	BioLegend, San Diego, CA, USA	423105	Zombie-NIR™	Dye	1:2000	-	-

Table 2.5 Composition of Mowial®488-DABCO Mounting Medium

Reagent	Vendor	Catalog	CAS	Quantity or Final Concentration
Mowial®488	MilliporeSigma	81381	9002-89-5	2.4 g ~10.5% w/v
DABCO	TCI America, Portland, OR, USA	D013425G	280-57-9	0.568 g ~2.5% w/v
Glycerol	FisherScientific	G33-4	56-81-5	6 g (4.758 mL) ~20.9% v/v
0.2M Tris-HCl (pH 8.5)	FisherScientific	BP153	1185-53-1	12 mL ~52.7% v/v
diH ₂ O	n/a	n/a	n/a	6 mL ~26.4% v/v

2.9.4 Embryoid Body and Cerebral Organoid Fixation

Three-dimensional samples such as EBs and cerebral organoids were washed once with $\text{Ca}^{2+}/\text{Mg}^{2+}$ -free PBS and fixed in 10% buffered formalin (Cat# CA71007-344, VWR). Day 5 EBs and small organoids (day 15 and younger) were fixed for 1 hour at room temperature whereas larger organoids (day 16 or older) were fixed overnight at 4°C. Fixed EBs and organoids were stored at 4°C in $\text{Ca}^{2+}/\text{Mg}^{2+}$ -free PBS + 0.1% (w/v) NaN_3 until use in whole-mount immunofluorescence (refer to Section 2.9.3) or cryogenic tissue processing (refer to Section 2.9.6).

2.9.5 Whole-Mount Immunostaining of Embryoid Bodies and Cerebral Organoids

For whole-mount imaging, fixed EBs and small organoids (day 15 and younger) were permeabilized and stained according to the methodology described previously in Section 2.9.3. Stained organoids or EBs in PBS-T were transferred to an 8-well μ -slide high-end microscopy chamber slide (Cat# 80826, ibidi, Martinsried, DEU) and immunofluorescence photos were taken (refer to confocal microscopy in Section 2.10.2).

2.9.6 Cryogenic Tissue Processing and Immunofluorescent Labeling

Fixed EBs and cerebral organoids (day 15+) were cryogenically prepared and immunolabelled according to the methodology described in STEMCELL Technologies' Document #27171, Version 1.0.0, Nov 2019. In summary, EBs and organoids were first dehydrated in $\text{Ca}^{2+}/\text{Mg}^{2+}$ -free PBS supplemented with 30%

(w/v) sucrose (Cat# 800-081-CG, WISENT Inc) for 1-4 days at 4°C until they sank. Dehydrated EBs and organoids were then incubated for 1 hour at 37°C in gelatin embedding solution consisting of 10% (w/v) sucrose and 7.5% (w/v) gelatin (Cat# G1890, MilliporeSigma) prepared in Ca²⁺/Mg²⁺-free PBS. The organoids and EBs in gelatin solution were then transferred to cryopreservation moulds and snap frozen in a slurry of dry ice and isopentane (Cat# M0167, TCI America). For each condition, a minimum of 2 organoids or 2 EBs were embedded together in a block and blocks were stored at -80°C until cryosectioning. Cryosectioning was performed at -26°C on a Microm HM 520 cryostat (Cat# 8243-30-1015, GMI, MN, USA). Slice thickness was set to 14 µm and the slices were affixed to positively charged glass Fisherbrand™ Superfrost™ microscope slides (Cat# ER4951PLUS, FisherScientific). Slides with cryosections were stored at -30°C until antigen retrieval and immunostaining. Antigen retrieval and gelatin clearance prior to immunolabelling was performed according to STEMCELL Technologies' Document #27171, Version 1.0.0, Nov 2019. In brief, slides were placed into a plastic container with citrate buffer, pH 6.0: 0.294% (w/v) Tri-sodium citrate (dihydrate) (Cat# A12274, Alfa Aesar, Tewksbury, MA, USA) with 0.05% (v/v) Tween®20. Samples were heated in a rice steamer (Cat# 37530, Hamilton Beach, Glen Allen, VA, USA) for 20 minutes. After retrieval, slides were washed 2X in Ca²⁺/Mg²⁺-free PBS-T followed by 1X in Ca²⁺/Mg²⁺-free PBS supplemented with 0.1% (v/v) Triton X-100. Each wash was performed at room temperature for 10 minutes with gentle mixing on an orbital shaker. Slides were removed from the wash and permitted to air dry for 5 minutes

at room temperature. Once dry, a DAKO hydrophobic pen (Cat# S2002, Agilent, Santa Clara, CA, USA) was used to create barriers around the tissue slices. Immunostaining with antibodies and dyes was performed as described above (refer to methodology in Section 2.9.3, Table 2.3, and Table 2.4). Slides were mounted using Mowial®488 reagent with 1,4-diazabicyclo[2.2.2]octane (DABCO) (as per Table 2.5) and cover slipped (Cat# 12-544G, FisherScientific).

2.10 Imaging

2.10.1 Phase Contrast

Phase contrast images of monolayer cells, EBs, and small organoids were taken on a Zeiss AxioObserver microscope using 5X/0.12 NA A-Plan, 10X/0.25 NA Ph1, and 20X/0.4 NA Korr objectives (Zeiss) whereas large organoids (day 40+) were imaged using a Zeiss Stemi-2000-C stereo microscope. Images from these microscopes were taken in 8-bit greyscale using an AxioCam MRm camera and AxioVision Version 4.8.2 software. All phase contrast imaging equipment is from Carl Zeiss Microscopy (Jena, DEU).

2.10.2 Confocal Microscopy

Fluorescent confocal images were acquired on a Fluoview FV10i—W3 confocal microscope fitted with a 10X/0.4NA or 60X/1.2NA lens and Fluoview version 2.1.17 software. The following lasers were used to visualize fluorophores: Hoechst/BV421 (405 nm laser); Alexa Fluor 488 (473 nm laser); Alexa Fluor

555/Phalloidin (559 nm laser); Alexa Fluor 647/TO-PRO-3 (635 nm laser). Occasionally, images were acquired using a Fluoview FV1000 confocal microscope fitted with 10X/0.4 NA, 20X/0.75NA, 40X/0.95NA or 60X/1.42NA and the following lasers: 405 nm, 458 nm, 568 nm, 633 nm. All confocal microscopy equipment is from Olympus Microscopy (Tokyo, JPN).

2.10.3 Image Analysis and Colocalization with FIJI

Images were analyzed using FIJI open source software (98). Fluorescent confocal images were occasionally subjected to equivalent brightness/contrast enhancement to facilitate visualization of phenomena.

Area measurements from phase contrast images of EBs and cerebral organoids were performed automatically using the batch macro code listed in Section 6.3. Area measurements from images that contained debris (fibers and unincorporated cells) were performed manually by tracing around the object's periphery and excluding debris protuberances.

We used Manders' colocalization coefficients to describe the fraction of PANX1 colocalizing with a second target and vice versa (66, 99). Manders' colocalization coefficient values range from 0 to 1.0 where values of 0 signify no pixel overlap and values of 1.0 denote identical spatial occupation between two signals (99). We performed colocalization analysis in FIJI using the JACoP plugin with Coste's automatic thresholding (100). We report the standard error of the mean for Manders' colocalization coefficients as indicated in the figure legends.

2.11 Flow Cytometry

Flow cytometry was performed on a CytoFLEX (Beckman Coulter, Brea, CA, USA) flow cytometer. Antibodies were titrated over a range of concentrations prior to use.

Briefly, secondary antibodies (when used) were first evaluated over a range of concentrations in the absence of a primary antibody. The highest possible concentration which did not increase cells' median fluorescence intensity (MFI) relative to that of unstained cells was selected. Next, each primary antibody was tested over a range of concentrations with the pre-determined concentration of secondary antibody. We identified the appropriate primary antibody concentration by calculating the sensitivity index (101) according to the formula below.

$$\text{Sensitivity index} = \frac{(MFI \text{ signal} - MFI \text{ background})}{[(84\text{th percentile } MFI \text{ background} - MFI \text{ background})/0.995]}$$

Similarly, directly conjugated primary antibodies were also titrated prior to use by staining control and negative cells (that should and not express the target, respectively) and calculating the sensitivity index (101). The caspase 3 antibody (Table 2.3) was titrated on a mixture of healthy iPSCs and those treated with 4 μ M camptothecin for 3.25 hours to elicit apoptosis (102).

The following controls were included in all flow cytometry assays: unstained control, secondary antibody-only control, fluorescence-minus-one (FMO) controls, and single-color compensation controls for fluorochromes.

UltraComp compensation beads (Cat# 01-2222-43, ThermoFisher) were used with antibodies raised in mice.

For assessment of intracellular targets by flow cytometry, live single-cell suspensions were portioned into wells of a 96-well round bottom plate at 100,000 – 400,000 cells per test. The plate was centrifuged at 300 x g for 5 minutes to pellet the cells and the excess liquid was decanted. A Zombie-NIR™ fixable viability dye (Cat# 423105, BioLegend®, San Diego, CA, USA) was included in flow cytometry experiments to eliminate dead cells during the analysis stage. Each well was washed with 300 μ L $\text{Ca}^{2+}\text{Mg}^{2+}$ -free PBS and the live cells were stained with Zombie-NIR™ prepared in $\text{Ca}^{2+}\text{Mg}^{2+}$ -free PBS (according to Table 2.4) for 15 minutes at 4°C in the dark. Each well was washed with cytometry buffer ($\text{Ca}^{2+}\text{Mg}^{2+}$ -free PBS with 1% (w/v) BSA or FBS) and the plate was centrifuged and decanted as before. Next, the cells in each well were fixed in 10% buffered formalin for 10 minutes at 4°C in the dark. After fixation, the plate was centrifuged and decanted as before. Cells were then permeabilized with permeabilization buffer ($\text{Ca}^{2+}\text{Mg}^{2+}$ -free PBS with 1% (w/v) BSA or FBS supplemented with 0.1% (v/v) Triton X-100) for 15 minutes at room temperature in the dark. Primary antibodies (used at dilutions according to Table 2.3) were prepared in cytometry buffer and cells were incubated for 30 minutes at 4°C in the dark. After incubation, cells were washed in cytometry buffer to remove unbound primary antibody.

Cells were then stained with secondary antibodies prepared in cytometry buffer. Secondary staining was performed for 30 minutes at 4°C in the dark. After incubation, cells were washed twice with cytometry buffer to remove unbound secondary antibodies. Finally, the cells from each test were resuspended in cytometry buffer and were transferred into 1.7 mL Eppendorf tubes for acquisition on the CytoFLEX cytometer.

Flow cytometric analysis was performed using FlowJo software (Version 10.7.1). Compensation was performed digitally using the software and the resultant compensation matrix was applied to the samples. Compensated samples were then subjected to several cleanup gating steps to exclude cell debris (FSC-SSC), doublets (FSC-A vs FSC-H), and dead cells. Gate placement for fluorochrome channels were determined using fluorescence-minus-one controls (FMOs) (101).

2.12 SDS-PAGE & Western Blot

Cells were washed with cold $\text{Ca}^{2+}/\text{Mg}^{2+}$ -free PBS and lysed using single detergent lysis buffer (consisting of 50mM Tris-HCl pH8, 150 mM NaCl, 0.02% (w/v) NaN_3 , and 1% (v/v) Triton X-100) supplemented with 1 mM NaVO_4 , 10 mM NaF, 2 $\mu\text{g}/\text{mL}$ leupeptin, and 2 $\mu\text{g}/\text{mL}$ aprotinin. Cells were scraped and lysates subjected to centrifugation at 15,000 x gravity for 10 min at 4°C to pellet insoluble material. Soluble protein concentration was determined in duplicate using Pierce BCA assay (Cat# PI23225, ThermoFisher) according to the manufacturer's instructions. Resultant colorimetry was assessed using a VICTOR multilabel plate

reader (Perkin Elmer, model 2030). Protein concentration was determined using a BSA standard curve (0, 0.125, 0.25, 0.5, 1, 2 µg/mL BSA) and extrapolated using the formula $y = mx + b$. Cell lysate protein was diluted in equal volumes to ensure equal loading and were denatured for 20 minutes at room temperature in 4X SDS (sodium dodecyl sulfate) loading buffer containing 2-mercaptoethanol (0.5M Tris HCl, pH 6.8, 8% (w/v) SDS, 0.4% (w/v) bromophenol blue, 40% (v/v) glycerol, 20% (v/v) 2-mercaptoethanol). To prevent aggregation of transmembrane proteins, samples were not heated above room temperature in the loading buffer (103).

Typically, 30 – 40 µg of denatured protein were separated using SDS-PAGE with a 10% resolving gel at 100V in a Mini-PROTEAN® Tetra Cell (Cat# 1658003, Bio-Rad) coupled with the PowerPac™ Basic Power Supply (Cat# 1645050, Bio-Rad) and using 1X PAGE electrophoresis buffer consisting of 25 mM Tris, 190 mM Glycine, and 0.1% (w/v) SDS. The Precision Plus Protein™ All Blue Prestained Protein Standards ladder (Cat# 1610393, Bio-Rad) was used to monitor migration of bands for SDS-PAGE. Proteins in the gel were transferred to a 0.45 µm nitrocellulose membrane (Cat# 1620115, Bio-Rad) using a Mini Trans-Blot® Module (Cat# 1703935, Bio-Rad) filled with cold transfer buffer (25 mM Tris Base, 192 mM Glycine, and 20% methanol) at 100V for 1 hour.

The membrane was stained with primary antibodies prepared in TBS-TWEEN®20 (TBST, consisting of 15.23 mM Tris HCl, 4.62 mM Tris Base, 150 mM NaCl, and 0.1% (v/v) TWEEN®20 adjusted to pH 7.6) + 3% (w/v) skim milk

(Carnation®). Primary antibodies were used at dilutions according to Table 2.3 and incubated with the membrane overnight at 4°C on a rocker. Primary antibody staining solution was removed and the membrane was washed 3X for 10 minutes each with TBST. Secondary antibodies conjugated to HRP were prepared in TBST + 3% (w/v) skim milk according to Table 2.4 and incubated for 1 hour at room temperature. After three, 10-minute washes with TBST, the membrane was developed with Bio-Rad Clarity™ Western ECL Substrate (Cat# 1705061, Bio-Rad) according to manufacturer's instructions and the resulting chemiluminescence was measured using a GE ImageQuant LAS 400 (Cat# 28955810, GE Healthcare) or a Biorad ChemiDoc imaging system (Cat# 17001401).

2.13 Statistics

Statistical analysis was performed in GraphPad PRISM Version 6.07. Error bars depict \pm standard error of the mean (SEM) when $n \geq 2$ biological replicates (independent experiments) unless otherwise stated. Statistical significance for comparisons between 2 groups was determined by unpaired Student's *t*-test. Statistical significance for comparisons between 3 or more groups was determined by 1-way or 2-way Analysis of Variance (ANOVA) followed by Tukey's multiple comparisons test unless otherwise indicated. A *p* value less than 0.05 is considered statistically significant. * $p \leq 0.05$, ** $p \leq 0.01$, *** $p \leq 0.001$, **** $p \leq 0.0001$.

3 Results

3.1 Human iPSCs Express PANX1

Transcripts expression for all three pannexin family members (*PANX1*, *PANX2*, and *PANX3*) have been previously reported in human embryonic and induced pluripotent stem cells (84). In our qPCR analysis, we were able to identify transcripts for *PANX1* and *PANX2* but not *PANX3* (Figure 3.1A). Using immunofluorescence imaging we observed PANX1 staining in OCT4-positive human iPSCs (Figure 3.1B). Although we identified *PANX2* mRNA expression in our iPSCs we could not identify a suitable antibody to detect the protein. As such, we restricted our investigations to PANX1.

3.2 *PANX1* Knockout iPSCs are Morphologically Indistinguishable from Control

To study the role of PANX1 in cellular differentiation we created *PANX1* knockout (*PANX1*^{-/-}) human iPSCs using CRISPR-Cas9 gene editing. The resulting clonal knockout iPSCs have a single base pair deletion in the third *PANX1* exon resulting in a frameshift mutation and numerous early stop codons (Figure 3.1C). The frameshift mutation alters the protein sequence near the end of the second transmembrane domain at amino acid position 126. After genetic ablation, the resulting *PANX1*^{-/-} iPSCs lack expression of the full-length PANX1 protein as assessed through flow cytometry and immunofluorescence imaging (Figure 3.1D-E).

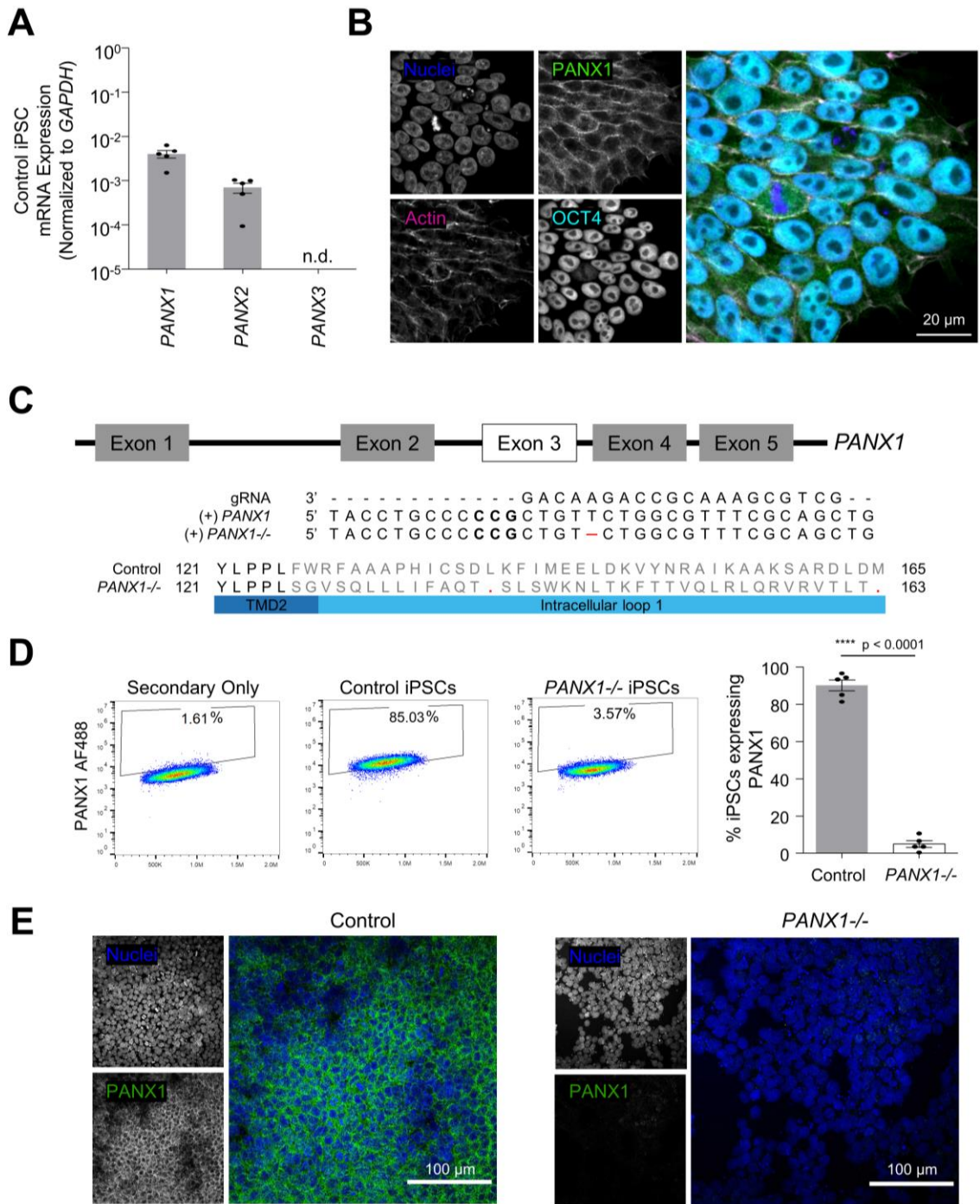


Figure 3.1 PANX1 expression and genetic ablation in iPSCs

(A) Quantitative RT-PCR (qPCR) demonstrates the presence of *PANX1* and *PANX2* transcripts in human iPSCs, but not *PANX3*. n.d. qPCR nondetect. (B) Immunofluorescence imaging reveals PANX1 (green) localization with actin (phalloidin, magenta) in OCT4-positive (cyan) control iPSCs. Nuclei (TO-PRO-3 iodide, blue). (C) CRISPR-Cas9 guide RNA (gRNA) was targeted to the third exon of the *PANX1* gene where CRISPR editing resulted in a single base pair deletion. The deletion alters the reading frame from the second transmembrane domain (TMD2) onward and elicits multiple early stop codons. After genetic ablation, human iPSCs no longer express full-length PANX1 protein as shown through (D) flow cytometry and (E) immunofluorescence. Flow cytometry data represent the standard error of the mean of 4-5 independent experiments. ****, $p \leq 0.0001$ compared to control as assessed through Student's t-test. Immunofluorescence images were acquired using consistent parameters and subjected to equal adjustments for brightness or contrast using FIJI. Scale bars as indicated. Representative fluorescence images shown in Panels B and E.

We then characterized the *PANX1*^{-/-} iPSCs to determine whether they exhibit altered cellular morphology, viability, growth, or pluripotency marker expression relative to control iPSCs. Like their control counterparts, *PANX1*^{-/-} iPSCs grew as compact, circular colonies with smooth borders and individual cells within the colonies had large nuclei with prominent, dark nucleoli (Figure 3.2A). Furthermore, we did not observe any apparent differences in growth kinetics or plating efficiency between the control and knockout iPSCs during routine pluripotent stem cell culture (data not shown). Using qPCR, we confirmed that both control and *PANX1*^{-/-} iPSCs express comparable levels of undifferentiated state genes, *POU5F1* (encodes OCT4) and *NANOG* (Figure 3.2B). We also confirmed that *PANX1*^{-/-} iPSCs do not compensate for the loss of functional PANX1 by upregulating expression of *PANX2*, *PANX3*, or *GJA1* (encoding Connexin43) (Figure 3.2C). To confirm that the *PANX1*^{-/-} iPSCs maintained in stem cell culture conditions retain their stemness and do not differentiate prematurely we quantified the expression of the undifferentiated state marker OCT4 as well as markers representative of the three germ layers (Figure 3.2D). Control and *PANX1*^{-/-} iPSCs both expressed high levels of OCT4 and minimal to no expression of T, (Brachyury, mesoderm marker), PAX6 (ectoderm marker), or SOX17 (endoderm marker). We observed comparable expression of the cell proliferation marker Ki67 in control and *PANX1*^{-/-} iPSCs where both conditions possessed a Ki67-bright population representative of cells in G2 and M phase (104) (Figure 3.2E). Additionally, we observed comparably low expression of the apoptosis marker cleaved caspase 3 (CC3) in control and

PANX1^{-/-} iPSCs (Figure 3.2E). Functionality of the CC3 antibody was verified on iPSCs treated with the apoptosis inducer, camptothecin as described in Section 2.11 (102). Together, our findings indicate that *PANX1* ablation is not detrimental to human iPSC morphology, survival, or pluripotency-associated gene expression.

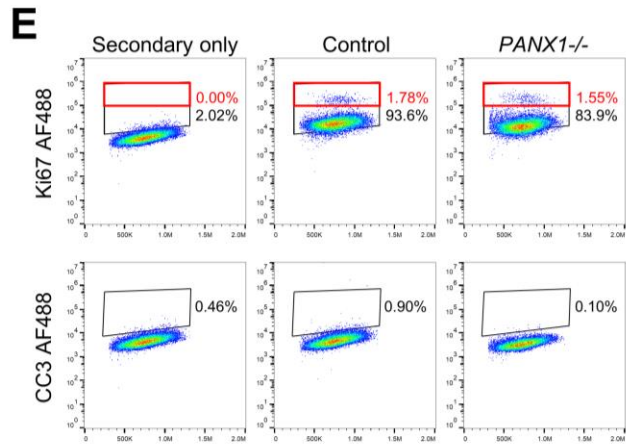
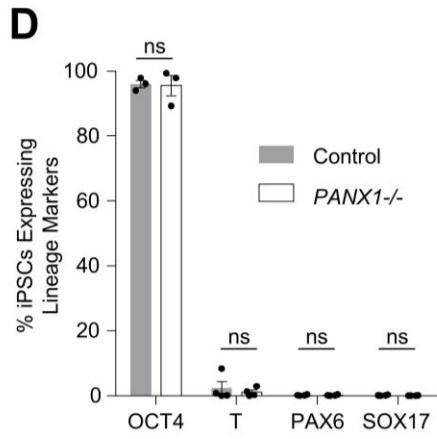
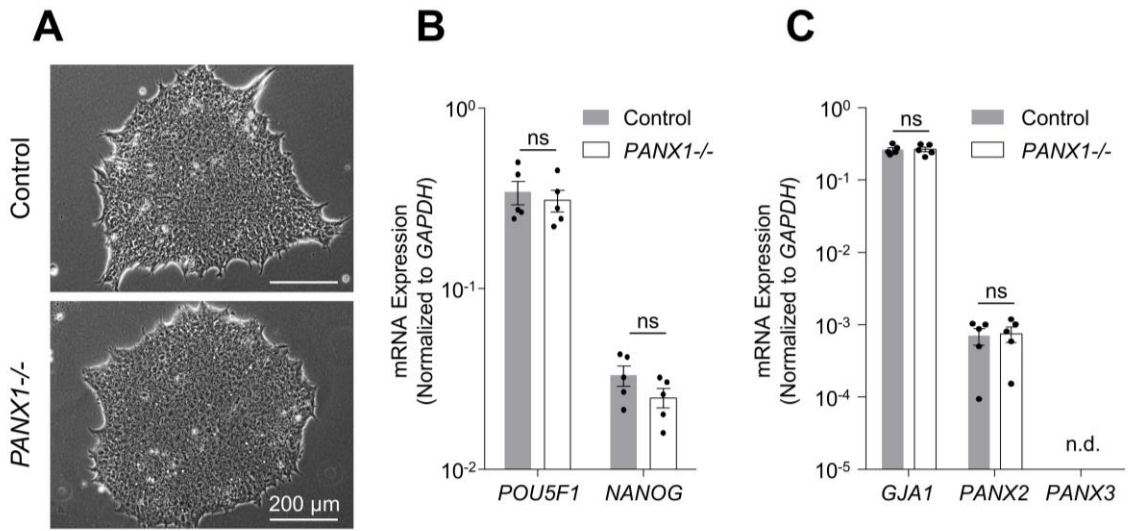


Figure 3.2 *PANX1* knockout iPSCs are morphologically indistinguishable from control iPSCs

(A) Phase contrast micrographs demonstrate that control and *PANX1*^{-/-} iPSCs each grow as large colonies of tightly packed cells with refractive borders and minimal differentiation. Scale bars as indicated. (B) qPCR analysis of key undifferentiated state genes *POU5F1* (encoding for OCT4) and *NANOG* as well as (C) *PANX2*, *PANX3* (qPCR non-detect) or *GJA1* (encoding for Connexin43) expression in control and *PANX1*^{-/-} iPSCs. Data represent the standard error of the mean of 5 independent experiments. n.d. qPCR non-detect. (D) Flow cytometric analysis from 3 independent experiments demonstrates that both control and *PANX1*^{-/-} iPSCs express high levels of the undifferentiated state marker, OCT4 and do not exhibit premature germ lineage commitment to Brachyury-positive mesoderm, PAX6-positive ectoderm, or SOX17-positive endoderm under iPSC maintenance culture in Essential 8 medium. (E) Control and *PANX1*^{-/-} iPSCs express high levels of the proliferation marker, Ki67 including a Ki67-bright population (outlined in red) representative of cells in G2 and M cell cycle phases. Both control and *PANX1*^{-/-} iPSCs possess very low levels of the apoptosis marker, cleaved caspase 3 (CC3) as measured with flow cytometry. Panel E displays results from 1 independent experiment. ns ($p > 0.05$, nonsignificant).

3.3 *PANX1* Knockout Embryoid Bodies Have Skewed Germ Layer Differentiation Potential

Although *PANX1* was not required for iPSC maintenance we wanted to see whether *PANX1*-mediated cell communication influences iPSC differentiation to the three germ layers. The EB model of spontaneous (cell-guided) differentiation generally produces cells from each of the three germ layers and their derivatives independently from exogenous cues. We singularized control and *PANX1*^{-/-} iPSCs and allowed them to form 3-dimensional EBs in culture medium free of exogenous differentiation cues (Figure 3.3A-B). Both control and *PANX1*^{-/-} iPSCs formed EBs within 24 hours and continued to grow thereafter, indicating that *PANX1* does not affect iPSC self-aggregation.

We then used qPCR to assess germ lineage marker expression in control and *PANX1*^{-/-} iPSCs, 5-day-old EBs, and 14-day-old EBs (Figure 3.3C-E). As anticipated, both control and *PANX1*^{-/-} knockout cells in day 5 and 14 EBs reduce expression of undifferentiated state markers *POU5F1* and *NANOG* relative to iPSCs indicating that cells within EBs lose pluripotent stemness and differentiate to downstream cell types. EBs from both conditions increase expression of *PAX6* and *NES* relative to starting iPSCs indicating commitment to the ectoderm germ layer. Strikingly, we observe that *PANX1*^{-/-} EBs, particularly at day 5 have higher transcript expression for mesendoderm (*MIXL1*), mesoderm (*T*, *NCAM1*) and endoderm transcripts (*SOX17*, *HNF1B*) when compared to day 5 control EBs (Figure 3.3C,E). After 14 days of spontaneous differentiation,

PANX1^{-/-} EBs display elevated expression of later-stage mesoderm genes (*WT1*, intermediate mesoderm; *PDGFRA*, paraxial mesoderm) indicative of more robust mesoderm differentiation trajectories than that of control EBs.

In control cells we observe a statistically significant increase in *PANX1* gene expression in EBs relative to the starting iPSCs (Figure 3.3D). *PANX2* expression was not significantly different throughout EB culture and *GJA1* (encoding Connexin43) steadily decreased relative to starting iPSCs for both control and *PANX1*^{-/-} conditions (Figure 3.3D). We did not detect any differences in *PANX2* or *GJA1* expression between control and *PANX1*^{-/-} cells nor did we detect transcripts for *PANX3* in iPSCs or EBs.

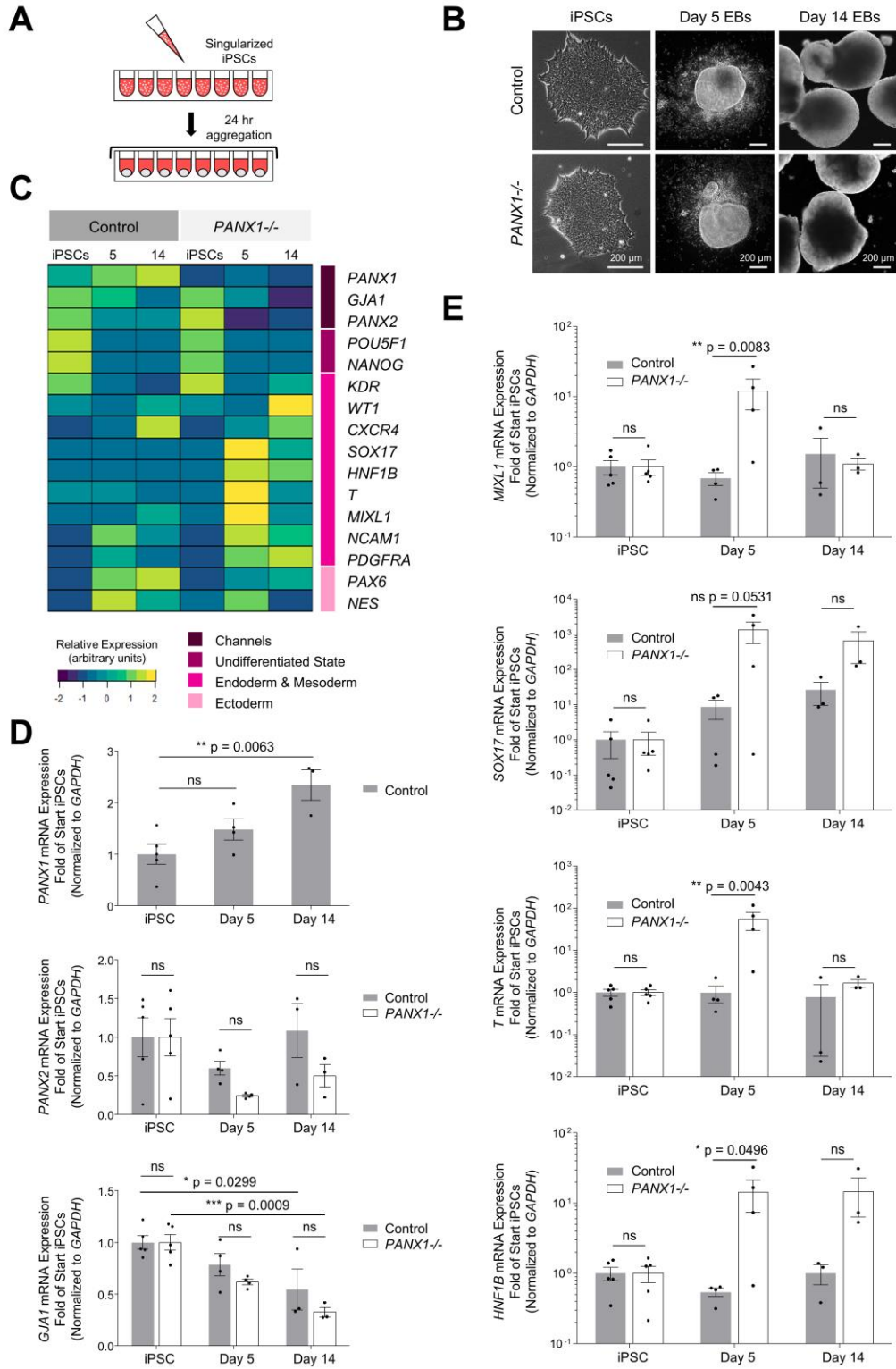


Figure 3.3 *PANX1*^{-/-} embryoid bodies exhibit skewed lineage specification during spontaneous differentiation

(A) Schematic depicting 3-dimensional EB formation. Aggregation of singularized cells into a unified mass occurs within 24 hours. (B) Control and *PANX1*^{-/-} iPSCs self-aggregate and form EBs. Scale bars as indicated. (C) Gene expression analysis of control and *PANX1*^{-/-} iPSCs as well as EBs after 5 and 14 days of spontaneous differentiation. The heatmap was generated using the average $2^{-\Delta CT}$ data value (normalized to *GAPDH*) for each condition using R Studio software with the ggplots.2 package and row clustering. Transcripts for *PANX3* were not detected at any point during differentiation. iPSCs and day 5 EBs n=5; day 14 EBs n=3. (D) qPCR analysis for *PANX1*, *PANX2*, and *GJA1* (Connexin43) channel transcripts in iPSCs and EBs. (E) Gene expression analysis of select mesendoderm, mesoderm, and endoderm gene targets of interest (*MIXL1*, *T*, *SOX17*, and *HNF1B*) expressed in iPSCs and EBs. qPCR bar graphs in **D-E** presented as $2^{-\Delta\Delta CT}$ (fold change of starting iPSCs for each cell line). Data represents the standard error of the mean for 3-5 independent experiments. P-values obtained with 1 or 2-way ANOVA as indicated. ns (p > 0.05, nonsignificant).

To verify our gene expression results we used immunofluorescence microscopy to assess representative markers of the three germ layers (Figure 3.4). Both control and *PANX1*^{-/-} EBs expressed ectoderm markers Nestin and PAX6 at day 5 (Figure 3.4A) and retained PAX6 expression after 14 days of spontaneous differentiation. On the other hand, *PANX1*^{-/-} EBs contained a greater proportion of Brachyury (mesoderm) and SOX17-positive (endoderm) cells relative to control (Figure 3.4B-C). Collectively, our results demonstrate *PANX1*^{-/-} EBs undergoing spontaneous differentiation have a greater propensity to form mesoderm and endoderm germ layers than control EBs.

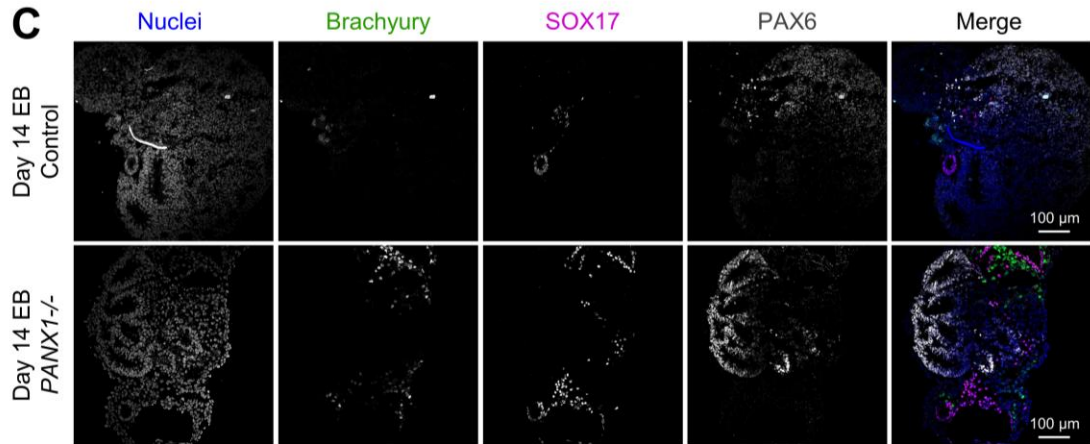
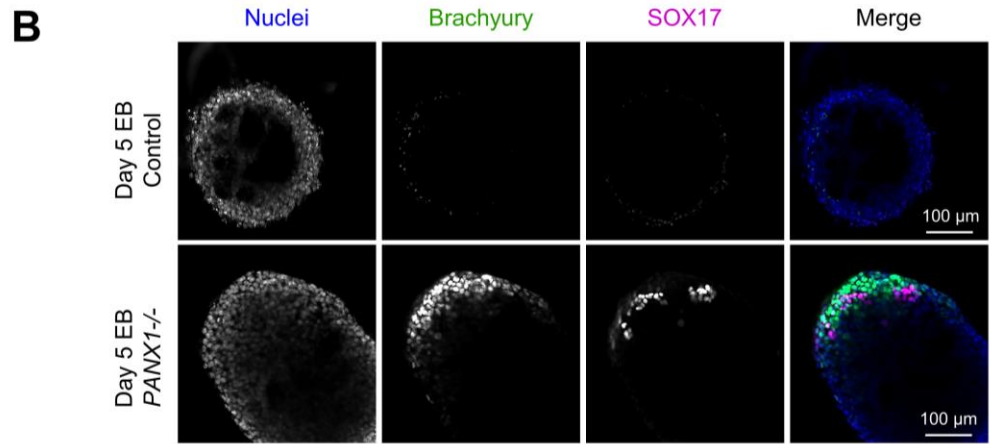
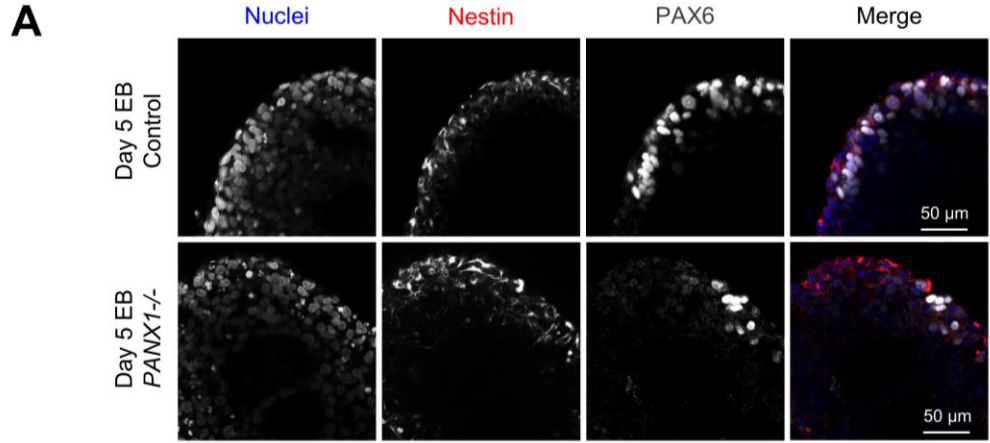


Figure 3.4 Immunofluorescent analysis of *PANX1*^{-/-} embryoid bodies

(A-B) Immunofluorescence of ectoderm (Nestin, red; PAX6, white), mesoderm (Brachyury, green), and endoderm (SOX17, magenta) in control and *PANX1*^{-/-} day 5 EB whole mount preparations. **(C)** After 14 days of spontaneous differentiation, control and *PANX1*^{-/-} EBs were cryosectioned and evaluated for germ lineage marker expression. Equal brightness and contrast enhancements were made in FIJI for picture clarity. Nuclei (Hoechst, blue). Scale bars as indicated. Images are representative of at least two technical replicates from 1 independent experiment.

3.4 Exogenous Pressures Override *PANX1*^{-/-} Germ Lineage Bias

Under spontaneous differentiation conditions we observed a bias toward mesoderm and endoderm in *PANX1*^{-/-} EBs. However, we wanted to see whether this bias is upheld during directed differentiation to the three germ layers under the guidance of exogenously applied signals. To that effect we used the STEMdiff™ Trilineage Differentiation Kit (STEMCELL Technologies) to create 2-dimensional monolayer cultures of ectoderm, definitive endoderm, and mesoderm from control and *PANX1*^{-/-} iPSCs (Figure 3.5). In control cells, *PANX1* mRNA was similarly expressed in each of the germ layers (Figure 3.5A). Additionally, transcripts for *PANX2* and *GJA1* (but not *PANX3*) were comparably expressed in each of the three germ layers produced with control or *PANX1*^{-/-} cells (Figure 3.5B-C). Using qPCR we found no significant difference in germ layer gene expression from control and *PANX1*^{-/-} iPSCs (Figure 3.5D). Finally, flow cytometric analysis revealed efficient differentiation of control and *PANX1*^{-/-} iPSCs to ectoderm (PAX6), definitive endoderm (SOX17), and mesoderm (Brachyury) (Figure 3.5E). Collectively, our data suggest that *PANX1*-mediated cell communication influences germ layer specification but is not required for this process.

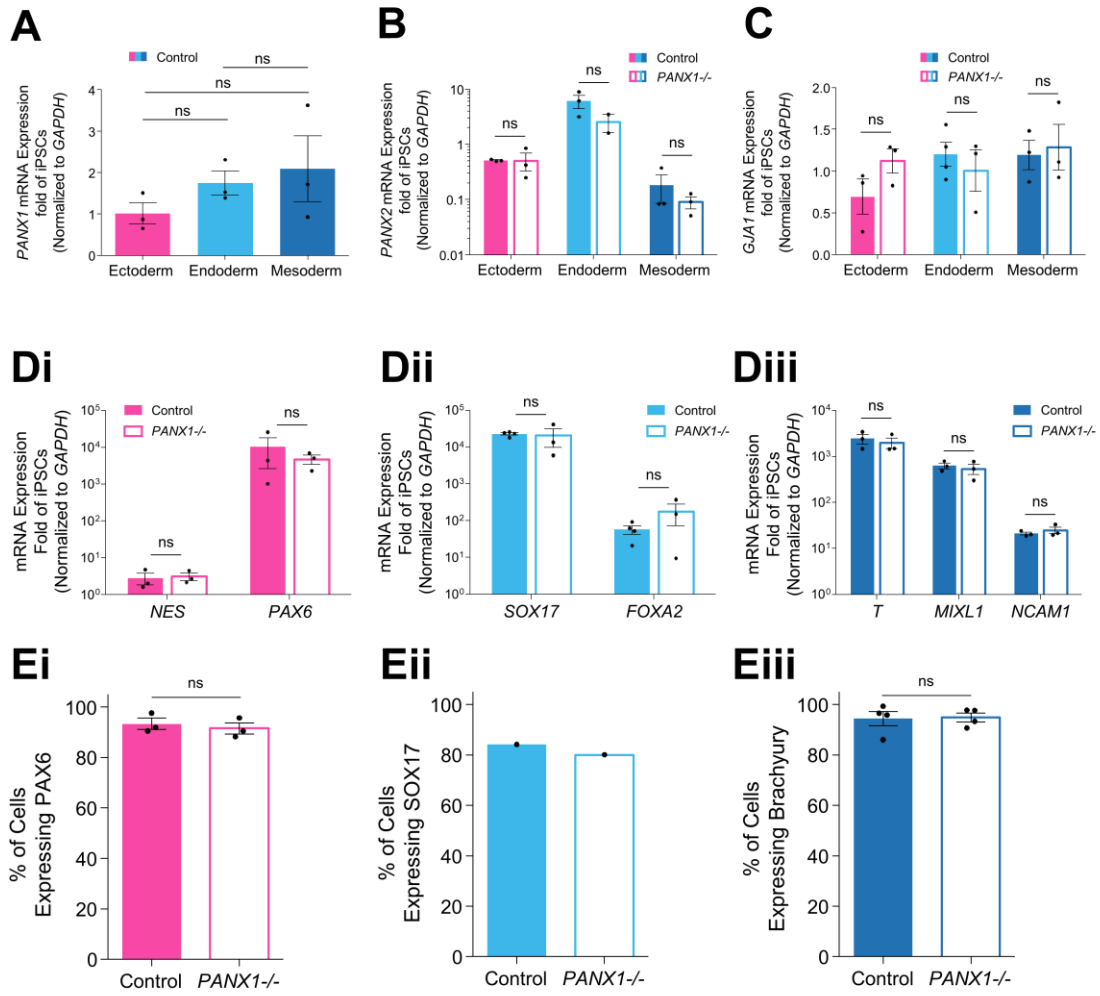


Figure 3.5 Exogenous pressures override *PANX1*^{-/-} lineage bias

Control and *PANX1*^{-/-} iPSCs form ectoderm (i and pink bars), definitive endoderm (ii and light blue bars), and mesoderm (iii and indigo bars) under monolayer directed differentiation with a commercially available kit. **(A-C)** Gene expression analysis of *PANX1*, *PANX2*, and *GJA1* (Connexin43) in control and *PANX1*^{-/-} germ lineages relative to each cell line's corresponding iPSC population. Transcripts for *PANX3* were not detected. **(D)** qPCR assessment of key germ lineage-associated targets for both control and *PANX1*^{-/-} iPSCs differentiated to ectoderm (**Di**), definitive endoderm (**Dii**), and mesoderm (**Diii**) relative to each cell line's corresponding iPSC population. **(E)** Control and *PANX1*^{-/-} cells robustly form PAX6-positive ectoderm (**Ei**), SOX17-positive definitive endoderm (**Eii**), and Brachyury-positive mesoderm (**Eiii**) as measured by flow cytometry. All panels depict the standard error of the mean for 3-4 independent experiments except for panel Eii which displays the average result from 1 independent experiment. ns ($p > 0.05$, nonsignificant).

3.5 PANX1 Expression in Neural Progenitor Cells and Neurons

Since PANX1 channels are implicated in several neurological pathologies and a human germline *PANX1* mutation is associated with sensorineural and learning deficits, we wanted to explore PANX1 expression in neural cell types. We created monolayer cultures of neural progenitor cells (NPCs) and neurons from control iPSCs to assess PANX1 expression (Figure 3.6 and Figure 3.7). qPCR analyses revealed similar *PANX1* transcript expression between control iPSCs, NPCs, and neurons (Figure 3.6A). Transcripts for *PANX2* were significantly reduced in neural progenitor cells relative to iPSCs and transcripts for *PANX3* were not detected (Figure 3.6B).

In contrast to the relatively equal *PANX1* transcript expression across cell types, Western blot analysis showed that NPCs and neurons express significantly more PANX1 protein than iPSCs (Figure 3.6C, D). Indeed, PANX1 was expressed 2.852 ± 0.522 fold more in NPCs compared to iPSCs, while neurons expressed 5.324 ± 0.357 higher levels compared to iPSCs (Figure 3.6C, D). We observed PANX1 migration as several distinct bands on a Western blot, corresponding to the level of putative glycosylation present on the protein (Gly0, Gly1, Gly2) as has been well-described by others (63, 64). In addition to higher overall PANX1 protein expression in NPCs and neurons compared to iPSCs, densitometric analysis shows that these differentiated cell types exhibit significantly elevated Gly2 PANX1 compared to iPSCs (Figure 3.6C-E, Table 3.1).

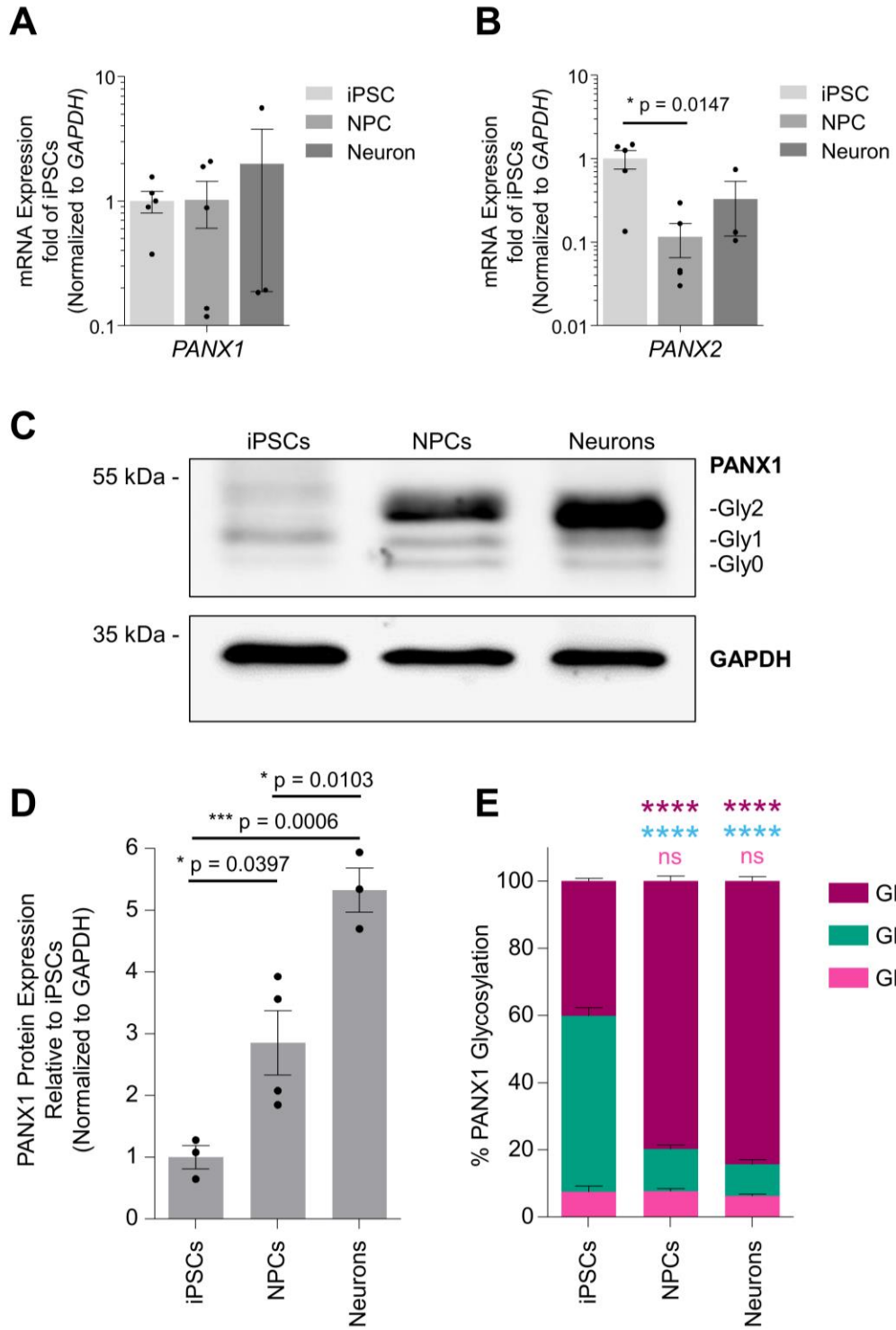


Figure 3.6 PANX1 is expressed in iPSC-derived neural progenitor cells and neurons

(A-B) qPCR analysis of *PANX1* and *PANX2* transcripts in control iPSCs, neural progenitor cells (NPCs), and neurons. Error bars depict standard error of the mean for 3-5 independent experiments. Data for each transcript shown as fold change from control iPSCs. *PANX3* was not detected. (C) Representative Western blot depicting PANX1 protein expression in control iPSCs, NPCs, and neurons. The PANX1 protein manifests as several discrete band sizes corresponding with the putative non-glycosylated protein (Gly0), high mannose (Gly1), and complex carbohydrate addition (Gly2). (D) Western blot quantitation of total PANX1 protein (all putative glycosylation states) in NPCs and neurons relative to iPSCs. (E) Proportion of PANX1 protein existing in each putative glycosylation state for iPSCs, NPCs, and neurons as determined from Western blots. Statistical analysis with 1-way ANOVA. P values as indicated except in panel (E) with comparisons relative to iPSCs where ****, $p \leq 0.0001$ and ns, non-significant. For panels D and E, error bars depict standard error of the mean for 3-4 independent experiments.

Table 3.1 Mean Putative PANX1 Glycosylation Species Frequency

	iPSCs	NPCs	Neurons
Gly2	40.150 ± 0.843 %	79.848 ± 1.551 %	84.370 ± 1.357 %
Gly1	52.390 ± 2.478 %	12.540 ± 1.219 %	9.447 ± 1.372 %
Gly0	7.460 ± 1.705 %	7.615 ± 0.855 %	6.183 ± 0.682 %
n	3	4	3

Because the PANX1 Gly2 isoform is associated with plasma membrane trafficking, we sought to uncover whether PANX1 does indeed localize to the cell surface in neural precursor cells and neurons. Immunofluorescence microscopy confirmed the presence of PANX1 in SOX2-positive NPCs and TUJ1-positive neurons where PANX1 colocalizes with actin (Figure 3.7A-B). Importantly, filamentous actin is a known interacting partner of PANX1, which can help anchor PANX1 to the plasma membrane. We measured the extent of colocalization between PANX1 and actin using Manders' correlation coefficients, where a perfect correlation is denoted by 1.0 and no correlation by 0.0. In NPCs, average colocalization for PANX1 with actin was 0.6988 ± 0.0122 (Figure 3.7C) while in neurons the average colocalization of PANX1 with actin was 0.7068 ± 0.0290 (Figure 3.7D) as calculated with Manders' correlation coefficient.

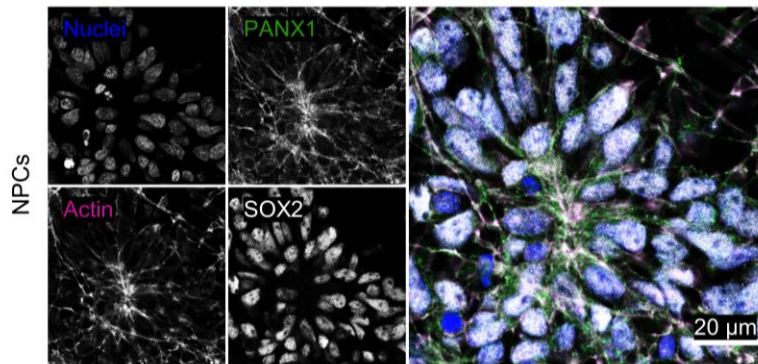
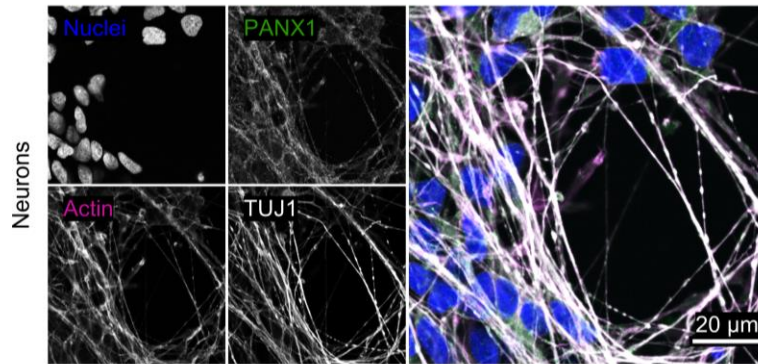
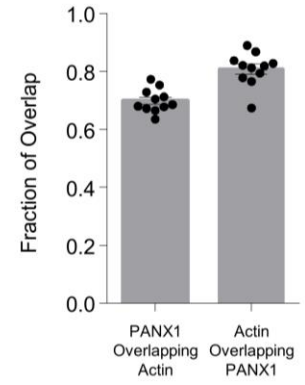
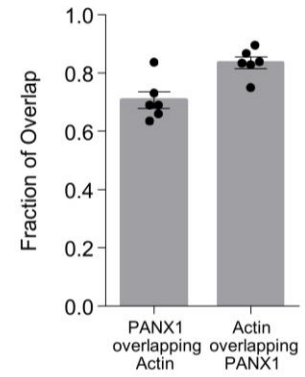
A**B****C****D**

Figure 3.7 PANX1 immunofluorescence in monolayer neural progenitor cells and neurons

Representative immunofluorescence micrographs of PANX1 (green) staining in SOX2-positive (white) neural progenitor cells (**A**) and in beta-III tubulin-positive (TUJ1, white) neurons (**B**). Fraction of overlap between PANX1 and actin filaments (phalloidin, magenta) in NPCs and neurons as assessed with Manders' correlation coefficient (**C-D**). Nuclei (Hoechst, blue). Scale bars as indicated. Error bars depict the standard error of the mean for analysis of 11 images from 2 independent experiments (A,C) or from 6 images from 1 experiment (B,D).

3.6 Human Cerebral Organoids Express PANX1

After we identified abundant PANX1 expression in monolayer NPCs and neurons we wanted to perform a comprehensive evaluation of PANX1 expression throughout early stages of human cerebral organoid development. We used the STEMdiff™ Cerebral Organoid Kit (STEMCELL Technologies) to create organoids that partially model the cellular organization and composition of the developing human cerebral cortex. Human cerebral organoids are created by first aggregating iPSCs into a spherical EB. The cells within the EB adopt a neural fate and the immature organoid produces neuroepithelia resembling bud-like structures. The developing cerebral organoid is then permitted to mature into a large structure containing a variety of neural cell types (Figure 3.8A). Control human iPSCs readily formed large 3D cerebral organoids which we cultured for up to 120 days.

We used whole mount immunofluorescence confocal microscopy to assess immature cerebral organoids for PANX1 expression at the end of the EB, neural induction, and neuroepithelial expansion stages (Figure 3.8B-D). After five days in culture and at the end of EB stage, organoids consisted of a dense cellular mass exhibiting some SOX2 and Nestin-positive regions. PANX1 was widely expressed throughout this day 5 organoid and did not segregate to any obvious cell type or tissue structures (Figure 3.8B). However, by the end of the neural induction stage (day 7) we observed several radially arranged SOX2-positive nuclei resembling neural rosettes within the organoids (Figure 3.8C). PANX1 was

expressed at the cell surface throughout the SOX2-positive rosettes. Moreover, PANX1 staining appeared somewhat concentrated toward the center of the neural rosette at the putative apical membrane domain. As developing cerebral organoids progress to the neuroepithelial expansion culture phase (starting on day 7), they are provided with extracellular matrix proteins to further support establishment of apical-basal polarity and the emergence of polarized neuroepithelium. By the end of this period, 10-day-old cerebral organoids possessed many spherical protuberances of tightly packed pseudostratified SOX2-positive cells. Within each expanding neuroepithelial sphere PANX1 expression was preferentially localized toward the center with minimal presence at the outer surfaces of the organoid (Figure 3.8D).

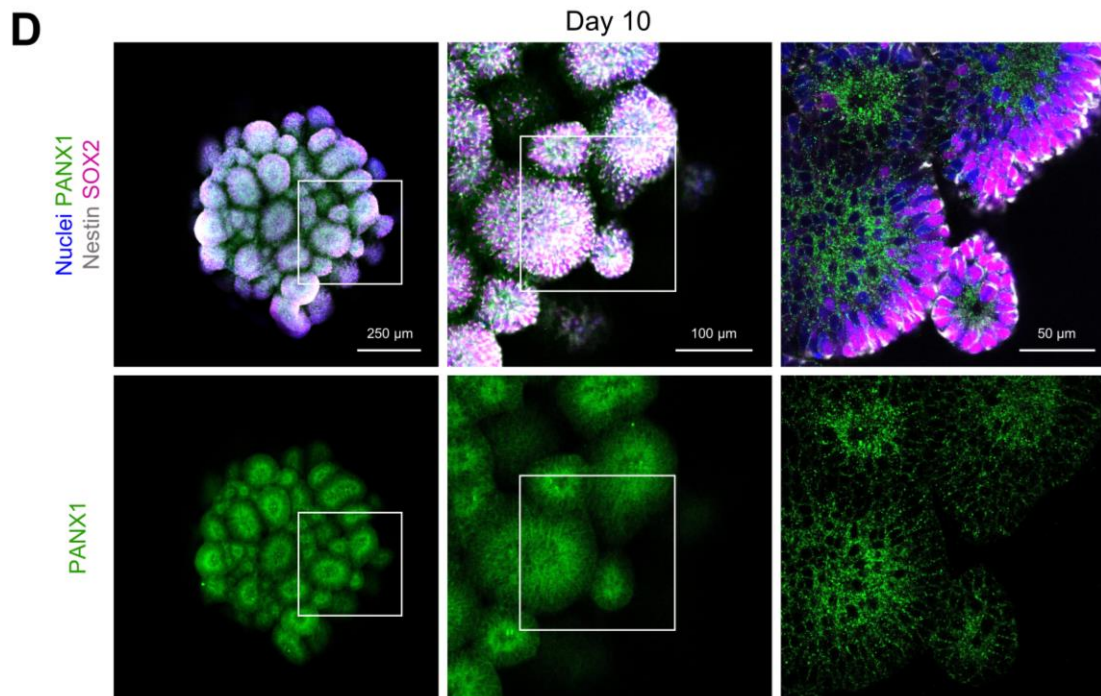
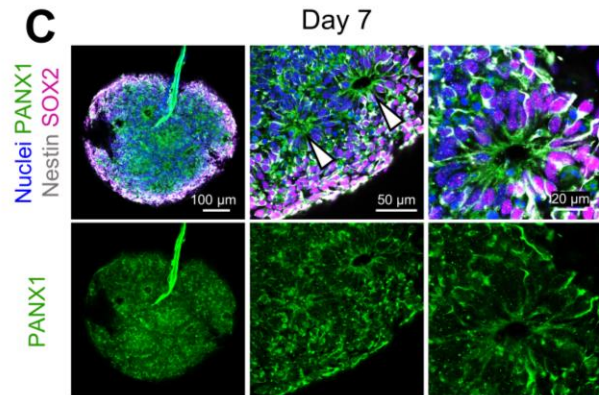
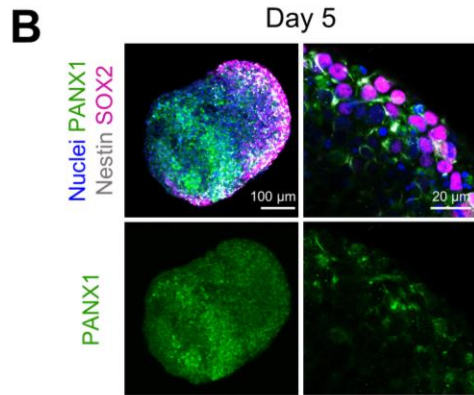
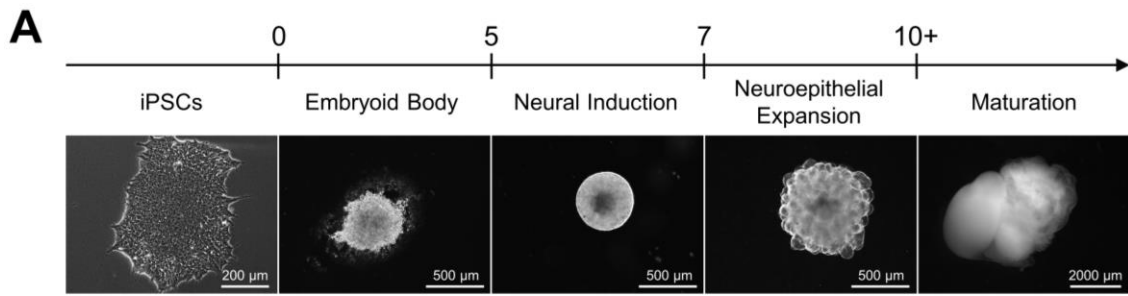


Figure 3.8 PANX1 is expressed at the earliest points of cerebral organoid development

(A) Schematic depicting the various stages of cerebral organoid culture and representative phase micrographs of control organoids. (B-D) Representative immunofluorescent confocal micrographs of whole mount control cerebral organoids at various developmental stages labelled for PANX1 (green), Nestin (white), and SOX2 (magenta). (B) PANX1 is widely expressed across the EB stage of cerebral organoid development (day 5). (C) At the end of the neural induction stage (day 7), PANX1 is expressed at the cell surface of radially arranged SOX2-positive neural rosettes (white arrowheads). (D) Day 10 cerebral organoids at the end of the neuroepithelial expansion stage develop many bulbous regions of radially arranged neuroepithelia with PANX1 staining concentrated toward the center of each bulb. Scale bars as indicated. Nuclei (Hoechst, blue). Images are representative of four biological replicates for panels A and D, or two replicates for panels B and C.

To better examine PANX1 localization at the neuroepithelial expansion stage, we cryosectioned 10-day-old cerebral organoids for analysis by confocal microscopy (Figure 3.9). Building on what we learned in the whole mount images, the cryosectioned slices revealed radially arranged SOX2-positive neural stem and progenitor cells surrounding hollow cavities reminiscent of brain ventricles (Figure 3.9A-B). These neural rosettes exhibit apical-basolateral polarity as demonstrated by the apical expression of adherens junctions β -catenin and N-cadherin as well as tight junction ZO-1 (Figure 3.9B). As predicted from the whole mount preparations, PANX1 protein localization is predominantly within the apical domain, residing at the interface of the neuroepithelium and ventricular space (Figure 3.9B). Furthermore, PANX1 colocalizes with adherens junctions β -catenin and N-cadherin and to a lesser extent with ZO-1 (Figure 3.9B-C). Mean colocalization for PANX1 with β -catenin is 0.4070 ± 0.06509 , PANX1 with N-cadherin is 0.5457 ± 0.05012 , and PANX1 colocalization with ZO-1 is 0.06847 ± 0.01272 as determined by Manders' correlation coefficients (Figure 3.9C). The high degree of colocalization between PANX1 and adherens junctions confirms occupancy of PANX1 in the apical compartments of neuroepithelia.

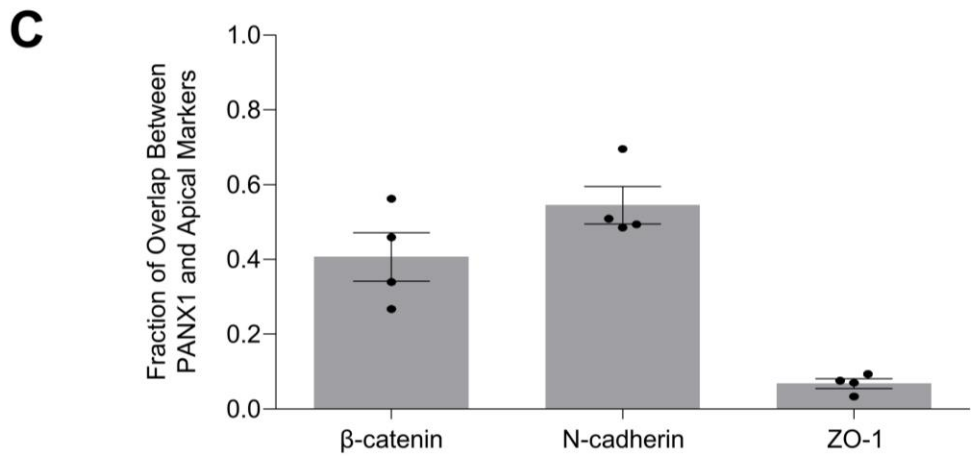
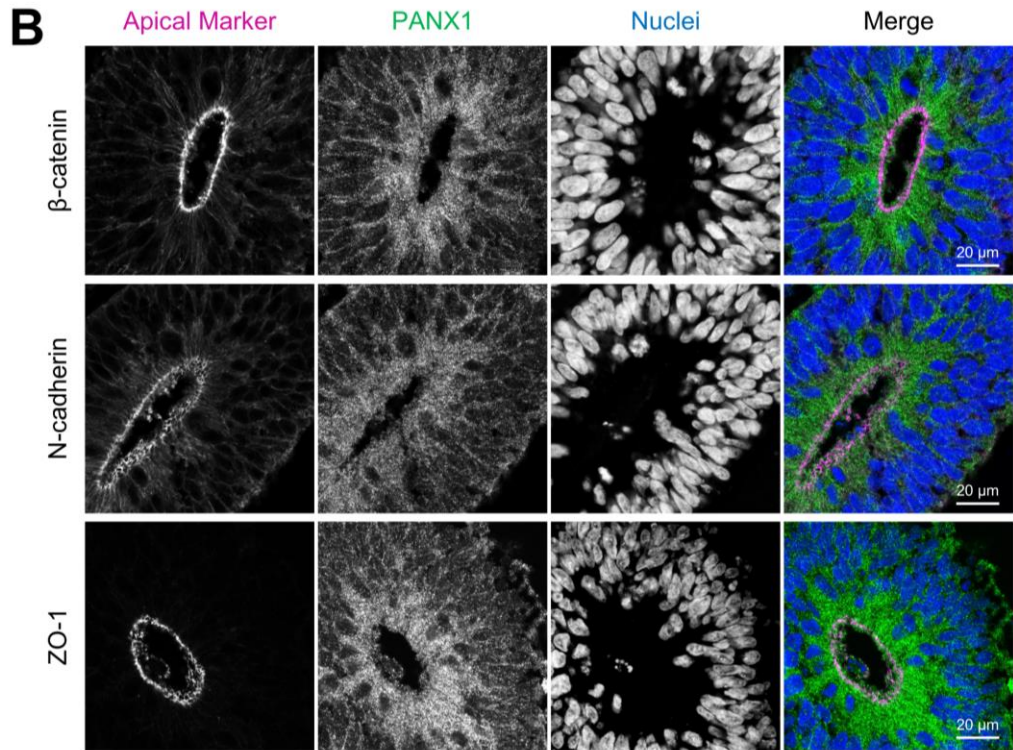
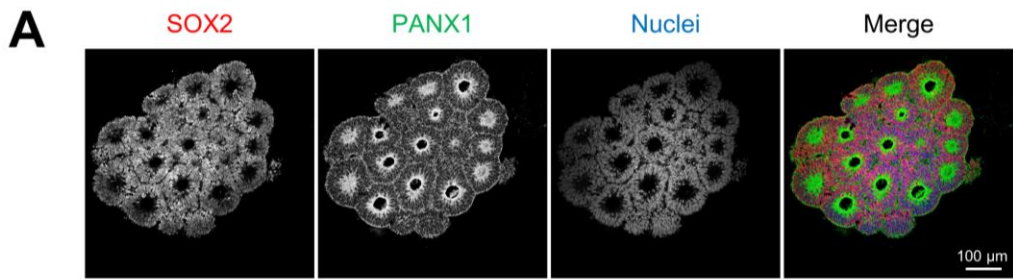


Figure 3.9 PANX1 is expressed in the apical domain of polarized neuroepithelial cells

(A) Immature control cerebral organoids at day 10 exhibit radially arranged SOX2-positive (red) cells surrounding fluid-filled spaces (neural rosettes). (B) Representative immunofluorescence confocal micrographs demonstrating PANX1 (green) co-localization with the apical membrane proteins β -catenin, N-cadherin, and ZO-1 (magenta) at the apical side (innermost) of the neuroepithelia. (C) Manders' correlation coefficients show the fraction of signal overlap for PANX1 with apically situated adherens junctions β -catenin and N-cadherin as well as with tight junction ZO-1. Error bars depict the standard error of the mean for 17-24 fields of view obtained from 4 independent experiments. Immunofluorescence images in panels A-B are representative of 4 independent experiments. Scale bars as indicated.

As cerebral organoids mature, the numerous neural rosettes continue to hollow out and elongate, forming ventricular-like spaces throughout the organoid. Furthermore, precursor cells begin to migrate from the ventricular-like zone to asymmetrically divide and ultimately differentiate into neurons and glia. To examine how *PANX1* expression and localization changes as organoids begin to mature and establish cortical layering, we examined mature cerebral organoids between 40 to 120 days (Figure 3.10). Using qPCR we detected transcripts for *PANX1* and *PANX2* but not *PANX3* (Figure 3.10A-B). One-way ANOVA did not reveal any statistical differences for *PANX1* or *PANX2* transcript abundance between iPSCs and cerebral organoids at 40, 80, or 120 days in culture. We also used IF in conjunction with qPCR to evaluate whether cerebral organoids expressed markers indicative of various cell types and developmental stages (Figure 3.10C-E). Day 40 organoids expressed neuroectodermal markers as demonstrated by abundant *PAX6* transcript expression and SOX2-positive staining by immunofluorescence (Figure 3.10Ci-ii). We confirmed that day 80 organoids contain many neuronal cells as indicated through TUJ1-positive immunostaining (Figure 3.10Dii). Furthermore, 80-day old organoids also possessed high levels of the neuronal transcript *MAP2* (Figure 3.10Di). Since gliogenesis (the production of glial cells) generally occurs following the onset of neurogenesis, we analyzed 120-day old organoids to determine whether cells with glial identity were present. Indeed, we observed GFAP-positive cells with astrocyte-like morphology using immunofluorescence and we also detected *GFAP* transcripts (Figure 3.10Ei-ii).

We used immunofluorescence microscopy to evaluate the localization of PANX1 throughout mature cerebral organoids. In organoids 40 days and older we observed apical expression of PANX1 in ventricular-like zones but noted the PANX1 signal appeared brightest outside the ventricular-like zones coinciding in regions with TUJ1-positive neurons (Figure 3.10Dii). This suggests that neurons may express more PANX1 protein than neural progenitor cells of ventricular-like zones. As organoids age they begin to produce glia cell types such as astrocytes which are characterized by GFAP expression. In 120-day old organoids we observed PANX1 expression within stellate GFAP-positive cells resembling astrocytes (Figure 3.10Eii). Our results indicate that mature organoids exhibit PANX1 localization at the apical side of the ventricular-like zones as well as in more developmentally advanced neural cell types such as neurons and GFAP-positive glia.

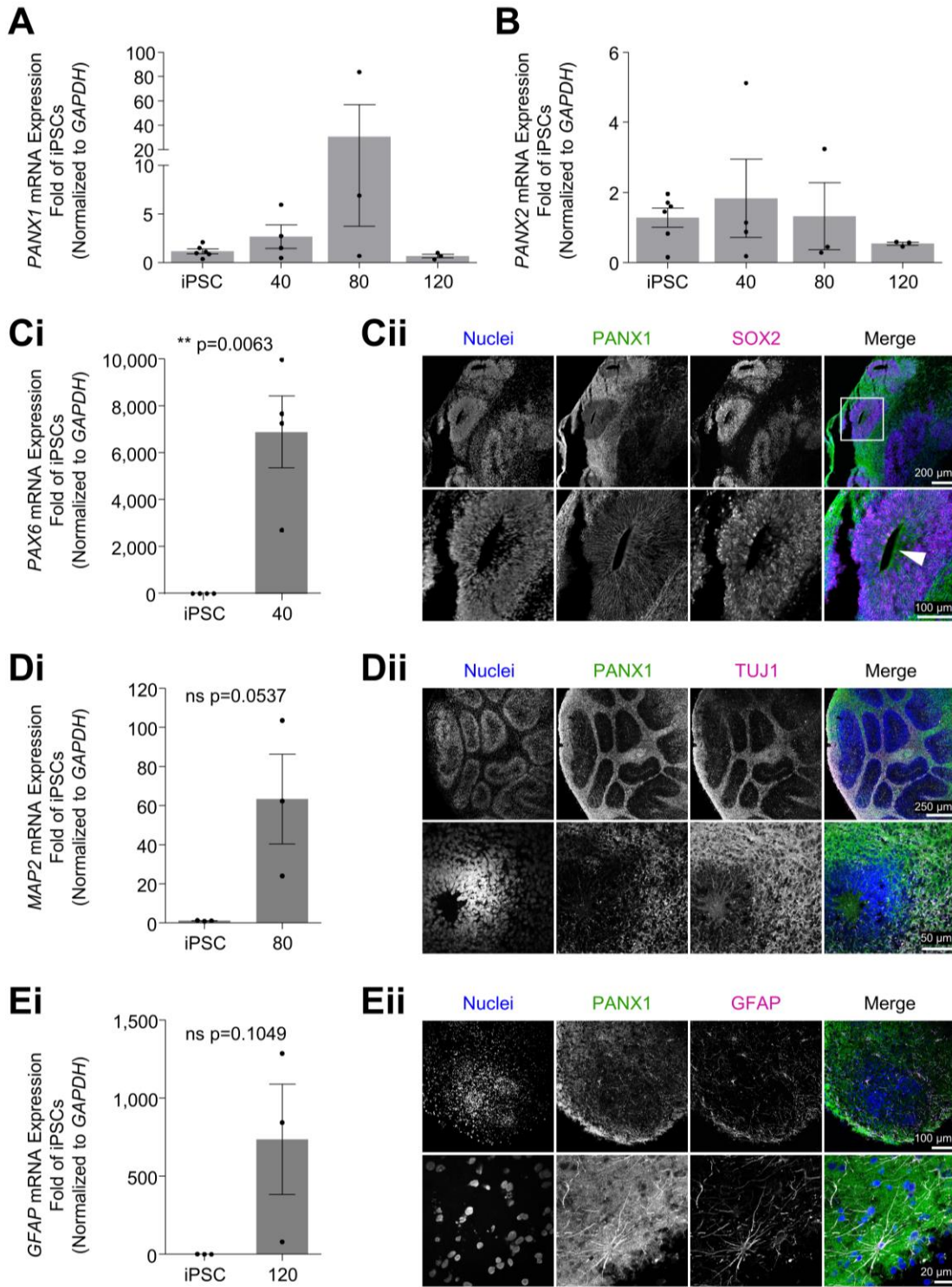


Figure 3.10 PANX1 localization in neural progenitor cells, neurons, and GFAP-positive glia within cerebral organoids

qPCR analysis of (A) *PANX1* and (B) *PANX2* mRNA expression in control iPSCs and control cerebral organoids aged 40 to 120 days. Transcripts for *PANX3* were not detected. (C*i-Ei*) Transcripts for neuroectoderm (*PAX6*), neurons (*MAP2*), and glial cells (*GFAP*) are generally elevated in cerebral organoids relative to iPSCs suggesting differentiation to these lineages. Data is expressed as a fold change from the control iPSCs. Error bars depict the standard error of the mean for 3-6 independent experiments in panels A-B or 3-4 independent experiments in panels C*i-Ei* with p values from Student's t-test as indicated. Representative immunofluorescence confocal micrographs from 2 independent experiments showing PANX1 (green) localization to various regions and cell types throughout control cerebral organoid maturation (C*ii- Eii*). (C*ii*) At 40 days in culture, cerebral organoids exhibit abundant PANX1 staining outside the SOX2-positive ventricular-like zones with some PANX1 expression persisting at the ventricular-like zone apical edge (arrowhead, inset). (D*ii*) Day 80 cerebral organoids display bright PANX1 expression in areas where TUJ1-positive neurons reside. (E*ii*) PANX1 expression is apparent in GFAP-positive glial cells with astrocyte morphology in 120-day-old cerebral organoids. Nuclei (Hoechst, blue). Neural cell type markers (SOX2, TUJ1, and GFAP in magenta). Scale bars as indicated.

3.7 Pharmacological Channel Inhibition with Probenecid Decreases Organoid Size

Given the wide expression and dynamic localization of PANX1 throughout each stage of cerebral organoid development, we hypothesized that PANX1-mediated cellular communication influences cerebral organoid development. Probenecid (PBN) is an FDA-approved drug frequently used to block PANX1 channel function *in vitro* (16, 58, 93, 105). To determine whether pharmacological PANX1 inhibition affects cerebral organoid development, we treated cerebral organoids with 1 mM PBN daily from day 5 until day 40 (Figure 3.11). By the end of the neuroepithelial expansion phase (day 10-11) PBN-treated organoids were significantly smaller ($0.1937 \pm 0.01020 \text{ mm}^2$) than control organoids ($0.6609 \pm 0.05481 \text{ mm}^2$) (Figure 3.11A-B). By day 40, we observed a trend where PBN-treated organoids were generally smaller compared to control (3.425 mm^2 compared to control organoids at $10.58 \pm 3.386 \text{ mm}^2$) (Figure 3.11A-B). Like the control, PBN-treated organoids continued to express the PANX1 protein in day 40 cerebral organoids (Figure 3.11C). Immunostaining revealed that both control and PBN-treated organoids developed TUJ1-positive neurons and that their SOX2-positive ventricular-like zones exhibit comparable thickness (Figure 3.11D-E). In summary, our PBN-treatment studies suggest that PANX1 may influence cerebral organoid size without impeding TUJ1-positive neuron production or enlargement of the ventricular like zone.

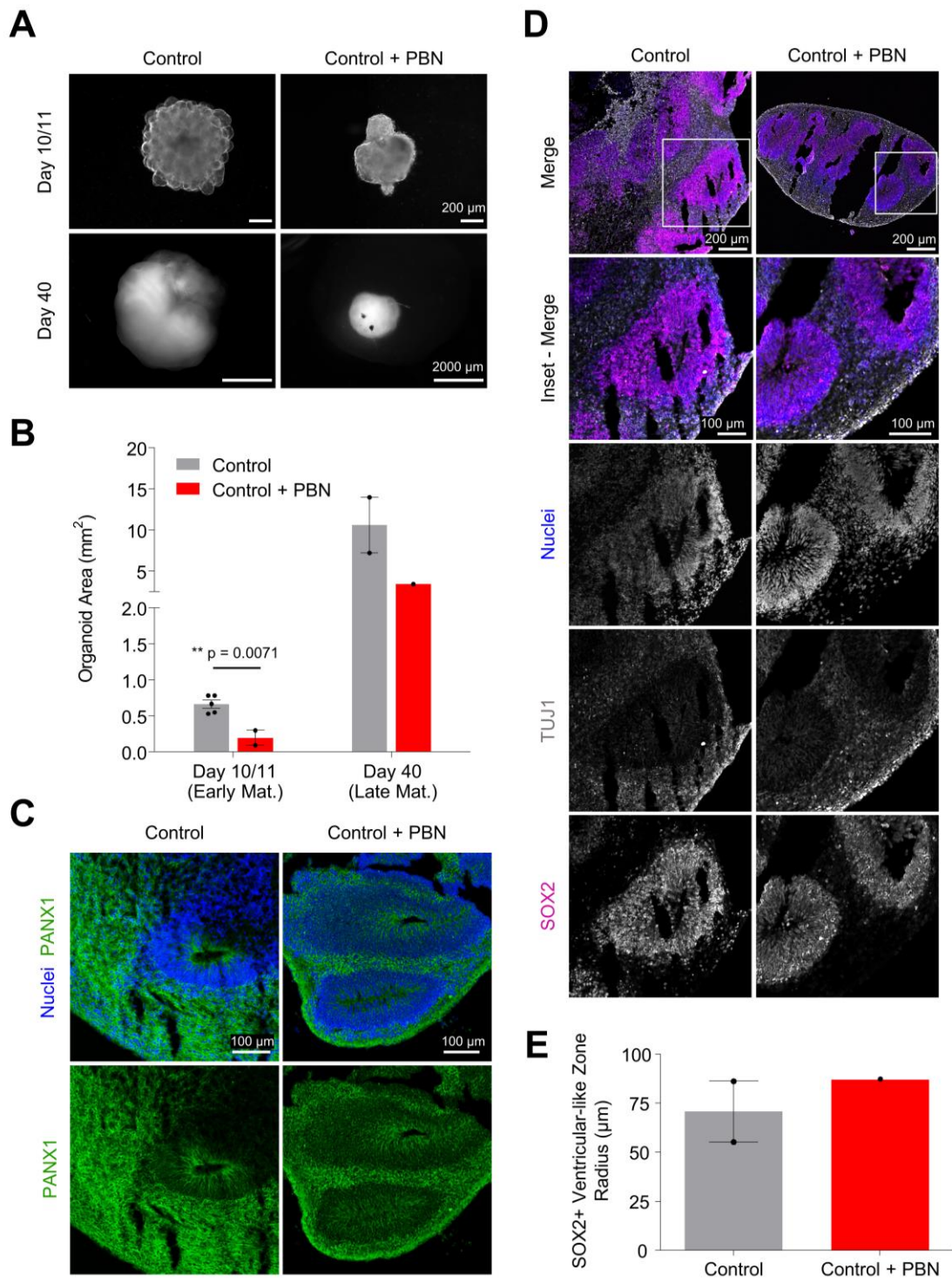


Figure 3.11 Probenecid-treated cerebral organoids display stunted growth

(A) Phase micrographs depicting representative morphologies of control and 1 mM probenecid (PBN)-treated cerebral organoids after neuroepithelial expansion (days 10/11) and at day 40 (mature organoids). (B) Cerebral organoid area measurements from phase micrographs of control and PBN-treated organoids. Data for day10/11 control is representative of 5 independent experiments comprising a total of 41 organoids whereas the PBN treatment is representative of 2 independent experiments containing a total of 9 organoids. P value for day10/11 obtained using Student's t-test. Day 40 data is representative of 2 independent experiments consisting of 14 control organoids and 1 experiment containing 2 PBN-treated organoids. (C) Representative immunofluorescence confocal micrographs of PANX1 (green) protein expression in mature day 40 control and PBN-treated organoids. (D) Control and PBN-treated organoids at day 40 contain SOX2-positive cells (magenta) in ventricular-like zones and TUJ1-positive (white) neurons outside the ventricular-like zones. Equivalent immunofluorescence image acquisition parameters and post processing were performed across conditions. Nuclei (Hoechst, blue). Scale bars as indicated. (E) SOX2-positive ventricular-like zone thickness (as measured from the apical to the basolateral edges of SOX2-positive regions) in day 40 control and PBN-treated cerebral organoids. Measurements taken from 2 independent experiments on a total of 4 control organoids and 34 measurements from 1 PBN-treated organoid. Error bars depict the standard error of the mean.

4 Discussion

Here we investigated PANX1 expression and localization in iPSCs and organoids as well as its influence over human pluripotent stem cell fate decisions. Since PANX1 is expressed in the embryo as well as adult tissues there is an underlying possibility for PANX1 involvement in cell fate specifications. However, potential contributions of PANX1 in the earliest stages of human development are poorly characterized. To address this gap, our study utilizes control and *PANX1* knockout iPSCs to model cell fate decisions to mesoderm, definitive endoderm, and ectoderm which collectively give rise to all bodily organs. Given PANX1's relatively high abundance in the embryonic brain, we also used cerebral organoids as a model system to evaluate PANX1 localization and the consequences of pharmacological inhibition during early stages of cortical development.

4.1 Human iPSCs Express PANX1

Human iPSCs and hESCs have previously been reported to express transcripts for *PANX1*, *PANX2* and *PANX3*, although the authors concluded that *PANX1* was the most highly expressed isoform (84). Using qPCR we observed expression of *PANX1* and *PANX2* mRNA transcripts in our iPSCs but were unable to detect *PANX3*. The disparity in our results compared to previously published reports could arise from differing PSC culture methodologies. We routinely maintain our iPSCs in feeder-free conditions in media with high levels of FGF2 in addition to TGF β , whereas the previous report (84) cultured PSCs on a

layer of murine embryonic fibroblasts (MEFs) in medium which lacks TGF β and contains very low levels of FGF2. It is unclear whether the presence of MEFs or the PSC culture medium influences pannexin expression in human PSCs.

Using Western blot, immunofluorescence, and flow cytometry, we show for the first time that PANX1 protein is also expressed in iPSCs where it is found at the cell surface and intracellularly. Previous work has demonstrated that the heavily glycosylated Gly2 isoform of PANX1 generally results in cell surface localization whereas the Gly1 modification sequesters PANX1 to the Golgi apparatus and Gly0 to the ER (64). Of note, PANX1 is predominantly localized to the cell surface of human oocytes as well as 2- and 4-cell embryos (69). Similarly, we found that PANX1 co-localized with actin at the surface of iPSCs with smaller populations of intracellular PANX1. To date we have not identified any specific messenger molecules that pass through PANX1 channels in iPSCs, but these studies would undoubtedly further our understanding of how PANX1 influences iPSCs.

4.2 PANX1 is Dispensable for Human iPSC Morphology, Survival, and Pluripotency Gene Expression

We are the first to describe *PANX1* CRISPR-Cas9 gene ablation in human iPSCs. Sanger sequencing revealed that gene editing with CRISPR-Cas9 resulted in a single base pair deletion in the third exon of *PANX1*, disrupting the reading frame and introducing 15 early stop codons. Immunofluorescence microscopy and flow cytometry confirmed the full-length PANX1 protein was no

longer present in our *PANX1*^{-/-} iPSCs. We found that *PANX1* knockout iPSCs do not compensate for the loss of full-length PANX1 protein by upregulating *PANX2*, *PANX3* or *GJA1*. In contrast, some cell types do indeed respond to the loss of functional PANX1 channels by upregulating other pannexins. For example, *PANX3* compensates for the loss of *PANX1* in dorsal skin of neonatal mice (106). Interestingly, we observed that *PANX1* knockout iPSCs have comparable survival, morphology, and marker expression relative to control. While loss of full-length PANX1 was well-tolerated in iPSCs, disruption of PANX1 channel function has been reported to be lethal in human oocytes. To date, four identified germline *PANX1* mutations cause aberrant PANX1 channel localization and oocyte death indicating that oocytes do not compensate for the loss of functional PANX1 channels (69). Our findings illustrate that although human iPSCs express PANX1, it is not essential for pluripotent stem cell renewal or survival.

4.3 PANX1 Influences Germ Layer Specification

Although PANX1 appeared to be dispensable for iPSC self-renewal or survival, we did uncover a role for PANX1 in germ lineage specification. We observed that under spontaneous differentiation conditions *PANX1*^{-/-} EBs have a propensity to elevate mesoderm and endoderm gene expression relative to control as measured with qPCR and immunofluorescence microscopy. There are several possible explanations for this skewed lineage representation, including an increase in mesendoderm cell proliferation, decreased apoptosis, or altered differentiation potential (107, 108). Alternatively, PANX1 could regulate iPSC

aggregation or even metabolism, both of which have been shown to influence cell fate specification (109-111). Again, uncovering the specific signaling molecules and PANX1 protein interacting partners involved in germ lineage specification is essential to fully understanding how PANX1 influences cell fate specification.

We assessed whether PANX1 channels are required for successful iPSC specification to the three germ layers. Interestingly, we observe that application of exogenous signals throughout monolayer directed differentiation overrides *PANX1*^{-/-} iPSC germ layer preferences. We demonstrate equal propensity for both control and *PANX1*^{-/-} iPSCs to form ectoderm, definitive endoderm, and mesoderm without apparent detriment to marker expression. Therefore, while PANX1 can influence cell fate specification to the three germ layers it is not essential to this process.

While we are the first to report a role for PANX1 in pluripotent stem cell fate decisions, others have shown the importance of these channels in various multipotent progenitor cells. PANX1 channels positively regulate self-renewal of neural stem and progenitor cells (16) and similarly, restrict differentiation of adipose-derived stromal cells to adipocytes (108). However, PANX1 channels in skeletal muscle progenitor cells have opposing functionality where they promote myoblast differentiation to skeletal myocytes (112). Since PANX1 channels do not have a singular effect in stem and progenitor cells, it will be increasingly important to investigate PANX1 channel functions across the progenitors of various tissues.

4.4 PANX1 is Expressed in NPCs, Neurons, and Astrocyte-Like Cells

Much of our understanding of PANX1 in brain development comes from animal models (where the earliest timepoints assessed are in the late embryonic period) and from limited human fetal tissue samples. It remains unclear how PANX1 influences the earliest stages of human brain development, or how PANX1 is expressed and regulated in the developing brain. Human iPSC-derived monolayer neural cultures and cerebral organoids allow us to study embryonic-like stages of brain development that are otherwise unobtainable in a human context.

Using monolayer and 3D cerebral organoid cultures we show that PANX1 is expressed in neural progenitor cells, neurons, and astrocyte-like cells expressing GFAP. Although *PANX1* transcripts in iPSCs, NPCs, and neurons cultured as monolayers were comparable, NPCs and neurons expressed significantly more PANX1 protein compared to undifferentiated iPSCs. The poor correlation between mRNA and protein expression in this instance is not understood but could be related to the relatively long half-life of PANX1 proteins or a difference in protein stability in neurons relative to iPSCs (54). Moreover, PANX1 in NPCs and neurons is predominantly expressed as a putative heavily glycosylated variant (Gly2) while immunofluorescence microscopy indicated PANX1 colocalization with actin in both cell types. Prior studies on postnatal murine NPCs, NSCs, and immortalized Neuro-2a cells demonstrate PANX1 expression predominantly at the cell surface (16, 59, 75). In these cells, the interaction between PANX1 and

P2X receptors facilitates self-renewal and prevents premature neuronal differentiation (16, 75). Further studies using cell-impermeant biotin which interacts with exposed lysine residues on transmembrane proteins to capture proteins at the cell surface would confirm PANX1 cell surface occupancy in neural progenitor cells and neurons. It would be interesting to evaluate whether PANX1 modulation of P2X receptor signal transduction also regulates self-renewal in human NPCs.

PANX1 is expressed in a variety of mature neuronal subtypes including cortical and hippocampal interneurons, neocortical pyramidal cells, dopaminergic neurons, excitatory principal cells, and others (57, 82). While the *PANX1* transcript levels between iPSCs and neurons were not significantly different, Western blotting revealed that neurons express roughly 5 times more PANX1 protein than iPSCs. Other studies reveal that PANX1 is often localized at neuronal synapses where it is believed PANX1 channels release ATP into the extracellular space which in turn helps to maintain the strength of neuronal connections (57, 81, 113, 114). We observed PANX1 expression in TUJ1-positive neurons produced in monolayer cultures and in cerebral organoids. Future investigations will reveal whether PANX1 localizes to neuronal postsynaptic sites in human cerebral organoids as has been shown in other systems (115).

Finally, we observed PANX1 expression in GFAP-positive cells with astrocytic morphology in 120-day old cerebral organoids, similar to reports in postnatal mice (116). Conflicting reports place PANX1 intracellularly or at the cell

surface in postnatal murine astrocytes and oligodendrocytes (116, 117). Using confocal microscopy, we observed robust PANX1 signal throughout the processes of GFAP-positive cells in 120-day old cerebral organoids. However, in the absence of cell surface biotinylation assays or high-resolution microscopy on purified populations of human glial cells, we cannot definitively comment on PANX1 subcellular localization in these cells.

4.4.1 PANX1 Localizes to the Apical Region of Cerebral Organoid Neuroepithelia

Previous studies describe apical membrane expression of the PANX1 protein in a variety of epithelial cell types including airway and kidney epithelia where apical PANX1 localization contributes to organ functionality (118, 119). For example, apically situated PANX1 channels release ATP which ultimately facilitates the reabsorption of salts and water from the kidney and mucous clearance from the airway (118, 119). Apical expression of *PANX1* transcripts is also observed along the telencephalic vesicle wall of E11.5 murine brains although a role for PANX1 in that location was not described (120).

Like the developing brain, cerebral organoids produce polarized neuroepithelia which initially form small neural rosettes (akin to the neural tube) containing neural stem and progenitor cells. We report apical localization of the PANX1 protein in polarized neuroepithelia of immature human cerebral organoids and in the ventricular zones of mature cerebral organoids. During cerebral organoid culture, this apical expression pattern of PANX1 is retained even up

until day 120 - the latest timepoint assessed which possibly indicates long-term functionality of PANX1 channels adjacent to the ventricular space.

Immunostaining during the neuroepithelial expansion stage revealed substantial colocalization between PANX1 and the adherens junction proteins N-cadherin and β -catenin which are also predominantly apical. PANX1 has few known interacting partners including actin, actin related protein 3, and P2X receptors (57). Future co-immunoprecipitation assays will confirm whether PANX1 physically interacts with N-cadherin, β -catenin, other scaffolding proteins, adhesion complexes, and/or polarity complexes in neuroepithelial cells.

While the role of apical PANX1 in the neuroepithelia of immature organoids and ventricular-like zones of mature organoids is currently unknown, evidence suggests that PANX1 contributes to maintenance and proliferation of neural stem and progenitor cells. ATP release through PANX1 channels positively regulates murine neurosphere stem and progenitor cell proliferation through P2 purinergic receptors (16). Additional studies are required to identify whether PANX1 channels at the apical domain of neuroepithelial or ventricular-like zones relay signaling molecules such as ATP into the fluid-filled ventricle to coordinate long-range developmental or proliferation events.

4.4.2 Pharmacological PANX1 Inhibition Reduces Cerebral Organoid Size

Since a germline mutation affecting PANX1 channel function is implicated with sensorineural deficits (68), we sought to explore the role of PANX1 in the developing human brain using cerebral organoids. To understand the

consequences of interrupted PANX1-mediated cell signaling throughout brain development, we treated our organoids with the FDA-approved drug probenecid, which is frequently used *in vitro* to block PANX1 channel function (16, 58, 93, 105). Our preliminary results indicate that forty-day old cerebral organoids treated with 1 mM PBN were visibly smaller than their vehicle control counterparts. A similar finding was made elsewhere wherein murine neurospheres treated with 1 mM PBN were smaller than control due to a reduction of neural stem and progenitor cell proliferation in response to impaired ATP release and P2 receptor activation (16). A follow-up study also demonstrated that loss of PANX1 channel function causes premature neural stem cell differentiation as indicated by enhanced neurite extension and cell migration (75). However, in our preliminary examination we observed that ventricular-like zone thickness between control and PBN-treated organoids were similar, suggesting that neural progenitor proliferation (and the subsequent enlargement of the ventricular-like zone) may not be adversely affected. However, more robust metrics such as radial glia cleavage angle may afford additional insights about cell proliferation and differentiation resulting from PANX1 channel blockade. It is also possible that PBN-treated organoids experience more cell death or reduced proliferation than control which could account for the size reduction. Staining for markers of apoptosis and proliferation would inform whether these parameters are affected by PBN treatment. We also noted that both control and drug-treated conditions produced TUJ1-positive neurons by day 40. Since others have reported a role for PANX1 in negatively regulating neurite extension (75, 113) it would be interesting

to see if PBN treatment enhances neurogenesis by increasing dendritic protrusion density.

Collectively, our preliminary findings indicate that PANX1 is expressed in neural progenitors, neurons, and GFAP-expressing glial cells with astrocytic morphology. In 3D cerebral organoid cultures we observe PANX1 expression along the apical edge of neuroepithelium in the rosettes of immature organoids and in the ventricular-like zones of mature organoids. Pharmacological PANX1 inhibition appears to negatively impact human cerebral organoid size beginning at the neuroepithelial expansion stage and results in smaller organoids.

4.5 Study Limitations

Using Sanger sequencing, we confirmed that our *PANX1*^{-/-} knockout iPSCs contain a frameshift mutation which disrupts the reading frame and generates multiple early stop codons. The first stop codons appear in the first intracellular loop, roughly halfway through the length of the PANX1 protein. Using an antibody raised against the C-terminus of PANX1 we confirmed that the full-length protein is no longer expressed in *PANX1*^{-/-} iPSCs. However, it is possible that *PANX1*^{-/-} iPSCs could produce truncated PANX1 proteins which are undetectable using the C-terminus PANX1 antibody. Assessment of PANX1 using an antibody raised against the N-terminus would confirm whether truncated PANX1 fragments translated upstream of the mutation site are present or whether the transcripts are subject to nonsense mediated decay. However, given that the *PANX1* mutation is introduced in the first half of the protein-coding

sequence, it is unlikely that any truncated PANX1 fragments could traffic to the cell surface given that the cell surface targeting motifs are located on the C-terminus near the end of protein (121).

To study PANX1 in early human development we used iPSC-based model systems including EBs and cerebral organoids. While these 3D systems offer advantages regarding cell-cell and cell-matrix organization, they are subject to a variety of limitations. Although EBs can provide useful information about germ layer formation, they do not faithfully recapitulate the cellular frequencies and organization of the human embryo. For example, although EBs can differentiate into cells of each of the three germ layers (19), PSCs have a propensity to “default” toward ectoderm and its derivatives (122). In line with this, our control EBs expressed far more PAX6-positive ectoderm cells compared to Brachyury-positive mesoderm and SOX17-positive endodermal cells. However, the EB model of spontaneous differentiation proved useful in modeling spontaneous human germ layer commitment as it was able to demonstrate a mesendoderm bias in *PANX1* knockout iPSCs relative to control.

A major limitation of cerebral organoid culture systems as a model of human brain development is the lack of vascular endothelial cells and resident immune cells called microglia (44, 123). Without vascularization, cerebral organoids are restricted in size and cannot reach the stature of the developing human cortex. Additionally, microglia play important roles in the differentiation and maturation of cortical neurons and astrocytes (123). Nevertheless,

transcriptional profiling of cerebral organoids revealed that the neural cells within attain greater maturation than those cultured in 2D systems and that 100-day old organoids have similar transcriptional profiles to those of 17-24 week human cerebral cortices (44). Like the developing brain, aging cerebral organoids display a greater diversity of cell types and heightened maturation of neurons and glia relative to younger organoids (44). Using this human-centric organoid culture system we identified PANX1 expression in neurons and glial cells as well as its apical localization in neural stem and progenitor cells lining the ventricular space.

In our present study, we used PBN to block PANX1 channel functions following the EB stage of cerebral organoid development. Although commonly used to block PANX1 channels *in vitro*, PBN has an unknown mechanism of action and can inhibit numerous channels and transporters (93, 124) (<https://go.drugbank.com/drugs/DB01032>). Therefore, the reduction in PBN-treated cerebral organoid size we observed may be due to off-target drug effects rather than specific PANX1 channel inhibition. Other drugs for PANX1 channel blockade such as trovafloxacin (125) and brilliant blue FCF (124, 126) may exhibit more PANX1 specificity and are worth investigating for use in temporal PANX1 channel inhibition studies. Since we have *PANX1*^{-/-} iPSCs in house, our future efforts will focus on using knockout cells rather than pharmacological inhibitors to evaluate PANX1 channel functions in cerebral organoids. However, our preliminary PBN study revealed a potential consequence of interrupted

PANX1 signaling which we will explore further using *PANX1* knockout cerebral organoids.

4.6 Conclusions

Here we report that human iPSCs express the PANX1 protein at the cell surface and within intracellular compartments. While PANX1-mediated cellular communication is not required for iPSC survival or morphology it does affect iPSC fate decisions. We found that *PANX1*^{-/-} iPSCs have a heightened propensity to generate mesoderm and endoderm relative to control iPSCs in an EB model of cell-guided, spontaneous differentiation. Interestingly, we saw comparable ability of control and *PANX1*^{-/-} iPSCs to form the three germ layers under directed differentiation strategies. We conclude that while PANX1 influences cell fate decisions during germ layer commitment, its participation in this process is not essential.

Additionally, we evaluated PANX1 expression in a cerebral organoid model of human cortical development. Immunofluorescence microscopy revealed PANX1 expression throughout all stages of cerebral organoid development and in cell types such as neurons, astrocyte-like cells, and neural progenitors. We noted that neurons and neural progenitors express more PANX1 protein than iPSCs and in these neural cells, PANX1 is heavily glycosylated (putatively) and colocalizes with actin. In the neuroepithelium of immature cerebral organoids, PANX1 was apically expressed where it colocalized with N-cadherin and β -catenin. This apical localization pattern was also observed in the ventricular-like

zones of mature cerebral organoids, suggestive of long-term channel functionality at this locale. Lastly, we found that pharmacological inhibition of PANX1 channels using PBN caused a reduction in cerebral organoid size relative to control. Together, our findings indicate that PANX1 channels are widely expressed in developing cortical tissues but may also play important regional roles, particularly in cells adjacent to the ventricular space.

4.7 Outlook and Future Directions

From studies on model organisms, we expect PANX1 is expressed in diverse neural cell types and brain regions that were not addressed in our present study (82, 83, 127, 128). For example, previous work on animal models have shown PANX1 expression across many brain regions including the hippocampus, cerebellum, thalamus, and retina as well as the spinal cord. (82, 83). The organoid model we used in this study predominantly generates cerebral cortex-like structures, but we could expand our investigations to other brain organoid culture systems (hippocampal, cerebellar, etc.) to study PANX1 expression and localization. Assessment of PANX1 expression in a variety of brain structures may reveal conserved functionality of PANX1 channels across the brain or help us understand why diverse structures possess abundant *PANX1* transcripts in the embryonic period but switch to *PANX2* in the fetal period.

To better understand how PANX1 is expressed across different neural cell types, we could assess publicly available single cell RNA sequencing (scRNA-seq) data from human cerebral organoids and fetal tissue samples to evaluate

PANX1 expression in specific neural cell types. This would help us identify neural cells of interest for further interrogation at the protein level. Precise identification of *PANX1* expression in discrete cell populations might provide clues about *PANX1*'s function or highlight developmental trajectories influenced by *PANX1*.

So far, disease-causing human *PANX1* mutations have only been reported in female patients (68, 69). However, this does not preclude the possibility that *PANX1* equally impacts males. Our current study evaluates control iPSCs of both sexes along with female *PANX1* knockout iPSCs. In the future we will use CRISPR-Cas9 genetic engineering to create male *PANX1*^{-/-} iPSCs for additional studies. We anticipate comparable germ layer emergence between sexes but are unsure how sex differences will impact cortical development. However, since several germline mutations are lethal to oocytes but not to sperm (69) we expect female PSCs will exhibit impaired differentiation to primordial germ cells relative to male PSCs.

Impaired cellular communication can prove detrimental during development, particularly at early stages where cell fate errors could prove lethal or be perpetuated throughout many downstream cell types and tissues. A thorough understanding of the cell fate decisions made during embryogenesis will improve our ability to identify and treat human developmental disorders. Since *PANX1* channels are expressed in oocytes, pluripotent stem cells, and many adult tissues, we expect that *PANX1*-mediated cellular communication impacts cell fate decisions throughout human development. Our continued efforts to

elucidate the role of PANX1-mediated communication in cell fate decisions will further our understanding of human embryogenesis and developmental pathologies.

5 References

1. K. K. Niakan, J. Han, R. A. Pedersen, C. Simon and R. A. Pera: Human pre-implantation embryo development. *Development*, 139(5), 829-41 (2012) doi:10.1242/dev.060426
2. C. Gerri, S. Menchero, S. K. Mahadevaiah, J. M. A. Turner and K. K. Niakan: Human Embryogenesis: A Comparative Perspective. *Annu Rev Cell Dev Biol*, 36, 411-440 (2020) doi:10.1146/annurev-cellbio-022020-024900
3. M. L. Condic: Totipotency: what it is and what it is not. *Stem Cells Dev*, 23(8), 796-812 (2014) doi:10.1089/scd.2013.0364
4. P. P. Tam and D. A. Loebel: Gene function in mouse embryogenesis: get set for gastrulation. *Nat Rev Genet*, 8(5), 368-81 (2007) doi:10.1038/nrg2084
5. T. Mikawa, A. M. Poh, K. A. Kelly, Y. Ishii and D. E. Reese: Induction and patterning of the primitive streak, an organizing center of gastrulation in the amniote. *Dev Dyn*, 229(3), 422-32 (2004) doi:10.1002/dvdy.10458
6. M. N. Shahbazi: Mechanisms of human embryo development: from cell fate to tissue shape and back. *Development*, 147(14) (2020) doi:10.1242/dev.190629
7. J. Y. Tan, G. Sriram, A. J. Rufaihah, K. G. Neoh and T. Cao: Efficient derivation of lateral plate and paraxial mesoderm subtypes from human embryonic stem cells through GSKi-mediated differentiation. *Stem Cells Dev*, 22(13), 1893-906 (2013) doi:10.1089/scd.2012.0590
8. S. Tada, T. Era, C. Furusawa, H. Sakurai, S. Nishikawa, M. Kinoshita, K. Nakao and T. Chiba: Characterization of mesendoderm: a diverging point of the definitive endoderm and mesoderm in embryonic stem cell differentiation culture. *Development*, 132(19), 4363-74 (2005) doi:10.1242/dev.02005
9. D. Evseenko, Y. Zhu, K. Schenke-Layland, J. Kuo, B. Latour, S. Ge, J. Scholes, G. David, X. Li, W. R. MacLellan and G. M. Crooks: Mapping the first stages of mesoderm commitment during differentiation of human embryonic stem cells. *Proc Natl Acad Sci U S A*, 107(31), 13742-7 (2010) doi:10.1073/pnas.1002077107
10. J. Tchieu, B. Zimmer, F. Fattahi, S. Amin, N. Zeltner, S. Chen and L. Studer: A Modular Platform for Differentiation of Human PSCs into All Major Ectodermal Lineages. *Cell Stem Cell*, 21(3), 399-410.e7 (2017) doi:10.1016/j.stem.2017.08.015
11. M. Thomson, S. J. Liu, L. N. Zou, Z. Smith, A. Meissner and S. Ramanathan: Pluripotency factors in embryonic stem cells regulate differentiation into germ layers. *Cell*, 145(6), 875-89 (2011) doi:10.1016/j.cell.2011.05.017
12. H. Liu, M. Yuan, Y. Yao, D. Wu, S. Dong and X. Tong: In vitro effect of Pannexin 1 channel on the invasion and migration of I-10 testicular cancer cells via ERK1/2 signaling pathway. *Biomed Pharmacother*, 117, 109090 (2019) doi:10.1016/j.biopha.2019.109090
13. J. Itskovitz-Eldor, M. Schuldiner, D. Karsenti, A. Eden, O. Yanuka, M. Amit, H. Soreq and N. Benvenisty: Differentiation of human embryonic stem cells into embryoid bodies compromising the three embryonic germ layers. *Mol Med*, 6(2), 88-95 (2000)
14. M. Amit, M. K. Carpenter, M. S. Inokuma, C. P. Chiu, C. P. Harris, M. A. Waknitz, J. Itskovitz-Eldor and J. A. Thomson: Clonally derived human embryonic stem cell lines maintain pluripotency and proliferative potential for prolonged periods of culture. *Dev Biol*, 227(2), 271-8 (2000) doi:10.1006/dbio.2000.9912
15. G. Liu, B. T. David, M. Trawczynski and R. G. Fessler: Advances in Pluripotent Stem Cells: History, Mechanisms, Technologies, and Applications. *Stem Cell Rev Rep*, 16(1), 3-32 (2020) doi:10.1007/s12015-019-09935-x
16. L. E. Wicki-Stordeur, A. D. Dzugalo, R. M. Swansburg, J. M. Suits and L. A. Swayne: Pannexin 1 regulates postnatal neural stem and progenitor cell proliferation. *Neural Dev*, 7, 11 (2012) doi:10.1186/1749-8104-7-11
17. M. A. Lancaster, M. Renner, C. A. Martin, D. Wenzel, L. S. Bicknell, M. E. Hurler, T. Homfray, J. M. Penninger, A. P. Jackson and J. A. Knoblich: Cerebral organoids model human brain development and microcephaly. *Nature*, 501(7467), 373-9 (2013) doi:10.1038/nature12517

18. K. Takahashi, K. Tanabe, M. Ohnuki, M. Narita, T. Ichisaka, K. Tomoda and S. Yamanaka: Induction of pluripotent stem cells from adult human fibroblasts by defined factors. *Cell*, 131(5), 861-72 (2007) doi:10.1016/j.cell.2007.11.019
19. I. Desbaillets, U. Ziegler, P. Groscurth and M. Gassmann: Embryoid bodies: an in vitro model of mouse embryogenesis. *Exp Physiol*, 85(6), 645-51 (2000)
20. J. A. Thomson, J. Itskovitz-Eldor, S. S. Shapiro, M. A. Waknitz, J. J. Swiergiel, V. S. Marshall and J. M. Jones: Embryonic stem cell lines derived from human blastocysts. *Science*, 282(5391), 1145-7 (1998) doi:10.1126/science.282.5391.1145
21. Y. Buganim, D. A. Faddah and R. Jaenisch: Mechanisms and models of somatic cell reprogramming. *Nat Rev Genet*, 14(6), 427-39 (2013) doi:10.1038/nrg3473
22. A. D. Panopoulos, O. Yanes, S. Ruiz, Y. S. Kida, D. Diep, R. Tautenhahn, A. Herreras, E. M. Batchelder, N. Plongthongkum, M. Lutz, W. T. Berggren, K. Zhang, R. M. Evans, G. Siuzdak and J. C. Izpisua Belmonte: The metabolome of induced pluripotent stem cells reveals metabolic changes occurring in somatic cell reprogramming. *Cell Res*, 22(1), 168-77 (2012) doi:10.1038/cr.2011.177
23. R. M. Marion, K. Strati, H. Li, A. Tejera, S. Schoeftner, S. Ortega, M. Serrano and M. A. Blasco: Telomeres acquire embryonic stem cell characteristics in induced pluripotent stem cells. *Cell Stem Cell*, 4(2), 141-54 (2009) doi:10.1016/j.stem.2008.12.010
24. T. Redmer, S. Diecke, T. Grigoryan, A. Quiroga-Negreira, W. Birchmeier and D. Besser: E-cadherin is crucial for embryonic stem cell pluripotency and can replace OCT4 during somatic cell reprogramming. *EMBO Rep*, 12(7), 720-6 (2011) doi:10.1038/embor.2011.88
25. G. Chen, D. R. Gulbranson, Z. Hou, J. M. Bolin, V. Ruotti, M. D. Probasco, K. Smuga-Otto, S. E. Howden, N. R. Diol, N. E. Propson, R. Wagner, G. O. Lee, J. Antosiewicz-Bourget, J. M. Teng and J. A. Thomson: Chemically defined conditions for human iPSC derivation and culture. *Nat Methods*, 8(5), 424-9 (2011) doi:10.1038/nmeth.1593
26. T. E. Ludwig, M. E. Levenstein, J. M. Jones, W. T. Berggren, E. R. Mitchen, J. L. Frane, L. J. Crandall, C. A. Daigh, K. R. Conard, M. S. Piekarczyk, R. A. Llanas and J. A. Thomson: Derivation of human embryonic stem cells in defined conditions. *Nat Biotechnol*, 24(2), 185-7 (2006) doi:10.1038/nbt1177
27. V. Akopian, P. W. Andrews, S. Beil, N. Benvenisty, J. Brehm, M. Christie, A. Ford, V. Fox, P. J. Gokhale, L. Healy, F. Holm, O. Hovatta, B. B. Knowles, T. E. Ludwig, R. D. McKay, T. Miyazaki, N. Nakatsuji, S. K. Oh, M. F. Pera, J. Rossant, G. N. Stacey, H. Suemori and I. S. C. I. Consortium: Comparison of defined culture systems for feeder cell free propagation of human embryonic stem cells. *In Vitro Cell Dev Biol Anim*, 46(3-4), 247-58 (2010) doi:10.1007/s11626-010-9297-z
28. T. E. Ludwig, V. Bergendahl, M. E. Levenstein, J. Yu, M. D. Probasco and J. A. Thomson: Feeder-independent culture of human embryonic stem cells. *Nat Methods*, 3(8), 637-46 (2006) doi:10.1038/nmeth902
29. M. Mossahebi-Mohammadi, M. Quan, J. S. Zhang and X. Li: FGF Signaling Pathway: A Key Regulator of Stem Cell Pluripotency. *Front Cell Dev Biol*, 8, 79 (2020) doi:10.3389/fcell.2020.00079
30. E. Sachlos and D. T. Auguste: Embryoid body morphology influences diffusive transport of inductive biochemicals: a strategy for stem cell differentiation. *Biomaterials*, 29(34), 4471-80 (2008) doi:10.1016/j.biomaterials.2008.08.012
31. Y. Qi, X. J. Zhang, N. Renier, Z. Wu, T. Atkin, Z. Sun, M. Z. Ozair, J. Tchieu, B. Zimmer, F. Fattahi, Y. Ganat, R. Azevedo, N. Zeltner, A. H. Brivanlou, M. Karayiorgou, J. Gogos, M. Tomishima, M. Tessier-Lavigne, S. H. Shi and L. Studer: Combined small-molecule inhibition accelerates the derivation of functional cortical neurons from human pluripotent stem cells. *Nat Biotechnol*, 35(2), 154-163 (2017) doi:10.1038/nbt.3777
32. S. M. Chambers, C. A. Fasano, E. P. Papapetrou, M. Tomishima, M. Sadelain and L. Studer: Highly efficient neural conversion of human ES and iPS cells by dual inhibition of SMAD signaling. *Nat Biotechnol*, 27(3), 275-80 (2009) doi:10.1038/nbt.1529

33. H. Hříbková, M. Grabiec, D. Klemová, I. Slaninová and Y. M. Sun: Calcium signaling mediates five types of cell morphological changes to form neural rosettes. *J Cell Sci*, 131(3) (2018) doi:10.1242/jcs.206896
34. D. ten Berge, W. Koole, C. Fuerer, M. Fish, E. Eroglu and R. Nusse: Wnt signaling mediates self-organization and axis formation in embryoid bodies. *Cell Stem Cell*, 3(5), 508-18 (2008) doi:10.1016/j.stem.2008.09.013
35. J. Friedrich, C. Seidel, R. Ebner and L. A. Kunz-Schughart: Spheroid-based drug screen: considerations and practical approach. *Nat Protoc*, 4(3), 309-24 (2009) doi:10.1038/nprot.2008.226
36. M. D. Ungrin, C. Joshi, A. Nica, C. Bauwens and P. W. Zandstra: Reproducible, ultra high-throughput formation of multicellular organization from single cell suspension-derived human embryonic stem cell aggregates. *PLoS One*, 3(2), e1565 (2008) doi:10.1371/journal.pone.0001565
37. Y. Lin and G. Chen: StemBook. In: *StemBook*. Ed T. S. C. R. Community. IOS Press, (2014) doi:doi/10.3824/stembook.1.98.1
38. J. Stiles and T. L. Jernigan: The basics of brain development. *Neuropsychol Rev*, 20(4), 327-48 (2010) doi:10.1007/s11065-010-9148-4
39. T. Mori, A. Buffo and M. Götz: The novel roles of glial cells revisited: the contribution of radial glia and astrocytes to neurogenesis. *Curr Top Dev Biol*, 69, 67-99 (2005) doi:10.1016/S0070-2153(05)69004-7
40. P. G. Wilson and S. S. Stice: Development and differentiation of neural rosettes derived from human embryonic stem cells. *Stem Cell Rev*, 2(1), 67-77 (2006) doi:10.1007/s12015-006-0011-1
41. A. Kriegstein and A. Alvarez-Buylla: The glial nature of embryonic and adult neural stem cells. *Annu Rev Neurosci*, 32, 149-84 (2009) doi:10.1146/annurev.neuro.051508.135600
42. D. V. Hansen, J. H. Lui, P. R. Parker and A. R. Kriegstein: Neurogenic radial glia in the outer subventricular zone of human neocortex. *Nature*, 464(7288), 554-561 (2010) doi:10.1038/nature08845
43. S. Jäkel and L. Dimou: Glial Cells and Their Function in the Adult Brain: A Journey through the History of Their Ablation. *Front Cell Neurosci*, 11, 24 (2017) doi:10.3389/fncel.2017.00024
44. E. Di Lullo and A. R. Kriegstein: The use of brain organoids to investigate neural development and disease. *Nat Rev Neurosci*, 18(10), 573-584 (2017) doi:10.1038/nrn.2017.107
45. M. Fujii and T. Sato: Somatic cell-derived organoids as prototypes of human epithelial tissues and diseases. *Nat Mater* (2020) doi:10.1038/s41563-020-0754-0
46. D. Dutta, I. Heo and H. Clevers: Disease Modeling in Stem Cell-Derived 3D Organoid Systems. *Trends Mol Med*, 23(5), 393-410 (2017) doi:10.1016/j.molmed.2017.02.007
47. M. Renner, M. A. Lancaster, S. Bian, H. Choi, T. Ku, A. Peer, K. Chung and J. A. Knoblich: Self-organized developmental patterning and differentiation in cerebral organoids. *EMBO J*, 36(10), 1316-1329 (2017) doi:10.15252/embj.201694700
48. M. T. Pham, K. M. Pollock, M. D. Rose, W. A. Cary, H. R. Stewart, P. Zhou, J. A. Nolte and B. Waldau: Generation of human vascularized brain organoids. *Neuroreport*, 29(7), 588-593 (2018) doi:10.1097/WNR.0000000000001014
49. L. Song, X. Yuan, Z. Jones, K. Griffin, Y. Zhou, T. Ma and Y. Li: Assembly of Human Stem Cell-Derived Cortical Spheroids and Vascular Spheroids to Model 3-D Brain-like Tissues. *Sci Rep*, 9(1), 5977 (2019) doi:10.1038/s41598-019-42439-9
50. P. R. Ormel, R. Vieira de Sá, E. J. van Bodegraven, H. Karst, O. Harschnitz, M. A. M. Sneeboer, L. E. Johansen, R. E. van Dijk, N. Scheefhals, A. Berdenis van Berlekom, E. Ribes Martínez, S. Kling, H. D. MacGillavry, L. H. van den Berg, R. S. Kahn, E. M. Hol, L. D. de Witte and R. J. Pasterkamp: Microglia innately develop within cerebral organoids. *Nat Commun*, 9(1), 4167 (2018) doi:10.1038/s41467-018-06684-2
51. M. Bershteyn, T. J. Nowakowski, A. A. Pollen, E. Di Lullo, A. Nene, A. Wynshaw-Boris and A. R. Kriegstein: Human iPSC-Derived Cerebral Organoids Model Cellular Features of

- Lissencephaly and Reveal Prolonged Mitosis of Outer Radial Glia. *Cell Stem Cell*, 20(4), 435-449.e4 (2017) doi:10.1016/j.stem.2016.12.007
52. H. Haegel, L. Larue, M. Ohsugi, L. Fedorov, K. Herrenknecht and R. Kemler: Lack of beta-catenin affects mouse development at gastrulation. *Development*, 121(11), 3529-37 (1995)
53. J. L. Esseltine and D. W. Laird: Next-Generation Connexin and Pannexin Cell Biology. *Trends Cell Biol*, 26(12), 944-955 (2016) doi:10.1016/j.tcb.2016.06.003
54. S. Penuela, R. Gehi and D. W. Laird: The biochemistry and function of pannexin channels. *Biochim Biophys Acta*, 1828(1), 15-22 (2013) doi:10.1016/j.bbamem.2012.01.017
55. Z. Iliodromiti, N. Antonakopoulos, S. Sifakis, P. Tsikouras, A. Daniilidis, K. Dafopoulos, D. Botsis and N. Vrachnis: Endocrine, paracrine, and autocrine placental mediators in labor. *Hormones (Athens)*, 11(4), 397-409 (2012) doi:10.14310/horm.2002.1371
56. A. Baranova, D. Ivanov, N. Petrash, A. Pestova, M. Skoblov, I. Kelmanson, D. Shagin, S. Nazarenko, E. Geraymovych, O. Litvin, A. Tiunova, T. L. Born, N. Usman, D. Staroverov, S. Lukyanov and Y. Panchin: The mammalian pannexin family is homologous to the invertebrate innexin gap junction proteins. *Genomics*, 83(4), 706-16 (2004) doi:10.1016/j.ygeno.2003.09.025
57. S. R. Bond and C. C. Naus: The pannexins: past and present. *Front Physiol*, 5, 58 (2014) doi:10.3389/fphys.2014.00058
58. E. Dossi, T. Blauwblomme, J. Moulard, O. Chever, F. Vasile, E. Guinard, M. Le Bert, I. Coullin, J. Pallud, L. Capelle, G. Huberfeld and N. Rouach: Pannexin-1 channels contribute to seizure generation in human epileptic brain tissue and in a mouse model of epilepsy. *Sci Transl Med*, 10(443) (2018) doi:10.1126/scitranslmed.aar3796
59. S. Penuela, S. J. Celetti, R. Bhalla, Q. Shao and D. W. Laird: Diverse subcellular distribution profiles of pannexin 1 and pannexin 3. *Cell Commun Adhes*, 15(1), 133-42 (2008) doi:10.1080/15419060802014115
60. M. G. Shum, Q. Shao, P. Lajoie and D. W. Laird: Destination and consequences of Panx1 and mutant expression in polarized MDCK cells. *Exp Cell Res*, 381(2), 235-247 (2019) doi:10.1016/j.yexcr.2019.05.016
61. R. Bhalla-Gehi, S. Penuela, J. M. Churko, Q. Shao and D. W. Laird: Pannexin1 and pannexin3 delivery, cell surface dynamics, and cytoskeletal interactions. *J Biol Chem*, 285(12), 9147-60 (2010) doi:10.1074/jbc.M109.082008
62. S. Penuela, A. W. Lohman, W. Lai, L. Gyenis, D. W. Litchfield, B. E. Isakson and D. W. Laird: Diverse post-translational modifications of the pannexin family of channel-forming proteins. *Channels (Austin)*, 8(2), 124-30 (2014) doi:10.4161/chan.27422
63. S. Penuela, R. Bhalla, K. Nag and D. W. Laird: Glycosylation regulates pannexin intermixing and cellular localization. *Mol Biol Cell*, 20(20), 4313-23 (2009) doi:10.1091/mbc.e09-01-0067
64. S. Penuela, R. Bhalla, X. Q. Gong, K. N. Cowan, S. J. Celetti, B. J. Cowan, D. Bai, Q. Shao and D. W. Laird: Pannexin 1 and pannexin 3 are glycoproteins that exhibit many distinct characteristics from the connexin family of gap junction proteins. *J Cell Sci*, 120(Pt 21), 3772-83 (2007) doi:10.1242/jcs.009514
65. M. Ishikawa, T. Iwamoto, T. Nakamura, A. Doyle, S. Fukumoto and Y. Yamada: Pannexin 3 functions as an ER Ca(2+) channel, hemichannel, and gap junction to promote osteoblast differentiation. *J Cell Biol*, 193(7), 1257-74 (2011) doi:10.1083/jcb.201101050
66. D. Boassa, P. Nguyen, J. Hu, M. H. Ellisman and G. E. Sosinsky: Pannexin2 oligomers localize in the membranes of endosomal vesicles in mammalian cells while Pannexin1 channels traffic to the plasma membrane. *Front Cell Neurosci*, 8, 468 (2014) doi:10.3389/fncel.2014.00468
67. L. E. Wicki-Stordeur, A. K. Boyce and L. A. Swayne: Analysis of a pannexin 2-pannexin 1 chimeric protein supports divergent roles for pannexin C-termini in cellular localization. *Cell Commun Adhes*, 20(3-4), 73-9 (2013) doi:10.3109/15419061.2013.791681
68. Q. Shao, K. Lindstrom, R. Shi, J. Kelly, A. Schroeder, J. Juusola, K. L. Levine, J. L. Esseltine, S. Penuela, M. F. Jackson and D. W. Laird: A Germline Variant in the PANX1 Gene Has Reduced Channel Function and Is Associated with Multisystem Dysfunction. *J Biol Chem*, 291(24), 12432-43 (2016) doi:10.1074/jbc.M116.717934

69. Q. Sang, Z. Zhang, J. Shi, X. Sun, B. Li, Z. Yan, S. Xue, A. Ai, Q. Lyu, W. Li, J. Zhang, L. Wu, X. Mao, B. Chen, J. Mu, Q. Li, J. Du, Q. Sun, L. Jin, L. He, S. Zhu, Y. Kuang and L. Wang: A pannexin 1 channelopathy causes human oocyte death. *Sci Transl Med*, 11(485) (2019) doi:10.1126/scitranslmed.aav8731
70. S. Penuela, L. Harland, J. Simek and D. W. Laird: Pannexin channels and their links to human disease. *Biochem J*, 461(3), 371-81 (2014) doi:10.1042/BJ20140447
71. Z. Ruan, I. J. Orozco, J. Du and W. Lü: Structures of human pannexin 1 reveal ion pathways and mechanism of gating. *Nature*, 584(7822), 646-651 (2020) doi:10.1038/s41586-020-2357-y
72. Q. Jin, B. Zhang, X. Zheng, N. Li, L. Xu, Y. Xie, F. Song, E. A. Bhat, Y. Chen, N. Gao, J. Guo, X. Zhang and S. Ye: Cryo-EM structures of human pannexin 1 channel. *Cell Res*, 30(5), 449-451 (2020) doi:10.1038/s41422-020-0310-0
73. K. Michalski, J. L. Syrjanen, E. Henze, J. Kumpf, H. Furukawa and T. Kawate: The Cryo-EM structure of pannexin 1 reveals unique motifs for ion selection and inhibition. *Elife*, 9 (2020) doi:10.7554/eLife.54670
74. J. K. Sandilos, Y. H. Chiu, F. B. Chekeni, A. J. Armstrong, S. F. Walk, K. S. Ravichandran and D. A. Bayliss: Pannexin 1, an ATP release channel, is activated by caspase cleavage of its pore-associated C-terminal autoinhibitory region. *J Biol Chem*, 287(14), 11303-11 (2012) doi:10.1074/jbc.M111.323378
75. L. E. Wicki-Stordeur and L. A. Swayne: Panx1 regulates neural stem and progenitor cell behaviours associated with cytoskeletal dynamics and interacts with multiple cytoskeletal elements. *Cell Commun Signal*, 11, 62 (2013) doi:10.1186/1478-811X-11-62
76. F. B. Chekeni, M. R. Elliott, J. K. Sandilos, S. F. Walk, J. M. Kinchen, E. R. Lazarowski, A. J. Armstrong, S. Penuela, D. W. Laird, G. S. Salvesen, B. E. Isakson, D. A. Bayliss and K. S. Ravichandran: Pannexin 1 channels mediate 'find-me' signal release and membrane permeability during apoptosis. *Nature*, 467(7317), 863-7 (2010) doi:10.1038/nature09413
77. A. Paoletti, S. Q. Raza, L. Voisin, F. Law, M. Caillet, I. Martins, E. Deutsch and J. L. Perfettini: Editorial: Pannexin-1--the hidden gatekeeper for HIV-1. *J Leukoc Biol*, 94(3), 390-2 (2013) doi:10.1189/jlb.0313148
78. C. Séror, M. T. Melki, F. Subra, S. Q. Raza, M. Bras, H. Saïdi, R. Nardacci, L. Voisin, A. Paoletti, F. Law, I. Martins, A. Amendola, A. A. Abdul-Sater, F. Ciccocanti, O. Delelis, F. Niedergang, S. Thierry, N. Said-Sadier, C. Lamaze, D. Métivier, J. Estaquier, G. M. Fimia, L. Falasca, R. Casetti, N. Modjtahedi, J. Kanellopoulos, J. F. Mouscadet, D. M. Ojcius, M. Piacentini, M. L. Gougeon, G. Kroemer and J. L. Perfettini: Extracellular ATP acts on P2Y2 purinergic receptors to facilitate HIV-1 infection. *J Exp Med*, 208(9), 1823-34 (2011) doi:10.1084/jem.20101805
79. R. J. Thompson, N. Zhou and B. A. MacVicar: Ischemia opens neuronal gap junction hemichannels. *Science*, 312(5775), 924-7 (2006) doi:10.1126/science.1126241
80. M. Freitas-Andrade, J. F. Bechberger, B. A. MacVicar, V. Viau and C. C. Naus: Pannexin1 knockout and blockade reduces ischemic stroke injury in female, but not in male mice. *Oncotarget*, 8(23), 36973-36983 (2017) doi:10.18632/oncotarget.16937
81. R. J. Thompson, M. F. Jackson, M. E. Olah, R. L. Rungta, D. J. Hines, M. A. Beazely, J. F. MacDonald and B. A. MacVicar: Activation of pannexin-1 hemichannels augments aberrant bursting in the hippocampus. *Science*, 322(5907), 1555-9 (2008) doi:10.1126/science.1165209
82. A. Ray, G. Zoidl, S. Weickert, P. Wahle and R. Dermietzel: Site-specific and developmental expression of pannexin1 in the mouse nervous system. *Eur J Neurosci*, 21(12), 3277-90 (2005) doi:10.1111/j.1460-9568.2005.04139.x
83. A. Vogt, S. G. Hormuzdi and H. Monyer: Pannexin1 and Pannexin2 expression in the developing and mature rat brain. *Brain Res Mol Brain Res*, 141(1), 113-20 (2005) doi:10.1016/j.molbrainres.2005.08.002
84. N. Hainz, A. Beckmann, M. Schubert, A. Haase, U. Martin, T. Tschernig and C. Meier: Human stem cells express pannexins. *BMC Res Notes*, 11(1), 54 (2018) doi:10.1186/s13104-018-3125-z

85. J. L. Esseltine, Q. Shao, C. Brooks, J. Sampson, D. H. Betts, C. A. Séguin and D. W. Laird: Connexin43 Mutant Patient-Derived Induced Pluripotent Stem Cells Exhibit Altered Differentiation Potential. *J Bone Miner Res*, 32(6), 1368-1385 (2017) doi:10.1002/jbmr.3098
86. J. L. Esseltine, C. R. Brooks, N. A. Edwards, M. Subasri, J. Sampson, C. Séguin, D. H. Betts and D. W. Laird: Dynamic regulation of connexins in stem cell pluripotency. *Stem Cells*, 38(1), 52-66 (2020) doi:10.1002/stem.3092
87. F. A. Ran, P. D. Hsu, J. Wright, V. Agarwala, D. A. Scott and F. Zhang: Genome engineering using the CRISPR-Cas9 system. *Nat Protoc*, 8(11), 2281-2308 (2013) doi:10.1038/nprot.2013.143
88. J. Beers, D. R. Gulbranson, N. George, L. I. Siniscalchi, J. Jones, J. A. Thomson and G. Chen: Passaging and colony expansion of human pluripotent stem cells by enzyme-free dissociation in chemically defined culture conditions. *Nat Protoc*, 7(11), 2029-40 (2012) doi:10.1038/nprot.2012.130
89. K. Watanabe, M. Ueno, D. Kamiya, A. Nishiyama, M. Matsumura, T. Wataya, J. B. Takahashi, S. Nishikawa, K. Muguruma and Y. Sasai: A ROCK inhibitor permits survival of dissociated human embryonic stem cells. *Nat Biotechnol*, 25(6), 681-6 (2007) doi:10.1038/nbt1310
90. J. Dahlmann, G. Kensah, H. Kempf, D. Skvorc, A. Gawol, D. A. Elliott, G. Dräger, R. Zweigerdt, U. Martin and I. Grub: The use of agarose microwells for scalable embryoid body formation and cardiac differentiation of human and murine pluripotent stem cells. *Biomaterials*, 34(10), 2463-71 (2013) doi:10.1016/j.biomaterials.2012.12.024
91. H. Kurosawa: Methods for inducing embryoid body formation: in vitro differentiation system of embryonic stem cells. *J Biosci Bioeng*, 103(5), 389-98 (2007) doi:10.1263/jbb.103.389
92. L. H. Chew, A. Anonuevo and E. Knock: Generating cerebral organoids from human pluripotent stem cells using standardized reagents. *Neural Progenitor Cells: Methods and Protocols*, Methods in Molecular Biology (2021)
93. Y. H. Chiu, M. S. Schappe, B. N. Desai and D. A. Bayliss: Revisiting multimodal activation and channel properties of Pannexin 1. *J Gen Physiol*, 150(1), 19-39 (2018) doi:10.1085/jgp.201711888
94. Y. Yan, S. Shin, B. S. Jha, Q. Liu, J. Sheng, F. Li, M. Zhan, J. Davis, K. Bharti, X. Zeng, M. Rao, N. Malik and M. C. Vemuri: Efficient and rapid derivation of primitive neural stem cells and generation of brain subtype neurons from human pluripotent stem cells. *Stem Cells Transl Med*, 2(11), 862-70 (2013) doi:10.5966/sctm.2013-0080
95. H. Zipper, H. Brunner, J. Bernhagen and F. Vitzthum: Investigations on DNA intercalation and surface binding by SYBR Green I, its structure determination and methodological implications. *Nucleic Acids Res*, 32(12), e103 (2004) doi:10.1093/nar/gnh101
96. T. D. Schmittgen and K. J. Livak: Analyzing real-time PCR data by the comparative C(T) method. *Nat Protoc*, 3(6), 1101-8 (2008) doi:10.1038/nprot.2008.73
97. C. S. H. Laboratory: Mowial-DABCO stock solution. *Cold Spring Harb. Protoc.* (2007) doi:doi:10.1101/pdb.rec10913
98. J. Schindelin, I. Arganda-Carreras, E. Frise, V. Kaynig, M. Longair, T. Pietzsch, S. Preibisch, C. Rueden, S. Saalfeld, B. Schmid, J. Y. Tinevez, D. J. White, V. Hartenstein, K. Eliceiri, P. Tomancak and A. Cardona: Fiji: an open-source platform for biological-image analysis. *Nat Methods*, 9(7), 676-82 (2012) doi:10.1038/nmeth.2019
99. K. W. Dunn, M. M. Kamocka and J. H. McDonald: A practical guide to evaluating colocalization in biological microscopy. *Am J Physiol Cell Physiol*, 300(4), C723-42 (2011) doi:10.1152/ajpcell.00462.2010
100. S. Bolte and F. P. Cordelières: A guided tour into subcellular colocalization analysis in light microscopy. *J Microsc*, 224(Pt 3), 213-32 (2006) doi:10.1111/j.1365-2818.2006.01706.x
101. H. T. Maecker and J. Trotter: Flow cytometry controls, instrument setup, and the determination of positivity. *Cytometry A*, 69(9), 1037-42 (2006) doi:10.1002/cyto.a.20333
102. C. P. García, G. A. Videla Richardson, L. Romorini, S. G. Miriuka, G. E. Sevlever and M. E. Scassa: Topoisomerase I inhibitor, camptothecin, induces apoptogenic signaling in human embryonic stem cells. *Stem Cell Res*, 12(2), 400-14 (2014) doi:10.1016/j.scr.2013.12.002

103. C. Sagné, M. F. Isambert, J. P. Henry and B. Gasnier: SDS-resistant aggregation of membrane proteins: application to the purification of the vesicular monoamine transporter. *Biochem J*, 316 (Pt 3), 825-31 (1996) doi:10.1042/bj3160825
104. M. Sobocki, K. Mrouj, A. Camasses, N. Parisi, E. Nicolas, D. Llères, F. Gerbe, S. Prieto, L. Krasinska, A. David, M. Eguren, M. C. Birling, S. Urbach, S. Hem, J. Déjardin, M. Malumbres, P. Jay, V. Dulic, D. L. j. Lafontaine, R. Feil and D. Fisher: The cell proliferation antigen Ki-67 organises heterochromatin. *Elife*, 5, e13722 (2016) doi:10.7554/eLife.13722
105. X. Xu, L. E. Wicki-Stordeur, J. C. Sanchez-Arias, M. Liu, M. S. Weaver, C. S. W. Choi and L. A. Swayne: Probenecid Disrupts a Novel Pannexin 1-Collapsin Response Mediator Protein 2 Interaction and Increases Microtubule Stability. *Front Cell Neurosci*, 12, 124 (2018) doi:10.3389/fncel.2018.00124
106. S. Penuela, J. J. Kelly, J. M. Churko, K. J. Barr, A. C. Berger and D. W. Laird: Panx1 regulates cellular properties of keratinocytes and dermal fibroblasts in skin development and wound healing. *J Invest Dermatol*, 134(7), 2026-2035 (2014) doi:10.1038/jid.2014.86
107. L. A. Swayne and S. A. Bennett: Connexins and pannexins in neuronal development and adult neurogenesis. *BMC Cell Biol*, 17 Suppl 1, 10 (2016) doi:10.1186/s12860-016-0089-5
108. V. R. Lee, K. J. Barr, J. J. Kelly, D. Johnston, C. F. C. Brown, K. P. Robb, S. Sayedyahosseini, K. Huang, R. Gros, L. E. Flynn and S. Penuela: Pannexin 1 regulates adipose stromal cell differentiation and fat accumulation. *Sci Rep*, 8(1), 16166 (2018) doi:10.1038/s41598-018-34234-9
109. A. W. Xie, B. Y. K. Binder, A. S. Khalil, S. K. Schmitt, H. J. Johnson, N. A. Zacharias and W. L. Murphy: Controlled Self-assembly of Stem Cell Aggregates Instructs Pluripotency and Lineage Bias. *Sci Rep*, 7(1), 14070 (2017) doi:10.1038/s41598-017-14325-9
110. H. Imamura, S. Sakamoto, T. Yoshida, Y. Matsui, S. Penuela, D. W. Laird, S. Mizukami, K. Kikuchi and A. Kakizuka: Single-cell dynamics of pannexin-1-facilitated programmed ATP loss during apoptosis. *Elife*, 9 (2020) doi:10.7554/eLife.61960
111. H. Miyazawa and A. Aulehla: Revisiting the role of metabolism during development. *Development*, 145(19) (2018) doi:10.1242/dev.131110
112. S. Langlois, X. Xiang, K. Young, B. J. Cowan, S. Penuela and K. N. Cowan: Pannexin 1 and pannexin 3 channels regulate skeletal muscle myoblast proliferation and differentiation. *J Biol Chem*, 289(44), 30717-30731 (2014) doi:10.1074/jbc.M114.572131
113. J. C. Sanchez-Arias, R. C. Candlish, E. van der Slagt and L. A. Swayne: Pannexin 1 Regulates Dendritic Protrusion Dynamics in Immature Cortical Neurons. *eNeuro*, 7(4) (2020) doi:10.1523/ENEURO.0079-20.2020
114. N. Prochnow, A. Abdulazim, S. Kurtenbach, V. Wildförster, G. Dvorientchikova, J. Hanske, E. Petrasch-Parwez, V. I. Shestopalov, R. Dermietzel, D. Manahan-Vaughan and G. Zoidl: Pannexin1 stabilizes synaptic plasticity and is needed for learning. *PLoS One*, 7(12), e51767 (2012) doi:10.1371/journal.pone.0051767
115. G. Zoidl, E. Petrasch-Parwez, A. Ray, C. Meier, S. Bunse, H. W. Habbes, G. Dahl and R. Dermietzel: Localization of the pannexin1 protein at postsynaptic sites in the cerebral cortex and hippocampus. *Neuroscience*, 146(1), 9-16 (2007) doi:10.1016/j.neuroscience.2007.01.061
116. Y. Huang, J. B. Grinspan, C. K. Abrams and S. S. Scherer: Pannexin1 is expressed by neurons and glia but does not form functional gap junctions. *Glia*, 55(1), 46-56 (2007) doi:10.1002/glia.20435
117. R. Iglesias, G. Dahl, F. Qiu, D. C. Spray and E. Scemes: Pannexin 1: the molecular substrate of astrocyte "hemichannels". *J Neurosci*, 29(21), 7092-7 (2009) doi:10.1523/JNEUROSCI.6062-08.2009
118. G. A. Ransford, N. Fregien, F. Qiu, G. Dahl, G. E. Conner and M. Salathe: Pannexin 1 contributes to ATP release in airway epithelia. *Am J Respir Cell Mol Biol*, 41(5), 525-34 (2009) doi:10.1165/rcmb.2008-0367OC
119. F. Hanner, L. Lam, M. T. Nguyen, A. Yu and J. Peti-Peterdi: Intrarenal localization of the plasma membrane ATP channel pannexin1. *Am J Physiol Renal Physiol*, 303(10), F1454-9 (2012) doi:10.1152/ajprenal.00206.2011

120. A. Raslan, N. Hainz, A. Beckmann, T. Tschernig and C. Meier: Pannexin-1 expression in developing mouse nervous system: new evidence for expression in sensory ganglia. *Cell Tissue Res*, 364(1), 29-41 (2016) doi:10.1007/s00441-015-2294-5
121. A. L. Epp, S. N. Ebert, J. C. Sanchez-Arias, L. E. Wicki-Stordeur, A. K. J. Boyce and L. A. Swayne: A novel motif in the proximal C-terminus of Pannexin 1 regulates cell surface localization. *Sci Rep*, 9(1), 9721 (2019) doi:10.1038/s41598-019-46144-5
122. C. E. Murry and G. Keller: Differentiation of embryonic stem cells to clinically relevant populations: lessons from embryonic development. *Cell*, 132(4), 661-80 (2008) doi:10.1016/j.cell.2008.02.008
123. D. Pacitti, R. Privolizzi and B. E. Bax: Organs to Cells and Cells to Organoids: The Evolution of. *Front Cell Neurosci*, 13, 129 (2019) doi:10.3389/fncel.2019.00129
124. F. Molica, M. J. Meens, G. Pelli, A. Hautefort, Y. Emre, B. A. Imhof, P. Fontana, E. Scemes, S. Morel and B. R. Kwak: Selective inhibition of Panx1 channels decreases hemostasis and thrombosis in vivo. *Thromb Res*, 183, 56-62 (2019) doi:10.1016/j.thromres.2019.09.028
125. I. K. Poon, Y. H. Chiu, A. J. Armstrong, J. M. Kinchen, I. J. Juncadella, D. A. Bayliss and K. S. Ravichandran: Unexpected link between an antibiotic, pannexin channels and apoptosis. *Nature*, 507(7492), 329-34 (2014) doi:10.1038/nature13147
126. J. Wang, D. G. Jackson and G. Dahl: The food dye FD&C Blue No. 1 is a selective inhibitor of the ATP release channel Panx1. *J Gen Physiol*, 141(5), 649-56 (2013) doi:10.1085/jgp.201310966
127. C. P. Lai, J. F. Bechberger, R. J. Thompson, B. A. MacVicar, R. Bruzzone and C. C. Naus: Tumor-suppressive effects of pannexin 1 in C6 glioma cells. *Cancer Res*, 67(4), 1545-54 (2007) doi:10.1158/0008-5472.CAN-06-1396
128. A. C. Cone, C. Ambrosi, E. Scemes, M. E. Martone and G. E. Sosinsky: A comparative antibody analysis of pannexin1 expression in four rat brain regions reveals varying subcellular localizations. *Front Pharmacol*, 4, 6 (2013) doi:10.3389/fphar.2013.00006

6 Appendices

For our qPCR transcript expression analyses we used *GAPDH* as the reference gene as it was stably expressed across all cell lines and tissues assessed in this study.

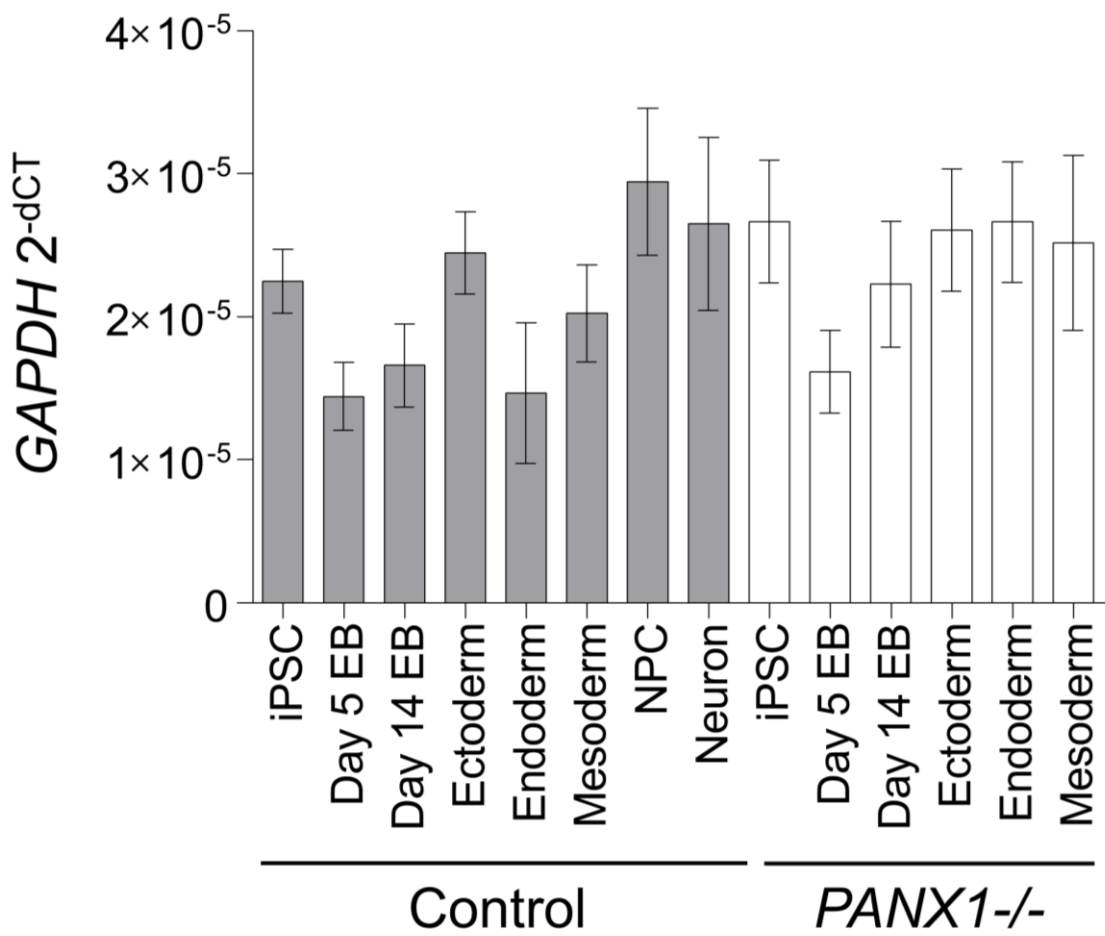


Figure 6.1 *GAPDH* transcript expression is stable across all cell lines and tissues assessed in this study

We evaluated the stability and suitability of *GAPDH* as a reference gene for qPCR analysis. This was performed according to the methodology described in Schmittgen and Livak (96) followed by 1-way ANOVA with Tukey post hoc testing. No significant differences were detected. n = 3 – 25 biological replicates per condition. Error bars depict the standard error of the mean.

6.1 Human Ethics Research Statement

2/15/2021

Memorial Webmail :: HREB - Approval of Ethics Renewal 510179

Subject HREB - Approval of Ethics Renewal 510179
From <administrator@hrea.ca>
To Esseltine Jessica(Principal Investigator) <jesseltine@mun.ca>
Cc <administrator@hrea.ca>
Date 2020-10-06 08:59



Researcher Portal File #: 20191777

Dear Dr. Jessica Esseltine:

This e-mail serves as notification that your ethics renewal for study HREB # 2018.210 – Connexins and Pannexins in Stem Cell Pluripotency and Cell Fate Decisions – has been **approved**. Please log in to the Researcher Portal to view the approved event.

Ethics approval for this project has been granted for a period of twelve months effective from **13 Nov 2020 to 13 Nov 2021**.

Please note, it is the responsibility of the Principal Investigator (PI) to ensure that the Ethics Renewal form is submitted prior to the renewal date each year. Though the Research Ethics Office makes every effort to remind the PI of this responsibility, the PI may not receive a reminder. The Ethics Renewal form can be found on the Researcher Portal as an "Event".

Thank you,

Research Ethics Office

(e) info@hrea.ca

(t) 709-777-6974

(f) 709-777-8776

(w) www.hrea.ca

Office Hours: 8:30 a.m. – 4:30 p.m. (NL TIME) Monday-Friday

This email is intended as a private communication for the sole use of the primary addressee and those individuals copied in the original message. If you are not an intended recipient of this message you are hereby notified that copying, forwarding or other dissemination or distribution of this communication by any means is prohibited. If you believe that you have received this message in error please notify the original sender immediately.

6.2 R Heatmap Code

The script listed below was used in R to scale qPCR data and produce a heatmap of the result. Lines preceded by # are included for information only and are not part of the code.

```
# Library import
install.packages("gplots") #if not installed already
library(gplots)
library(cluster) #clustering algorithms

#Install and load the ggplot package to make heatmaps
install.packages("ggplot2") #if not installed already
library("ggplot2")

#Import the csv data (should be a pivot table where gene names are in the rows and conditions/treatments are in the columns)
df=read.csv("pathway to the pivot table file saved as a csv", row.names=1)
View(df)
attach(df)
# for an example of the csv data table as it appears in R studio refer to Figure 6.2 below.
# for an example of the csv data converted into a dataframe where row names have been set to column 1 (row.names=1) refer to Figure 6.3 below.

#turn our dataframe into a matrix (only numbers)
matrix=data.matrix(df)
View(matrix)

#Make a heatmap using heatmap.2 (UQ Library Version)
heatmap.2(matrix)
heatmap.2(matrix, scale="row") #specified to do the scaling by row (scale across conditions/treatments)
# but the above script does the clustering before the scaling!
#scale the data before visualizing
matrix_scaled=t(scale(t(matrix)))
heatmap.2(matrix_scaled) #scaling and clustering is now performed correctly
# can use colors from heat.colors
heatmap.2(matrix_scaled,
          col = hcl.colors(n=10, palette = "viridis"), #use viridis blue/yellow colors with 10 gradations
          main = "Title of Heatmap", #add a title
          trace ="none", #get rid of count trace on heatmap
          #Rowv = NA, #can remove row dendogram if you want
          #ColV=NA, #can remove dendograms from columns
          margins = c(8,10), #the lower the #s the narrower the margins on x y
          cexRow = 1.1, #modifies font size for row names
          cexCol = 0.8, #modifies font size for column names
          key.title=NA, #adds a legend to the color key
          key.ylab=NA,
          keysize = 1.2,
          density.info='none',#get rid of the histogram on the color key
          )
```

i.Gene	D0.iPSC.CX43Ko.3	D0.iPSC.PANX1Ko.2	D0.iPSC.PANX1Ko.4	D0.iPSC.WT	D5.EB.CX43Ko.3	D5.EB.PANX1Ko.2	D5.EB.PANX1Ko.4
1 CX43	1.89e-01	3.07e-01	2.85e-01	2.78e-01	1.05e-01	0.168000	0.205000
2 CXCR4	1.32e-04	2.48e-04	1.59e-04	2.81e-04	1.21e-02	0.010100	0.016200
3 MIXL1	8.77e-05	7.45e-05	8.30e-05	1.03e-04	1.03e-04	0.001440	0.000303
4 NANOG	3.16e-02	1.59e-02	2.32e-02	2.68e-02	2.20e-04	0.002980	0.000332
5 NCAM1	6.10e-04	6.64e-04	1.14e-03	7.47e-04	9.26e-03	0.007850	0.008060
6 NES	3.94e-02	3.52e-02	4.20e-02	2.40e-02	4.18e-02	0.044500	0.070700
7 PANX1	4.24e-03	1.25e-03	3.85e-03	3.58e-03	5.45e-03	0.002000	0.003440
8 PANX2	6.98e-04	7.50e-04	8.93e-04	4.99e-04	2.59e-04	0.000134	0.000167
9 PAX6	1.69e-05	2.62e-05	2.51e-05	1.26e-05	1.22e-02	0.006510	0.022500
10 POU5F1	3.24e-01	2.43e-01	3.81e-01	2.73e-01	5.44e-03	0.021900	0.003560
11 SOX17	8.51e-07	1.58e-06	1.90e-06	6.77e-07	3.47e-05	0.001960	0.000228
12 TBXT	2.68e-05	4.45e-05	9.14e-05	6.40e-05	9.36e-05	0.001800	0.000216

Figure 6.2 Example of csv file imported into R

Values in the table are ΔC_T values normalized to *GAPDH* expression. The first data column contains the gene names.

i.Gene	D0.iPSC.CX43Ko.3	D0.iPSC.PANX1Ko.2	D0.iPSC.PANX1Ko.4	D0.iPSC.WT	D5.EB.CX43Ko.3	D5.EB.PANX1Ko.2	D5.EB.PANX1Ko.4	D5.EB
CX43	1.89e-01	3.07e-01	2.85e-01	2.78e-01	1.05e-01	0.168000	0.205000	2.05e-
CXCR4	1.32e-04	2.48e-04	1.59e-04	2.81e-04	1.21e-02	0.010100	0.016200	7.26e-
MIXL1	8.77e-05	7.45e-05	8.30e-05	1.03e-04	1.03e-04	0.001440	0.000303	6.81e-
NANOG	3.16e-02	1.59e-02	2.32e-02	2.68e-02	2.20e-04	0.002980	0.000332	1.32e-
NCAM1	6.10e-04	6.64e-04	1.14e-03	7.47e-04	9.26e-03	0.007850	0.008060	8.05e-
NES	3.94e-02	3.52e-02	4.20e-02	2.40e-02	4.18e-02	0.044500	0.070700	5.41e-
PANX1	4.24e-03	1.25e-03	3.85e-03	3.58e-03	5.45e-03	0.002000	0.003440	4.29e-
PANX2	6.98e-04	7.50e-04	8.93e-04	4.99e-04	2.59e-04	0.000134	0.000167	1.99e-
PAX6	1.69e-05	2.62e-05	2.51e-05	1.26e-05	1.22e-02	0.006510	0.022500	1.77e-
POU5F1	3.24e-01	2.43e-01	3.81e-01	2.73e-01	5.44e-03	0.021900	0.003560	1.53e-
SOX17	8.51e-07	1.58e-06	1.90e-06	6.77e-07	3.47e-05	0.001960	0.000228	1.22e-
TBXT	2.68e-05	4.45e-05	9.14e-05	6.40e-05	9.36e-05	0.001800	0.000216	2.23e-

Figure 6.3 Example of csv file converted to a dataframe (df)

Rows are now labeled by the gene name rather than a numerical row position.

Gene names are no longer located in a data column.

6.3 FIJI Area Measurement Macro

The macro shown here computes object area for entire folders of phase contrast images that were taken on the same microscope, at the same magnification. The macro can be adjusted for different magnifications and microscopes by changing the parameters in "Set Scale". Instructions that are not part of the code are preceded by //.

```
//This FIJI Macro - Whole folder analysis of spheroids taken on Zeiss AxioObserver 5X Objective
// This macro batch measures a folder of images.
// Use the Analyze>Set Measurements command to specify the measurement parameters. Check
// "Display Label" in the Set Measurements dialog and the file names will be added to the first column of
// the "Results" table.

//start of batch macro code
macro "Batch Measure" {
  dir = getDirectory("Choose a Directory ");
  list = getFileList(dir);
  if (getVersion>="1.40e")
    setOption("display labels", true);
  setBatchMode(true);
  for (i=0; i<list.length; i++) {
    path = dir+list[i];
    showProgress(i, list.length);
    if (!endsWith(path,"/")) open(path);
    if (nImages>=1) {
//customizable instructions
run("8-bit");
run("Set Scale...", "distance=388 known=500 pixel=1 unit=microns global");
run("Enhance Contrast...", "saturated=0.3 normalize");
run("Auto Local Threshold", "method=Phansalkar radius=15 parameter_1=0 parameter_2=0 white");
run("Analyze Particles...", "size=40000-Infinity display include add");
selectWindow("Results");
//Final piece of batch macro code
      close();
    }
  }
}
```